INTEGRATION EXPERIMENTS USING AN ENERGY CONSERVING DIABATIC MODEL IN ISENTROPIC COORDINATES

by

Lawrence Marx

Submitted in Partial Fulfillment

of the Requirements for the

Degree of Master of Science

at the

MASSACHUSETTS INSTITUTE OF TECHNOLOGY

September, 1977

Signature redacted

Signature of Author.....
Department of Meteorology, August 12, 1977

Signature redacted

Certified by.....
Thesis Supervisor

Accepted by.....
Department Chairman

CONTENTS

LIST OF FIGURES

Integration Experiments Using an Energy Conserving Diabatic Model in Isentropic Coordinates

by Lawrence Marx

Eugenia Kalnay-Rivas, Assistant Professor, Thesis Supervisor

ABSTRACT

A quadratically conservative diabatic model based on isentropic coordinates has been developed. It is the first isentropic model that allows for an exact energy conservation equation for adiabatic motion and the first model to include diabatic processes.

The model has been run in a periodic channel. Although the numerical scheme allows for long integrations, the problem of the boundary conditions at the walls has not been completely solved and limits integrations to about ten days.

Short time adiabatic integrations compare well with previous integrations of Eliassen and Raustein (1968,1970). Preliminary integrations including very simple newtonian heating and cooling have been performed with reasonable results.

For long time integrations further work is necessary in the parameterization of heating, inclusion of moist processes, the treatment of the intersection of isentropic surfaces with the ground, and the meridional boundary conditions.

The model should prove useful in investigating processes in which heating effects are important for baroclinic developement, as for example coastal cyclogenesis.

CHAPTER 1

INTRODUCTION

In a paper by Starr (1945) the usefulness of a quasi-Lagrangian model based on material surfaces was pointed out: since no flux occurs through material surfaces, only the horizontal terms need be considered in the primitive equations. Isentropic surfaces (i.e. surfaces of constant potential temperature) behave as material surfaces under adiabatic conditions, so that the choice of these surfaces under adiabatic flow as the vertical coordinate would seem natural.

However, due to the simplicity of the primitive equations using pressure as the vertical coordinate and due to the difficulty in treating the intersection of an isentropic surface with the ground, isentropic coordinate models received little attention until the mid 1960's. At this time a primitive equation model in isentropic coordinates for two layers was developped by Eliassen and Raustein (1968). Their treatment of the intersection of an isentrope with the ground proved feasible, and the model simulated a "life like" cyclone developement over a period of three days. This led to the developement of a six level model (Eliassen and Raustein, 1970). This last model and the treatment of the intersection problem in the first model became the basis for several subsequent models using primitive equations.

Bleck (1974) compared a primitive equation model in isentropic coordinates and an earlier filtered (quasigeostrophic)

model (Bleck,1973) based on the conservation of potential vorticity in isentropic coordinates. These models were used to make actual forecasts using real data. The primitive equation model was based on the Eliassen and Raustein approach. The isentropic coordinate forecasts could be shown to be consistently better than other coordinate model forecasts; however certain synoptic developements such as rapid cyclogenesis were much better predicted by the isentropic coordinate models. Shapiro (1975) used a model similar to the model of Eliassen and Raustein to show the advantages of an isentropic coordinate model in forecasting upper level frontogenesis. Papers by Eliassen and Hellevik (1975) and Hellevik (1976) proposed an improved treatment of the isentrope and ground intersection. These (and more recently Trevisan (1976) and Bleck (1977)) have included orography. A model including parameterized moist adiabatic processes developed by Reimer (1976) has given reasonable results. An attempt to combine isentropic and sigma coordinates into one model by Friend et al. (1976) has had mixed results.

However, all of these models have been based on the assumption of adiabatic motion. This, as Starr showed, has the advantage that the primitive equations are simplified since the terms involving heating, $\dot{\theta}$, vanish. This assumption may be valid for short time integrations of two days or less. It has often been assumed that the inclusion of heating makes isentropic models no better than other coordiante models such as sigma

and pressure because isentropes cease to be material surfaces. This is not really the case because of the fact that isentropic surfaces are closely spaced in the vicinity of cyclones and frontal surfaces (see figure 1.1). Therefore, even though the continuous forms of the primitive equations in the various coordinate systems are equivalent, the discrete approximations to the different coordinate systems are not. In a numerical model the dynamics of cyclones and fronts will be better resolved in an isentropic model than in other models with the same number of horizontal grid points and vertical levels.

In this thesis a new numerical model based on isentropic is developed. The model includes the heating (diabatic) terms in the primitive equations. Its structure allows for the conservation of mass, momentum, and total energy. The finite difference techniques differ from those used by Eliassen and Raustein and other subsequent primitive equation models. The Eliassen and Raustein technique uses a staggered grid with the non linear terms calculated in advective form. The present model uses a box type grid with the non linear terms computed in a flux form. This allows for the formulation of an exact energy integral equation which apparently cannot be done using the Eliassen and Raustein numerical scheme. For comparison purposes the same model parameters are used wherever they can be made compatible with the Eliassen and Raustein model. The time integrations are performed in a beta-plane reentrant channel. The model is first run adiabatically to compare with the

Eliassen and Raustein (1968) model. Diffusion and heating terms are then included, and the model is run beyond the traditional three or four days for which previous models have been run.

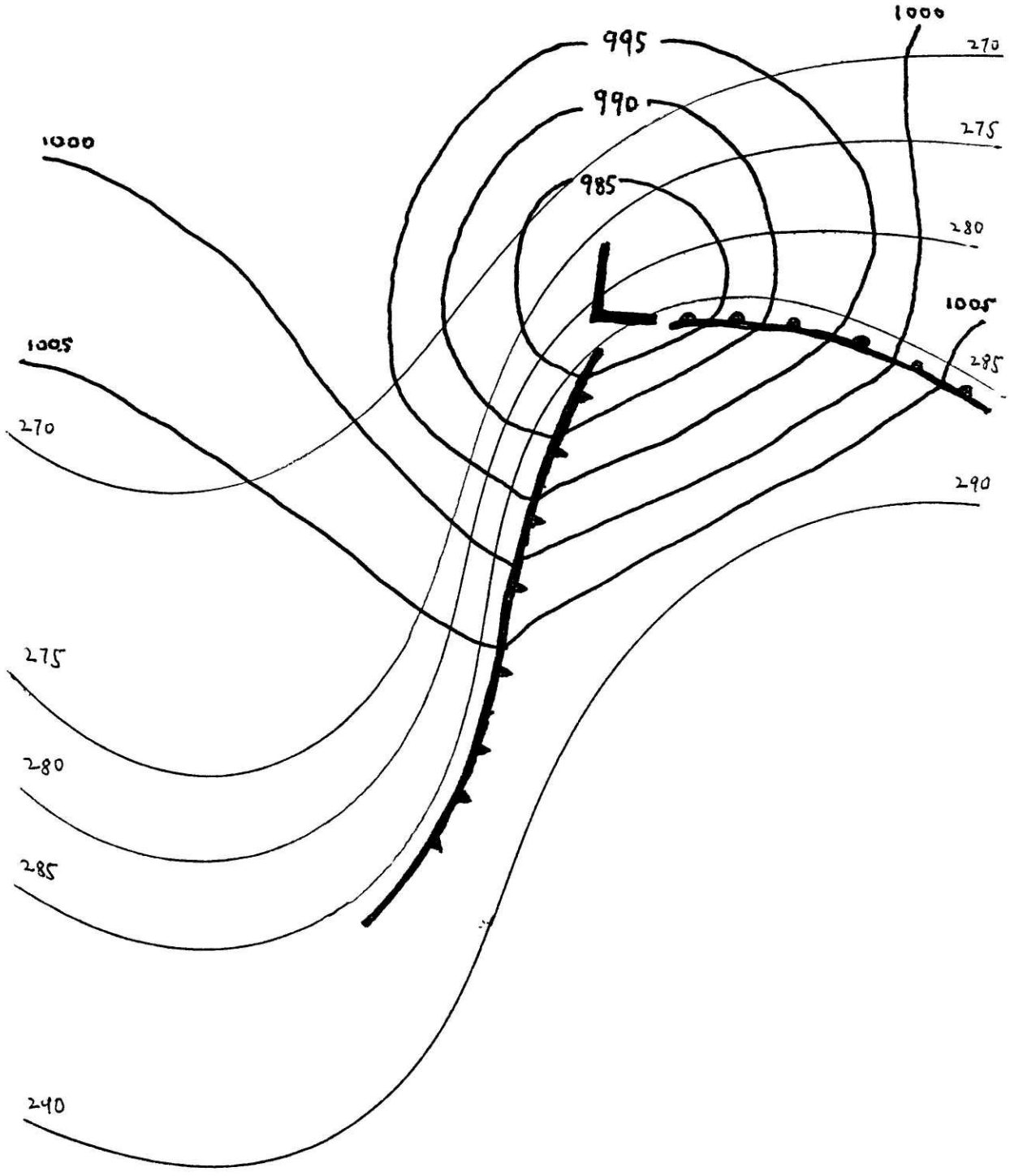

Figure 1.1 A typical low with potential isotherms at the ground (light lines). Isobars in heavy lines 5mb spacing.

CHAPTER 2

THE DIABATIC EQUATIONS IN ISENTROPIC COORDINATES

2.1 Notation Used for Equations

Independent Variables

x,y	horizontal Cartesian coordinates
t	time
θ	potential temperature

Dependent Variables

$\vec{V}$	horizontal velocity vector
$u \equiv \frac{dx}{dt}$	horizontal velocity component in the x direction
$v \equiv \frac{dy}{dt}$	horizontal velocity component in the y direction
$\dot{\theta} \equiv \frac{d\theta}{dt}$	"vertical velocity" in isentropic coordinates (equivalent to heating)
p	pressure
z	height
$w \equiv \frac{dz}{dt}$	vertical velocity
$\pi = C_p (p/10^5 \text{ Pascals})^{R/C_p}$	Exner function
T	temperature
$\phi = gz$	geopotential
$h = C_p T = \theta \pi$	dry enthalpy
$M = \phi + h$	Montgomery potential
$f = f_o + \beta y$	Coriolis parameter

F	friction vector
F_x	friction component in the x direction
F_y	friction component in the y direction
ρ	density

Constants

R	gas constant for dry air
C_p	specific heat at constant pressure
g	gravitational acceleration

Subscripts

$( )_z$	at constant height
$( )_s$	at a material surface (usually the ground)
$( )_\theta$	at constant potential temperature
	(used for emphasis or clarification)

2.2 Introduction

The model equations are derived in a flux form allowing for diabatic heating and cooling. The equations developed in a flux form are more complicated than in the advective form, however this allows for quadratically conservative numerical integration.

2.3 Substantial Time Derivative

The substantial time derivative in isentropic coordinates as shown by Thompson (1961) is:

$$\frac{d\eta}{dt} = \left(\frac{\partial \eta}{\partial t}\right)_\theta + u\left(\frac{\partial \eta}{\partial x}\right)_\theta + v\left(\frac{\partial \eta}{\partial y}\right)_\theta + \dot{\theta}\,\frac{\partial \eta}{\partial \theta} \qquad (2.3.1)$$

where η is an arbitrary variable.

2.4 The Continuity Equation

The derivation of the diabatic continuity equation in isentropic coordinates is similar to the derivation performed by Thompson (1961) for the adiabatic case. The same procedure will be followed, but the terms involving $\dot{\theta}$ will be retained. Using (2.3.1) and substituting $\frac{\partial z}{\partial \theta}$ for η gives:

$$\frac{d}{dt}\left(\frac{\partial z}{\partial \theta}\right) = \frac{\partial}{\partial \theta}\left(\frac{\partial z}{\partial t}\right)_\theta + u\frac{\partial}{\partial \theta}\left(\frac{\partial z}{\partial x}\right)_\theta + v\frac{\partial}{\partial \theta}\left(\frac{\partial z}{\partial y}\right)_\theta + \dot{\theta}\,\frac{\partial^2 z}{\partial \theta^2} \qquad (2.4.1)$$

$$= \frac{\partial}{\partial \theta}\left(\frac{dz}{dt}\right) - \frac{\partial u}{\partial \theta}\left(\frac{\partial z}{\partial x}\right)_\theta - \frac{\partial v}{\partial \theta}\left(\frac{\partial z}{\partial y}\right)_\theta - \frac{\partial \dot{\theta}}{\partial \theta}\left(\frac{\partial z}{\partial \theta}\right) \qquad (2.4.2)$$

Since $\frac{dz}{dt}$ is w, by rearrangement of terms (2.4.2) becomes:

$$\frac{\partial w}{\partial \theta} = \frac{d}{dt}\left(\frac{\partial z}{\partial \theta}\right) + \frac{\partial u}{\partial \theta}\left(\frac{\partial z}{\partial x}\right)_\theta + \frac{\partial v}{\partial \theta}\left(\frac{\partial z}{\partial y}\right)_\theta + \frac{\partial \dot{\theta}}{\partial \theta}\left(\frac{\partial z}{\partial \theta}\right) \qquad (2.4.3)$$

The continuity equation in Cartesian coordinates is:

$$\frac{1}{\rho}\frac{d\rho}{dt} + \left(\frac{\partial u}{\partial x}\right)_z + \left(\frac{\partial v}{\partial y}\right)_z + \frac{\partial w}{\partial z} = 0 \qquad (2.4.4)$$

Assign $\frac{\partial w}{\partial z} = \frac{\partial \theta}{\partial z}\frac{\partial w}{\partial \theta}$ and substitute (2.4.3) for $\frac{\partial w}{\partial \theta}$:

$$\frac{1}{\rho}\frac{d\rho}{dt} + \frac{\partial \theta}{\partial z}\frac{d}{dt}\left(\frac{\partial z}{\partial \theta}\right) + \left(\frac{\partial u}{\partial x}\right)_z + \left(\frac{\partial v}{\partial y}\right)_z + \frac{\partial u}{\partial z}\left(\frac{\partial z}{\partial x}\right)_\theta + \frac{\partial v}{\partial z}\left(\frac{\partial z}{\partial y}\right)_\theta + \frac{\partial \dot{\theta}}{\partial z}\left(\frac{\partial z}{\partial \theta}\right) = 0 \qquad (2.4.5)$$

Multiply by $\rho\frac{\partial z}{\partial \theta}$ and combine terms one and two, three and five,

and four and six to obtain:

$$\frac{d}{dt}\left(\rho\frac{\partial z}{\partial\theta}\right)+\rho\frac{\partial z}{\partial\theta}\left(\frac{\partial u}{\partial x}\right)_\theta+\rho\frac{\partial z}{\partial\theta}\left(\frac{\partial v}{\partial y}\right)_\theta+\rho\frac{\partial\dot{\theta}}{\partial z}\left(\frac{\partial z}{\partial\theta}\right)^2=0 \qquad (2.4.6)$$

The combinations can be done since $\left(\frac{\partial u}{\partial x}\right)_\theta=\left(\frac{\partial u}{\partial x}\right)_z+\frac{\partial u}{\partial z}\left(\frac{\partial z}{\partial x}\right)_\theta$ and likewise for v. Using the following form of the hydrostatic equation:

$$\rho\frac{\partial z}{\partial\theta}=-\frac{1}{g}\frac{\partial z}{\partial\theta}\frac{\partial\theta}{\partial z}=-\frac{1}{g}\frac{\partial p}{\partial\theta} \qquad (2.4.7)$$

and substituting this for $\rho\frac{\partial z}{\partial\theta}$ yields:

$$\frac{d}{dt}\left(\frac{\partial p}{\partial\theta}\right)+\frac{\partial u}{\partial\theta}\left(\frac{\partial u}{\partial x}\right)+\frac{\partial p}{\partial\theta}\left(\frac{\partial v}{\partial y}\right)_\theta+\frac{\partial p}{\partial\theta}\frac{\partial\dot{\theta}}{\partial\theta}=0 \qquad (2.4.8)$$

Expanding the first term by (2.3.1):

$$\frac{\partial p}{\partial t}\left(\frac{\partial\theta}{\partial p}\right)_\theta+u\frac{\partial}{\partial x}\left(\frac{\partial\theta}{\partial p}\right)_\theta+v\frac{\partial}{\partial y}\left(\frac{\partial\theta}{\partial p}\right)_\theta+\dot{\theta}\left(\frac{\partial^2\theta}{\partial\theta^2}\right)+\frac{\partial\theta}{\partial p}\left(\frac{\partial u}{\partial x}\right)_\theta+\frac{\partial\theta}{\partial p}\left(\frac{\partial v}{\partial y}\right)_\theta+\frac{\partial\theta}{\partial p}\frac{\partial\dot{\theta}}{\partial\theta}=0 \qquad (2.4.9)$$

combining terms yields:

$$\frac{\partial}{\partial t}\left(\frac{\partial\theta}{\partial p}\right)_\theta+\frac{\partial}{\partial x}\left(\frac{\partial\theta}{\partial p}u\right)_\theta+\frac{\partial}{\partial y}\left(\frac{\partial\theta}{\partial p}v\right)_\theta+\frac{\partial}{\partial\theta}\left(\frac{\partial\theta}{\partial p}\dot{\theta}\right)=0 \qquad (2.4.10)$$

This is the analytical form of the continuity equation for isentropic coordinates used in the model.

2.5 The Equations of Motion

The equations of motion in z coordinates are:

$$\frac{du}{dt}+\frac{1}{\rho}\left(\frac{\partial p}{\partial x}\right)_z-fv+F_x=0 \qquad (2.5.1)$$

$$\frac{dv}{dt}+\frac{1}{\rho}\left(\frac{\partial p}{\partial y}\right)_z+fu+F_y=0 \qquad (2.5.2)$$

The parameterizaton of the friction terms will be discussed in a later chapter. The pressure gradient terms, $\frac{1}{\rho}\left(\frac{\partial p}{\partial x}\right)_z$ and $\frac{1}{\rho}\left(\frac{\partial p}{\partial y}\right)_z$, can be written in isentropic coordinates as shown by Thompson (1961) as:

$$\frac{1}{\rho}\left(\frac{\partial p}{\partial x}\right)_z = \left(\frac{\partial M}{\partial x}\right)_\theta \qquad \text{and} \qquad \frac{1}{\rho}\left(\frac{\partial p}{\partial y}\right)_z = \left(\frac{\partial M}{\partial y}\right)_\theta$$

Where $M=C_p T+gz= \theta\eta+\phi$ is the Montgomery potential. To transform (2.5.1) and (2.5.2) into isentropic coordinates, all that is required is to substitute for the pressure gradient terms, since the remaining terms are independent of the coordinate system used. Further expanding the first term of (2.5.1) by (2.3.1) and solving for $\left(\frac{\partial u}{\partial t}\right)_\theta$:

$$\left(\frac{\partial u}{\partial t}\right)_\theta = -u\left(\frac{\partial u}{\partial x}\right)_\theta - v\left(\frac{\partial u}{\partial y}\right)_\theta - \dot{\theta}\frac{\partial u}{\partial \theta} - \left(\frac{\partial M}{\partial x}\right)_\theta + fv - F_x \qquad (2.5.3)$$

This is the advective form of the u equation of motion in isentropic coordinates. Multiply (2.5.3) by $\frac{\partial p}{\partial \theta}$ and (2.4.10) by u, adding and combining terms to get:

$$\frac{\partial}{\partial t}\left(\frac{\partial p}{\partial \theta}u\right)_\theta = -\frac{\partial}{\partial x}\left(\left(\frac{\partial p}{\partial \theta}u\right)u\right)_\theta - \frac{\partial}{\partial y}\left(\left(\frac{\partial p}{\partial \theta}v\right)u\right)_\theta - \frac{\partial}{\partial \theta}\left(\left(\frac{\partial p}{\partial \theta}\dot{\theta}\right)u\right)$$

$$- \frac{\partial p}{\partial \theta}\left(\frac{\partial M}{\partial x}\right)_\theta + \frac{\partial p}{\partial \theta}fv - \frac{\partial p}{\partial \theta}F_x \qquad (2.5.4)$$

This is the zonal momentum equation used in the model. It may appear to be somewhat more awkward than the advective u equation (2.5.3), however, as will be shown in the following chapter,

(2.5.4) can be treated with little difficulty and has several advantages for numerical integration. Following the same procedure, the meridional momentum equation is:

$$\frac{\partial}{\partial t}\left(\frac{\partial p}{\partial \theta} v\right)_\theta = -\frac{\partial}{\partial x}\left(\left(\frac{\partial p}{\partial \theta} u\right) v\right)_\theta - \frac{\partial}{\partial y}\left(\left(\frac{\partial p}{\partial \theta} v\right) v\right)_\theta - \frac{\partial}{\partial \theta}\left(\left(\frac{\partial p}{\partial \theta} \dot{\theta}\right) v\right)$$

$$- \frac{\partial p}{\partial \theta}\left(\frac{\partial M}{\partial y}\right)_\theta - \frac{\partial p}{\partial \theta} f u - \frac{\partial p}{\partial \theta} F_y \qquad (2.5.5)$$

2.6 The Thermodynamic Equation

The analytical form of the thermodynamic equation is simply:

$$\frac{d\theta}{dt} = \dot{\theta} \qquad (2.6.1)$$

If the model atmosphere is bounded by isentropes, (2.6.1) becomes redundant. If, however, a non-isentropic surface is one of the model boundaries, a prognostic equation for θ on that surface will arise.

2.7 The Hydrostatic Equation

The hydrostatic equation used in this model is:

$$\frac{\partial M}{\partial \theta} = -\pi \qquad (2.7.1)$$

This is the same equation used by Eliassen and Raustein (1968)

CHAPTER 3

THE FINITE DIFFERENCE APPROXIMATIONS AND THE BOUNDARY CONDITIONS

3.1 Introduction

Since the equations cannot be solved analytically, finite difference techniques are required. Using a scheme developed by Kálnay-Rivas (1976, private communication), the model atmosphere is approximated by a box type grid in the horizontal, where each grid point is representative of the center (horizontally) of each box. In the vertical a staggered grid is used. The thermodynamic variables, such as pressure, potential temperature, and geopotential, are defined at each level. The wind components are defined at each layer between levels.

3.2 Finite Difference Notation

Let i be any grid point along the x direction with grid spacing Δx.

Let k be any level or the layer immediately below level k.

Let Q_k and R_k be any variables defined at level k.

Let u_k and v_k be any variables defined at layer k.

Using centered differences in the horizontal, each has the following definition:

$$\Delta Q_k = Q_k - Q_{k-1} \qquad \overline{Q_k}^{\theta} = \frac{Q_k + Q_{k-1}}{2}$$

$$\overline{u_k}^{\theta} = \frac{u_{k+1} + u_k}{2} \qquad \overline{u_i}^{x} = \frac{u_{i-\frac{1}{2}} + u_{i+\frac{1}{2}}}{2}$$

$$\delta_x u_i = \frac{u_{i+\frac{1}{2}} - u_{i-\frac{1}{2}}}{\Delta x} \qquad \overline{uv_i}^{x} = \frac{u_{i+\frac{1}{2}} v_{i+\frac{1}{2}} + u_{i-\frac{1}{2}} v_{i-\frac{1}{2}}}{2}$$

$$\widetilde{uv_i}^{x} = \frac{u_{i-\frac{1}{2}} v_{i+\frac{1}{2}} + u_{i+\frac{1}{2}} v_{i-\frac{1}{2}}}{2} \qquad \widetilde{QR_k}^{\theta} = \frac{Q_k R_{k-1} + Q_{k-1} R_k}{2}$$

(3.2.1)

The following properties will be used:

$$\overline{\overline{u_i}^{x}\,\overline{v_i}^{x}}^{x} = \frac{1}{2}\overline{uv_i}^{x} + \frac{1}{2}\widetilde{uv_i}^{x} \qquad (3.2.2)$$

$$\delta_x \widetilde{uv_i}^{x} = u_i \delta_x \overline{v_i}^{x} + v_i \delta_x \overline{u_i}^{x} \qquad (3.2.3)$$

$$v_i \delta_x \overline{u_i}^{x} \overline{v_i}^{x} = \frac{v_i^2}{2} \delta_x \overline{u_i}^{x} + \delta_x\left(\overline{u_i}^{x} \widetilde{\frac{v_i^2}{2}}^{x}\right) = \frac{v_i^2}{2} \delta_x \overline{u_i}^{x} + \frac{1}{2} \delta_x \widetilde{(uv)v_i}^{x} \qquad (3.2.4)$$

$$\overline{u_k}^{\theta} \Delta v_k = \Delta u v_k - \overline{v_k}^{\theta} \Delta u_k \qquad (3.2.5)$$

Similar definitions and properties hold for y as for x.

3.3 Material and Isentropic Surfaces

A material surface is a surface through which no mass flux occurs. The ground is then a material surface, particularly

under dry conditions. An isentropic surface is by definition a surface of constant potential temperature. Under adiabatic conditions an isentropic surface becomes a material surface. Under diabatic conditions, however, an isentropic surface no longer remains a material surface; the mass flux through the isentropic surface is then proportional to the heating at the surface. Since the ground is not an isentropic surface, the potential temperature must be specified through all time in order to sucessfully intergrate the governing equations. It will thus be assumed in the early sections of this chapter that the potential temperature at the ground, θ_s , is a known function of space and time. In a later section the specification of the potential temperature at the ground will outlined. In this model the ground is assumed to be flat at height z=0. The top of the model will be both an isentropic and a material surface. This is not a realistic approximation for the atmosphere, but given the other limitations of the model, will suffice to show the capabilites of the model.

3.4 The Finite Difference Approximation to the Diabatic Continuity Equation

Assume that a discrete set of potential temperatures is chosen as the set of isentropic surfaces where the information of the atmosphere will be retained. Some of these surfaces may intersect the ground, and this problem will be discussed in detail in the next chapter. In this chapter it will be assumed

that the finite difference computations will be performed away from such intersections.

Given the continuity equation (2.4.10):

$$\frac{\partial}{\partial t}\left(\frac{\partial p}{\partial \theta}\right) = -\frac{\partial}{\partial x}\left(\frac{\partial p}{\partial \theta} u\right) - \frac{\partial}{\partial y}\left(\frac{\partial p}{\partial \theta} v\right) - \frac{\partial}{\partial \theta}\left(\frac{\partial p}{\partial \theta} \dot{\theta}\right)$$

Integration in the vertical will now be done between two arbitrary consecutive isentropes, θ_{k-1} and θ_k. The left hand side becomes:

$$\int_{\theta_{k-1}}^{\theta_k} \frac{\partial}{\partial t}\left(\frac{\partial p}{\partial \theta}\right) d\theta = \frac{\partial}{\partial t}\int_{\theta_{k-1}}^{\theta_k} \frac{\partial p}{\partial \theta}\, d\theta - \left(\frac{\partial p}{\partial \theta}\frac{\partial \theta}{\partial t}\right)\Big|_{\theta_{k-1}}^{\theta_k} \qquad (3.4.1)$$

Each term of the right hand side becomes:

$$-\int_{\theta_{k-1}}^{\theta_k} \frac{\partial}{\partial x}\left(\frac{\partial p}{\partial \theta} u\right) d\theta = -\frac{\partial}{\partial x}\int_{\theta_{k-1}}^{\theta_k} \left(\frac{\partial p}{\partial \theta} u\right) d\theta + \left(\frac{\partial p}{\partial \theta} u \frac{\partial \theta}{\partial x}\right)\Big|_{\theta_{k-1}}^{\theta_k} \qquad (3.4.2)$$

$$-\int_{\theta_{k-1}}^{\theta_k} \frac{\partial}{\partial y}\left(\frac{\partial p}{\partial \theta} v\right) d\theta = -\frac{\partial}{\partial y}\int_{\theta_{k-1}}^{\theta_k} \left(\frac{\partial p}{\partial \theta} v\right) d\theta + \left(\frac{\partial p}{\partial \theta} v \frac{\partial \theta}{\partial y}\right)\Big|_{\theta_{k-1}}^{\theta_k} \qquad (3.4.3)$$

$$-\int_{\theta_{k-1}}^{\theta_k} \frac{\partial}{\partial \theta}\left(\frac{\partial p}{\partial \theta} \dot{\theta}\right) d\theta = -\left(\frac{\partial p}{\partial \theta} \dot{\theta}\right)\Big|_{\theta_{k-1}}^{\theta_k} \qquad (3.4.4)$$

If θ_{k-1} and θ_k are fixed isentropic surfaces, they are invariant in space and time. The last terms of (3.4.1), (3.4.2), and (3.4.3) each vanish and when recombined yield:

$$\frac{\partial}{\partial t}\int_{\theta_{k-1}}^{\theta_k} \frac{\partial p}{\partial \theta}\, d\theta = -\frac{\partial}{\partial x}\int_{\theta_{k-1}}^{\theta_k} \frac{\partial p}{\partial \theta} u\, d\theta - \frac{\partial}{\partial y}\int_{\theta_{k-1}}^{\theta_k} \frac{\partial p}{\partial \theta} v\, d\theta - \left(\frac{\partial p}{\partial \theta}\dot{\theta}\right)\Big|_{\theta_{k-1}}^{\theta_k} \qquad (3.4.5)$$

If θ_{k-1} is not an isentropic surface, but is the ground surface, $\theta_s = \theta_s(x, y, t)$, then since $\dot{\theta}_s = \frac{\partial \theta_s}{\partial t} + u\frac{\partial \theta_s}{\partial x} + v\frac{\partial \theta_s}{\partial y}$, the lower

limits of the second terms of (3.4.1), (3.4.2), and (3.4.3) cancel the lower limit of (3.4.4). Therefore, the lower limit of the last term of (3.4.5) vanishes. The integral $\int_{\theta_{K-1}}^{\theta_K} \frac{\partial \rho}{\partial \theta}\, d\theta$ is $\Delta\rho_K$. The integrals $\int_{\theta_{K-1}}^{\theta_K} \frac{\partial \rho}{\partial \theta}\, u\, d\theta$ and $\int_{\theta_{K-1}}^{\theta_K} \frac{\partial \rho}{\partial \theta}\, v\, d\theta$ will be represented by $(\Delta\rho u)_K$ and $(\Delta\rho v)_K$. It can be easily shown that $(\Delta\rho u)_K = \Delta\rho_K u_K + O(\Delta\theta_K)^2$ since $\Delta\rho_K$ and u_K are defined at the center of each layer. Introducing centered finite differences in the horizontal direction, the finite difference form of equation (3.4.5) becomes:

$$\frac{\partial \Delta\rho_K}{\partial t} = -\delta_x \overline{\Delta\rho u}^x - \delta_y \overline{\Delta\rho v}^y - \Delta\left(\left(\overline{\frac{\Delta\rho}{\Delta\theta}}\right)^\theta \dot{\theta}\,\alpha\right)_K \qquad (3.4.6)$$

where $\alpha = 1$ for non material isentropic surfaces

$\alpha = 0$ for material surfaces.

3.5 Conservation Properties of the Finite Difference Scheme

The finite difference form of the continuity equation (3.4.6) ensures conservation of total mass, with the exception of time truncation errors. From (3.4.6) it can be shown that $\sum_x \sum_y \sum_\theta \frac{\partial \Delta\rho}{\partial t} \Delta x \Delta y$ (or equivalently $\frac{\partial}{\partial t} \sum_x \sum_y \sum_\theta \Delta\rho \Delta x \Delta y$) is zero as long as the boundaries are periodic or have no flux through them. In this model a channel cyclic in the x direction, with no flux at the walls in the y direction, and bounded at the top and bottom by material surfaces is used. Thus, the model will conserve mass.

Consider a conservation equation for a scalar field f of the form:

$$\frac{\partial f}{\partial t} + u\frac{\partial f}{\partial x} + v\frac{\partial f}{\partial y} + \dot{\theta}\frac{\partial f}{\partial \theta} = 0 \qquad (3.5.1)$$

Using the same procedure as outlined in chapter 2, (3.5.1) can be written in flux form as:

$$\frac{\partial}{\partial t}\left(\frac{\partial p}{\partial \theta} f\right) + \frac{\partial}{\partial x}\left(\left(\frac{\partial p}{\partial \theta} u\right) f\right) + \frac{\partial}{\partial y}\left(\left(\frac{\partial p}{\partial \theta} v\right) f\right) + \frac{\partial}{\partial \theta}\left(\left(\frac{\partial p}{\partial \theta} \dot{\theta}\right) f\right) = 0 \qquad (3.5.2)$$

Integrating between two arbitrary consecutive isentropes, θ_{K-1} and θ_K, each term becomes:

$$\int_{\theta_{K-1}}^{\theta_K} \frac{\partial}{\partial t}\left(\frac{\partial p}{\partial \theta} f\right) d\theta = \frac{\partial}{\partial t}\int_{\theta_{K-1}}^{\theta_K} \frac{\partial p}{\partial \theta} f \, d\theta - \left(\frac{\partial p}{\partial \theta} f \frac{\partial \theta}{\partial t}\right)\Bigg|_{\theta_{K-1}}^{\theta_K} \qquad (3.5.3)$$

$$\int_{\theta_{K-1}}^{\theta_K} \frac{\partial}{\partial x}\left(\left(\frac{\partial p}{\partial \theta} u\right) f\right) d\theta = \frac{\partial}{\partial x}\int_{\theta_{K-1}}^{\theta_K} \left(\frac{\partial p}{\partial \theta} u\right) f \, d\theta - \left(\frac{\partial p}{\partial \theta} u f \frac{\partial \theta}{\partial x}\right)\Bigg|_{\theta_{K-1}}^{\theta_K} \qquad (3.5.4)$$

$$\int_{\theta_{K-1}}^{\theta_K} \frac{\partial}{\partial y}\left(\left(\frac{\partial p}{\partial \theta} v\right) f\right) d\theta = \frac{\partial}{\partial y}\int_{\theta_{K-1}}^{\theta_K} \left(\frac{\partial p}{\partial \theta} v\right) f \, d\theta - \left(\frac{\partial p}{\partial \theta} v f \frac{\partial \theta}{\partial y}\right)\Bigg|_{\theta_{K-1}}^{\theta_K} \qquad (3.5.5)$$

$$\int_{\theta_{K-1}}^{\theta_K} \frac{\partial}{\partial \theta}\left(\left(\frac{\partial p}{\partial \theta} \dot{\theta}\right) f\right) d\theta = \left(\frac{\partial p}{\partial \theta} \dot{\theta} f\right)\Bigg|_{\theta_{K-1}}^{\theta_K} \qquad (3.5.6)$$

The second terms of the right hand sides of (3.5.3-3.5.5) will vanish if θ_{K-1} and θ_K are isentropes. If, as before, θ_{K-1} is replaced by the potential temperature at the ground, θ_s $\theta_s = \theta_s(x, y, t)$, then since $\dot{\theta}_s = \frac{\partial \theta_s}{\partial t} + u\frac{\partial \theta_s}{\partial x} + v\frac{\partial \theta_s}{\partial y}$, the lower limits of the second terms of (3.5.3-3.5.5) will cancel the lower limit of (3.5.6). The integral $\frac{\partial}{\partial t}\int_{\theta_{K-1}}^{\theta_K} \frac{\partial p}{\partial \theta} f \, d\theta$ will be

represented by $\frac{\partial(\Delta\rho f)_\kappa}{\partial t}$. The integral $\frac{\partial}{\partial x}\int_{\theta_{\kappa-1}}^{\theta_\kappa}\left(\frac{\partial\rho}{\partial\theta}u\right)f\,d\theta$ will be represented by $\delta_x(\overline{\Delta\rho u}^x\bar{f}^x)_\kappa$. A similar form will occur for v. The final finite difference form is then:

$$\frac{\partial(\Delta\rho f)_\kappa}{\partial t}+\delta_x(\overline{\Delta\rho u}^x\bar{f}^x)_\kappa+\delta_y(\overline{\Delta\rho v}^y\bar{f}^y)_\kappa+\Delta\left(\left(\frac{\overline{\Delta\rho}}{\Delta\theta}\right)^\theta\dot{\theta}\,\alpha\,\bar{f}^\theta\right)_\kappa=0 \quad (3.5.7)$$

where α is as in (3.4.6).

It is clear that the total volume integral, $\frac{\partial}{\partial t}\sum_x\sum_y\sum_\theta\Delta\rho f\Delta x\Delta y$, will also vanish. This again is because flux form finite differences are used; the non-boundary terms will add out leaving only the boundary terms. As long as the boundaries are not sources or sinks of f, which is the case for cyclic or no flux conditions, the boundary terms will also vanish. Thus, the mass average mean value of f will be conserved.

Lastly, it can be shown that the mass average mean square value of f will also be conserved. Multiplying (3.5.7) by f and (3.4.6) by $-\frac{f^2}{2}$ and adding gives:

$$\frac{\partial\Delta\rho\frac{f^2}{2}}{\partial t}+\delta_x\left(\overline{\Delta\rho u}^x\widetilde{\frac{f^2}{2}}^x\right)+\delta_y\left(\overline{\Delta\rho v}^y\widetilde{\frac{f^2}{2}}^y\right)+\Delta\left(\left(\frac{\overline{\Delta\rho}}{\Delta\theta}\right)^\theta\dot{\theta}\,\alpha\,\widetilde{\frac{f^2}{2}}^\theta\right)=0 \quad (3.5.8)$$

where properties (3.2.2-3.2.5) have been used.

The volume integral of (3.5.8) will vanish:

$$\frac{\partial}{\partial t}\sum_x\sum_y\sum_\theta\Delta\rho\frac{f^2}{2}\Delta x\Delta y=0$$

This means that the possibility of nonlinear instability will be greatly reduced. It also allows for the formulation of the energy equation which will be discussed in section 3.7.

3.6 The Finite Difference Approximations to the Momentum Equations.

The finite difference form of the equations of momentum are derived in similar fashion to equation (3.5.7). Following this method, equation (2.5.4) becomes:

$$\left(\frac{\partial \Delta\rho u}{\partial t}\right)_k = -\delta_x\left(\overline{\Delta\rho u}^x\,\overline{u}^x\right)_k - \delta_y\left(\overline{\Delta\rho v}^y\,\overline{u}^y\right)_k - \Delta\left(\left(\frac{\overline{\Delta\rho}}{\Delta\theta}\right)^\theta \dot{\theta}\,\alpha\,\overline{u}^\theta\right)_k$$

$$-\left(\Delta\rho\,\delta_x\overline{M}^{\theta x}\right)_k + \left(\Delta\rho\,\beta\,\pi_s\,\delta_x\overline{\theta_s}^x\right)_k + \left(\Delta\rho f v\right)_k - \left(\Delta\rho F_x\right)_k \qquad (3.6.1)$$

where $\beta=0$ for isentrope bounded layer

$\beta=\frac{1}{2}$ for ground bounded layer

$\alpha=0$ for material surfaces

$\alpha=1$ for isentropic surfaces as before

The fifth term on the right side is a correction to the pressure gradient term. This is required because of the averaging of M over θ, and the fact that the pressure gradient force at the ground is $-\theta_s\frac{\partial \pi_s}{\partial x}$. Similarly for v, the finite difference form of equation (2.5.5) is:

$$\left(\frac{\partial \Delta\rho v}{\partial t}\right)_k = -\delta_x\left(\overline{\Delta\rho u}^x\,\overline{v}^x\right)_k - \delta_y\left(\overline{\Delta\rho v}^y\,\overline{v}^y\right)_k - \Delta\left(\left(\frac{\overline{\Delta\rho}}{\Delta\theta}\right)^\theta \dot{\theta}\,\alpha\,\overline{v}^\theta\right)_k$$

$$-\left(\Delta\rho\,\delta_y\overline{M}^{\theta y}\right)_k + \left(\Delta\rho\,\beta\,\pi_s\,\delta_y\overline{\theta_s}^y\right)_k - \left(\Delta\rho f u\right)_k - \left(\Delta\rho F_y\right)_k \qquad (3.6.2)$$

These equations are consistent with the equation of continuity (3.4.6). The terms involving M require further lateral boundary conditions in order for the model to remain quadratically

conservative. This will be discussed in section 3.10.

3.7 The Exact Energy Integral Equation

In Eliassen and Hellevik (1975) they are only able to arrive at an approximate energy integral equation. They state:

"Clearly it would be desirable if the isentropic surface model could be designed with an exact energy integral, as was done by Lorenz for isobaric surface models. It is not known whether this is possible."

Contrary to their model and other previous models in isentropic coordinates, an exact energy equation can be derived for the present model.

Multiply equation (3,6.1) by u, (3.6.2) by v, and (3.4.6) by $-\frac{u^2+v^2}{2}$ and adding to obtain:

$$\frac{\partial}{\partial t}\Delta\rho K + \delta_x\left[\overline{\Delta\rho u}^x \tilde{K}^x\right] + \delta_y\left[\overline{\Delta\rho v}^y \tilde{K}^y\right] + \Delta\left[\left(\overline{\frac{\Delta\rho}{\Delta\theta}}\right)^\theta \dot{\theta}\alpha \tilde{K}^\theta\right] =$$

$$-\Delta\rho u \delta_x\left(\overline{\bar{M}^\theta}^x\right) - \Delta\rho v \delta_y\left(\overline{\bar{M}^\theta}^y\right) + \Delta\rho u \beta \pi_s \delta_x \bar{\theta}_s^x$$

$$+\Delta\rho v \beta \pi_s \delta_y \bar{\theta}_s^y - \Delta\rho(uF_x + vF_y) \qquad (3,7,1)$$

Where $K=\frac{u^2+v^2}{2}$ and α and β have their usual meanings. Using equation (3.4.6), the right side can be rewritten as:

$$-\delta_x\widetilde{(\Delta\rho u)\bar{M}^\theta}^x - \delta_y\widetilde{(\Delta\rho v)\bar{M}^\theta}^y - \bar{M}^\theta\left[\frac{\partial\Delta\rho}{\partial t} + \Delta\left(\left(\overline{\frac{\Delta\rho}{\Delta\theta}}\right)^\theta \dot{\theta}\alpha\right)\right]$$

$$+\Delta P u \beta \pi_s \delta_x \overline{\theta_s}^x + \Delta P v \beta \pi_s \delta_y \overline{\theta_s}^y - \Delta P (u F_x + v F_y)$$

Adding $\Delta P \cdot \frac{\partial \overline{\theta\pi}^\theta}{\partial t}$ to each side and rearranging terms gives:

$$\frac{\partial}{\partial t} \Delta P (K + \overline{\theta\pi}^\theta) + \delta_x [\overline{\Delta P u}^x \tilde{K}^x + \widetilde{(\Delta P u)\bar{M}^\theta}^x] + \delta_y [\overline{\Delta P v}^y \tilde{K}^y + \widetilde{(\Delta P v)\bar{M}^\theta}^y]$$

$$+ \Delta [(\overline{\frac{\Delta P}{\Delta\theta}})^\theta \dot{\theta} \alpha \tilde{K}^\theta + (\overline{\frac{\Delta P}{\Delta\theta}})^\theta \dot{\theta} \alpha M] = -\overline{\phi}^\theta \frac{\partial \Delta P}{\partial t} + \Delta P \frac{\partial \overline{\theta\pi}^\theta}{\partial t}$$

$$+ \overline{(\overline{\frac{\Delta P}{\Delta\theta}})^\theta \dot{\theta} \alpha}^\theta \Delta M + \Delta P \beta \pi_s \vec{V} \cdot [\delta_x \overline{\theta_s}^x \vec{i} + \delta_y \overline{\theta_s}^y \vec{j}] - \Delta P \vec{V} \cdot \vec{F} \quad (3.7.2)$$

Rewriting $\Delta P \frac{\partial \overline{\theta\pi}^\theta}{\partial t}$ as $\Delta P \overline{\theta \frac{\partial \pi}{\partial t}}^\theta + \Delta P \beta \pi_s \frac{\partial \theta_s}{\partial t}$, the right hand side becomes:

$$-\overline{\phi}^\theta \frac{\partial \Delta P}{\partial t} + \Delta P \overline{\theta \frac{\partial \pi}{\partial t}}^\theta + \Delta P \beta \pi_s \frac{\partial \theta_s}{\partial t} + \Delta P \beta \pi_s \vec{V} \cdot [\delta_x \overline{\theta_s}^x \vec{i} + \delta_y \overline{\theta_s}^y \vec{j}]$$

$$+ \overline{(\overline{\frac{\Delta P}{\Delta\theta}})^\theta \dot{\theta} \alpha}^\theta \Delta M - \vec{V} \cdot \vec{F}$$

The following form of the hydrostatic approximation, $-\theta = \frac{\partial \phi}{\partial \pi}$, is equivalent to $\frac{\partial M}{\partial \theta} = \pi$ in finite difference form as will be shown in section 3.9. Substituting for the second term:

$$\Delta P \overline{\theta \frac{\partial \pi}{\partial t}}^\theta = -\Delta P \overline{\frac{\partial \phi}{\partial \pi} \frac{\partial \pi}{\partial t}}^\theta = -\Delta P \overline{\frac{\partial \phi}{\partial t}}^\theta$$

This and the first term combine to form $-\frac{\partial \Delta P \overline{\phi}^\theta}{\partial t}$. This can be placed on the left hand side. Since $\dot{\theta}_s = \frac{\partial \theta_s}{\partial t} + u \frac{\partial \theta_s}{\partial x} + v \frac{\partial \theta_s}{\partial y}$, the

third and fourth terms can be combined. Integrating over the total volume of the model atmosphere yields:

$$\frac{\partial}{\partial t}\sum_{i,j,k}\Delta p\,(h+\overline{M}^{\theta})\Delta x\,\Delta y = \sum_{i,j,k}\overline{\left(\frac{\Delta p}{\Delta\theta}\right)^{\theta}\dot{\theta}\,\alpha\,\Delta M}^{\theta} + \Delta p_{v}\frac{\pi_{s}}{2}\dot{\theta}_{s} - \sum_{i,j,k}\Delta p(\vec{V}\cdot\vec{F}) \qquad (3.7.3)$$

where the subscript v is the index of the lowest layer. This form of the energy equation is the finite difference equivalent of the continuous form of the energy equation (26) of Eliassen and Hellevik (1975), except that the diabatic and friction terms are included.

3.8 The Finite Difference Form of the Thermodynamic Equation

The basic thermodynamic equation, $\dot{\theta}=\frac{d\theta}{dt}$, would be a tautology if the top and bottom boundaries were isentropes. However, in the present model the bottom boundary is not an isentrope. This requires a thermodynamic equation to specify the potential temperature at the ground, θ_s. Expanding $\frac{d\theta}{dt}$ by (2.3.1):

$$\left(\frac{\partial\theta}{\partial t}\right)_{\theta} + u\left(\frac{\partial\theta}{\partial x}\right)_{\theta} + v\left(\frac{\partial\theta}{\partial y}\right)_{\theta} + \dot{\theta}\,\frac{\partial\theta}{\partial\theta} = \dot{\theta} \qquad (3.8.1)$$

Multiplying (3.8.1) by $\frac{\partial p}{\partial\theta}$, retaining all terms, then multiplying (2.4.10) by θ, adding, and combining terms to get:

$$\frac{\partial}{\partial t}\left(\frac{\partial p}{\partial\theta}\theta\right) + \frac{\partial}{\partial x}\left(\left(\frac{\partial p}{\partial\theta}u\right)\theta\right) + \frac{\partial}{\partial y}\left(\left(\frac{\partial p}{\partial\theta}v\right)\theta\right) + \frac{\partial}{\partial\theta}\left(\left(\frac{\partial p}{\partial\theta}\dot{\theta}\right)\theta\right) = \frac{\partial p}{\partial\theta}\dot{\theta} \qquad (3.8.2)$$

Integrating again between two arbitrary consecutive isentropes would yield a tautology; if the lower boundary is instead $\theta_s=\theta_s(x,y,t)$, then the left hand side becomes:

$$\int_{\theta_s}^{\theta_K} \frac{\partial}{\partial t}\left(\frac{\partial p}{\partial \theta}\right)\theta\, d\theta = \frac{\partial}{\partial t}\int_{\theta_s}^{\theta_K} \frac{\partial p}{\partial \theta}\,\theta\, d\theta - \frac{\partial p}{\partial \theta}\,\theta\,\frac{\partial \theta}{\partial t}\Big|_{\theta_s}^{\theta_K} \qquad (3.8.3)$$

$$\int_{\theta_s}^{\theta_K} \frac{\partial}{\partial x}\left(\frac{\partial p}{\partial \theta}\, u\theta\right) d\theta = \frac{\partial}{\partial x}\int_{\theta_s}^{\theta_K} \frac{\partial p}{\partial \theta}\, u\theta\, d\theta - \left(\frac{\partial p}{\partial \theta}\, u\theta\,\frac{\partial \theta}{\partial x}\right)\Big|_{\theta_s}^{\theta_K} \qquad (3.8.4)$$

$$\int_{\theta_s}^{\theta_K} \frac{\partial}{\partial y}\left(\frac{\partial p}{\partial \theta}\, v\theta\right) d\theta = \frac{\partial}{\partial y}\int_{\theta_s}^{\theta_K} \frac{\partial p}{\partial \theta}\, v\theta\, d\theta - \left(\frac{\partial p}{\partial \theta}\, v\theta\,\frac{\partial \theta}{\partial y}\right)\Big|_{\theta_s}^{\theta_K} \qquad (3.8.5)$$

$$\int_{\theta_s}^{\theta_K} \frac{\partial}{\partial \theta}\left(\frac{\partial p}{\partial \theta}\,\dot{\theta}\,\theta\right) d\theta = \frac{\partial p}{\partial \theta}\,\dot{\theta}\,\theta\Big|_{\theta_s}^{\theta_K} \qquad (3.8.6)$$

Again since $\dot{\theta}_s = \frac{\partial \theta_s}{\partial t} + u\frac{\partial \theta_s}{\partial x} + v\frac{\partial \theta_s}{\partial y}$, all the lower limit terms will cancel, and the upper limit terms of (3.8.3-3.8.5) will each vanish because θ_K is an isentrope. The integral $\int_{\theta_s}^{\theta_K} \frac{\partial p}{\partial \theta}\,\theta\, d\theta$ is represented by $\Delta p\,\bar{\theta}^{\theta}$. $\bar{\theta}^{\theta}$ is used as the mean potential temperature of a <u>layer</u> since θ is defined at the boundaries of the layer. Using the same approximation consistent with (3.5.7), a prognostic equation for $\Delta p\,\bar{\theta}^{\theta}$ results:

$$\frac{\partial}{\partial t}\Delta p\,\bar{\theta}^{\theta} + \delta_x\left(\overline{\Delta p u}^{x}\,\overline{\bar{\theta}^{\theta}}^{x}\right) + \delta_y\left(\overline{\Delta p v}^{y}\,\overline{\bar{\theta}^{\theta}}^{y}\right) + \Delta\left(\overline{\left(\frac{\Delta p}{\Delta \theta}\right)}^{\theta}\,\dot{\theta}\,\overline{\bar{\theta}^{\theta}}^{\theta}\right) = \Delta p\,\dot{\bar{\theta}}^{\theta} \qquad (3.8.7)$$

This equation is the quadratically conservative form of the thermodynamic equation. However, it has been found in this equation that the truncation errors introduced by the double vertical average $\overline{\bar{\theta}}^{\theta}$ are significant near the ground where there is large variation of the thickness of the layers. Therefore, $\overline{\bar{\theta}}^{\theta}$, which approximates the value of θ at the

boundary of the layer, is replaced by the exact value θ_K. Thus, equation (3.8.7) becomes:

$$\frac{\partial \Delta p \bar{\theta}^{\theta}}{\partial t} + \delta_x\left(\overline{\Delta p u}^{x}\,\overline{\bar{\theta}^{\theta}}^{x}\right) + \delta_y\left(\overline{\Delta p v}^{y}\,\overline{\bar{\theta}^{\theta}}^{y}\right) + \Delta\left(\left(\overline{\frac{\Delta p}{\Delta\theta}}^{\theta}\dot{\theta}\,\alpha\,\theta\right)\right) = \Delta p\,\overline{\dot{\theta}}^{\theta} \qquad (3.8.8)$$

This is the finite difference form of the thermodynamic equation used in the model. While it is no longer strictly quadratically conservative, the departures from this are not large.

3.9 The Finite Difference Approximation to the Hydrostatic Equation

The finite difference form of the hydrostatic equation (2.7.1) is:

$$\frac{\Delta M}{\Delta\theta} = \overline{\pi}^{\theta} \qquad (3.9.1)$$

This is equivalent to the form:

$$\frac{\Delta\phi}{\Delta\eta} = -\bar{\theta}^{\theta} \qquad (3.9.2)$$

which is the finite difference form of the hydrostatic equation used in deriving the energy equation. In effect (3.9.1) can be rewritten as:

$$\Delta(\phi + \theta\pi)_K = \Delta\theta_K\left(\overline{\pi}^{\theta}\right)_K \qquad (3.9.3)$$

Expanding this:

$$\phi_K - \phi_{K-1} + \theta\pi_K - \theta\pi_{K-1} = (\theta_K - \theta_{K-1})\left(\frac{\pi_K + \pi_{K-1}}{2}\right) \qquad (3.9.4)$$

or

$$\phi_K - \phi_{K-1} = \frac{\theta_K \pi_K}{2} + \frac{\theta_K \pi_{K-1}}{2} - \frac{\theta_{K-1} \pi_K}{2} - \frac{\theta_{K-1} \pi_{K-1}}{2} - \theta \pi_K + \theta \pi_{K-1} \quad (3.9.5)$$

$$= -\frac{\theta_K \pi_K}{2} + \frac{\theta_K \pi_{K-1}}{2} - \frac{\theta_{K-1} \pi_K}{2} + \frac{\theta_{K-1} \pi_{K-1}}{2} \quad (3.9.6)$$

$$= -\frac{\theta_K \pi_K}{2} - \frac{\theta_{K-1} \pi_K}{2} + \frac{\theta_K \pi_{K-1}}{2} + \frac{\theta_{K-1} \pi_{K-1}}{2} \quad (3.9.7)$$

$$= -(\pi_K - \pi_{K-1}) \left(\frac{\theta_K + \theta_{K-1}}{2} \right) \quad (3.9.6)$$

Or

$$\Delta\phi_K = -\Delta\pi_K \left(\bar{\theta}^{\theta} \right)_K \quad (3.9.7)$$

which is equivalent to (3.92).

3.10 Lateral Boundary Conditions

The model is cyclic in the x direction with a period L. The distance L in the model is set to a typical value of the synoptic scale.

As stated in in section 3.5, there is no flux through the northern and southern walls (which are at y=B and y=0 respectively); i.e. the flux $\overline{\Delta pv}^{y}$ vanishes at the walls which are defined between two grid points. This, as previously shown, ensures mass conservation, and that the model remains quadratically conservative.

The Δpv-momentum equation requires further boundary conditions. This is because the gradient $\delta_y \overline{M}^{y}$ cannot be calculated at the y boundary grid points. Since M must be specified out-

side the boundaries, two methods have been tested: the first assumes geostrophic balance in the Δpv equation at the boundary grid points, the second imposes $v\equiv 0$ at the boundary grid points through all time. The first method proved inadequate since after 24 hours standing gravity waves of meridional wavelength $4\Delta y$ manifested themselves and continued to amplify. The second method proved adequate for the two layer version of the model since no signs of gravity waves or nonlinear instability were observed for serval days of integration. For a multilayer version other complications set in. This will be discussed in chapter 6. The setting of $v\equiv 0$ at the two sets of boundary grid points eliminates the calculation of the Δpv momentum equation at the boundaries.

3.11 Numerical Time Scheme

The prognostic equations are integrated using the modified (improved) N-cycle scheme of Lorenz (1971). The basic scheme is an algorithm such that its form repeats itself every N iterations and gives the best results at the end of each N iterations. The form of the basic scheme is:

Let Δt be the time step for every N iterations.

Let δt be the time step for each iteration. ($\Delta t = N\delta t$)

Let y be the field(s) with time derivative(s) F(y).

Let Δy be the time increment such that for iteration n

$y_{n+1} = \Delta y_n + y_n$.

Then the algorithm with iteration n is:

Step

1 Set $a=0$, $b=\frac{1}{\delta t}$

2 $\Delta y_n=\frac{1}{b}(a\cdot\Delta y_{n-1}+F(y_n))$

3 $y_{n+1}=\Delta y_n+y_n$

4 Replace a by $a-\frac{1}{\Delta t}$ and b by $b-\frac{1}{\Delta t}$

5 For $b>0$ go to step 2, for $b=0$ N-cycle iteration is complete

The modified N-cycle scheme changes the basic algorithm to:

Step

1 Let $a=0$, $b=\frac{1}{\delta t}$

2 $\Delta y_n=\frac{1}{b}(a\cdot\Delta y_{n-1}+F(y_n))$

3 $y_{n+1}=\Delta y_n+y_n$

4 If $a=0$ replace a by $a-\frac{1}{\delta t}$ and b by $b-\frac{1}{\delta t}$. If $a<0$, do nothing.

5 Replace a by $a+\frac{1}{\Delta t}$ and b by $b+\frac{1}{\Delta t}$

6 If $a<0$, return to step 2; if $a=0$, the procedure is completed.

This algorithm modifies the original algorithm such that the basic scheme is used once, an altered scheme is used twice, and the basic scheme is used once again, at the end of which the best results are obtained. The modified scheme allows for better error cancelation and requires little addition work as compared to the basic scheme. In this model N is chosen as 4, which gives the scheme fourth order accuracy. The use of this scheme leads to some difficulties for the intersection of an isentrope with the ground which will be described in section 4.8.

CHAPTER 4

THE TREATMENT OF THE INTERSECTION OF AN ISENTROPIC SURFACE WITH THE GROUND

4.1 Introduction

The possibility that one or more isentropic surfaces may intersect the ground has been a major difficulty of isentropic coordinate models. Several techniques to solve this problem have been developed by Eliassen and others.

A modification of the method developed by Eliassen and Hellevik (1975) is used in the present model. The surface of θ_1 (or any isentropic surface θ_K which intersects the ground) is assumed to continue below the ground, and other associated variables are either interpolated or extrapolated in such a way as to preserve some of the properties stated in the previous chapter.

The layer number corresponding to the lowest layer still above the ground at a given point shall be denoted by ν. Any layer or level above the ground (with an index greater than or equal to ν) will be an active layer or level. Others will be considered inactive.

Eliassen and Hellevik define extraordinary points as all those points which satisfy:

$p_s - p_H < 2000$ Pascals (20 mb) or $\theta_H - \theta_s < 1^\circ K$

All other points are defined as ordinary.

In the present model the following cases are distinguished:

1) An isentrope is just above the ground.

2) An isentrope goes below the ground.

3) An isentrope rises above the ground.

4) An isentrope remains below the ground.

5) None of the above cases apply (ordinary case).

The treatment of the variables in these cases requires separate criteria and formulations.

4.2 Case 1: An isentrope is just above the ground

Due to the fact that both Δp_v and $\Delta p\bar{\theta}^{\theta}$ indicate the spacing of θ_s and θ_v, it is necessary to choose one of these variables as the correct one when the isentrope θ_v is near θ_s, specifically when $0° < \theta_v - \theta_s < 1°K$ or $0 < p_s - p_v < 1000$ Pascals. This is required since $\Delta p\bar{\theta}^{\theta}$ and Δp_v are subjected to large relative truncation errors (i.e. $\Delta t \cdot \frac{\partial \Delta p}{\partial t}$ is of the same order or larger than Δp). The variable Δp is chosen as the reliable variable since $\Delta p\bar{\theta}^{\theta}$ is a composite variable of Δp and is no more accurate than Δp. Thus, θ_s must be extrapolated to make $\Delta p\bar{\theta}^{\theta}$ consistent with Δp. θ_s is extrapolated in the vertical by:

$$\theta_s = \theta_v - (\theta_{v+1} - \theta_v) \cdot (p_s - p_v) / (p_v - p_{v+1}) \qquad (4.2.1)$$

In addition Δpu and Δpv suffer the same difficulties as $\Delta p\bar{\theta}^{\theta}$. Thus, u (and similarly for v) is extrapolated in the horizontal by:

$$u_v = \frac{\Sigma \Delta p u_v}{\Sigma \Delta p_v} \qquad (4.2.2)$$

The summations are performed for those points in the immediate vicinity of u_v (points with horizontal indices that differ by less than 2 from the horizontal indices of u_v). Only those points which are poleward of $\theta_v = \theta_s$ and which are well defined (points which are ordinary or have been extrapolated) are used. The variables $\bar{\theta}^{\theta}$, $\Delta p \bar{\theta}^{\theta}$, $\Delta p u$ and $\Delta p v$ must be redefined accordingly after these formulas have been used.

4.3 Case 2: An isentrope goes below the ground

For the reasons stated in the previous section, Δp_v becoming negative is used to determine when θ_v becomes less than θ_s. This requires θ_s to be interpolated in the vertical by:

$$\theta_s = \theta_k - \left(\frac{p_s - p_k}{p_k - p_{k+1}} \right) \cdot (\theta_{k+1} - \theta_k) \qquad (4.3.1)$$

The subscript k refers to the level which just submerged. The value of v must be increased by one, and the new fields of Δp_v, $\Delta p \bar{\theta}^{\theta}$, $\Delta p u_v$, and $\Delta p v_v$ must be redefined by:

$$\Delta p_v = p_s - p_{v_{new}} = p_s - p_{v_{old}+1} \qquad (4.3.2)$$

$$\Delta p \bar{\theta}^{\theta} = \Delta p_{v_{new}} \cdot \bar{\theta}^{\theta}_{new} = (p_s - p_{v_{new}}) \cdot \left(\frac{\theta_{s_{new}} + \theta_{v_{new}}}{2} \right) \qquad (4.3.3)$$

$$\Delta p u_v = \Delta p_{v_{new}} \cdot u_{v_{new}} = (p_s - p_{v_{new}}) \cdot u_{v_{new}} \qquad (4.3.4)$$

$$\Delta PV_r = \Delta P_{r_{new}} \cdot V_{r_{new}} = (P_s - P_{r_{new}}) \cdot V_{r_{new}} \qquad (4.3.5)$$

The winds at the layer that submerged are extrapolated as in case 4 (section 4.6). The value of $\Delta P_{r_{old}}$ is left unchanged, and $\Delta PU_{r_{old}}$ and $\Delta PV_{r_{old}}$ are adjusted accordingly.

4.4 Case 3: An Isentrope Rises Above the Ground

An isentrope, θ_K, is defined to rise above the ground when the value of θ_S becomes less than θ_K. Because the variables associated with θ_K have been inactive, they must be interpolated or extrapolated and appropiate adjustments must be made. The pressure p_k is interpolated by:

$$P_k = P_{K+1} + \left(\frac{\theta_{K+1} - \theta_K}{\theta_{K+1} - \theta_S}\right)(P_s - P_{K+1}) \qquad (4.4.1)$$

The values of u_k and v_k are extrapolated as for case 1. The values of ΔP_K, ΔP_{K+1}, $\Delta P\bar{\theta}^{\theta}$, ΔPU_K, ΔPU_{K+1}, ΔPV_K and ΔPV_{K+1} must all be readjusted by:

$$\Delta P_K = P_s - P_K \qquad (4.4.2)$$

$$\Delta P_{K+1} = P_K - P_{K+1} \qquad (4.4.3)$$

$$\Delta P\bar{\theta}^{\theta} = (P_s - P_K) \cdot \left(\frac{\theta_K + \theta_S}{2}\right) \qquad (4.4.4)$$

$$\Delta PU_K = (P_s - P_K) \cdot U_K \qquad (4.4.5)$$

$$\Delta\rho\, u_{k+1} = (\rho_k - \rho_{k+1}) \cdot u_{k+1} \qquad (4.4.6)$$

and similar formulas for $\Delta\rho v_k$ and $\Delta\rho v_{k+1}$.
Subsequent values of these variables are determined in ordinary fashion. Note that ν must be decreased by one, and that in (4.4.5) both $\Delta\rho_k$ and u_k have been redefined.

4.5 Case 4: Treatment of the Pressure below the Ground

At each point where $\vartheta_s > \theta_k$ at the present as well as at the previous time step, the pressure for θ_k is horizontally extrapolated following Eliassen and Hellevik (1975). The procedure is to extrapolate the pressure by:

$$\rho_k = \rho_s + \bar{r}\,(\theta_s - \theta_k) \qquad (4.5.1)$$

where $\bar{r}$ is the arithmetic mean of:

$$r = \frac{\rho_k - \rho_s}{\theta_k - \theta_s} \qquad (4.5.2)$$

for all points in the immediate vicinity of p_k.
The points cover both sides of the intersection, but these must be well defined with each p_k ordinary or previously extrapolated. Once p_k is calculated, $\Delta\rho_k$ is updated. Note that $\Delta\rho_k$ is negative since $\Delta\rho_k = \rho_s - \rho_k$ at all times. All points below the ground are extrapolated, but only those which are contiguous to the intersection are ever used in flux calculations.

4.6 Treatment of the Fluxes Associated with the Intersection and the Extrapolation of u and v below the Ground

One of the most important characteristics of the model is that it conserves mass. The method for maintaining mass conservation when dealing with an intersecting isentrope may be seen by starting with the continuity equation (3.4.6). Consider the mass fluxes in the x direction near the intersection of θ_1 and θ_3 (figure 4.1) with cold air to the right. As indicated by figure 4.2, fluxes coming out of (or going into) a box are computed as horizontal averages of fluxes defined between the same vertical boundaries as the box. Thus, for this case the continuity equation will have the following forms for points near the intersection:

$$\left(\frac{\partial \Delta p}{\partial t}\right)_{2A} = \left(\frac{\partial (p_3 - p_2)}{\partial t}\right)_A = - \frac{\Delta \rho u_{2B'} - \Delta \rho u_{2C}}{\Delta x} \qquad (4.6.1)$$

$$\left(\frac{\partial \Delta p}{\partial t}\right)_{2D} = \left(\frac{\partial (p_1 - p_2)}{\partial t}\right)_D = - \frac{\Delta \rho u_{2F} - \Delta \rho u_{2B''}}{\Delta x} \qquad (4.6.2)$$

$$\left(\frac{\partial \Delta p}{\partial t}\right)_{1D} = \left(\frac{\partial (p_3 - p_1)}{\partial t}\right)_D = - \frac{\Delta \rho u_{1F} - \Delta \rho u_{1B}}{\Delta x} \qquad (4.6.3)$$

where the fluxes $\Delta \rho u_{2C}$, $\Delta \rho u_{2F}$, and $\Delta \rho u_{1F}$ have their usual definitions, and $\Delta \rho u_{2B'}$, $\Delta \rho u_{2B''}$, and $\Delta \rho u_{1B}$ are:

$$\Delta \rho u_{2B'} = \frac{[(p_3 - p_1) u_1 + (p_1 - p_2) u_2]_D + [(p_3 - p_2) u_2]_A}{2} \qquad (4.6.4)$$

$$\Delta\rho u_{2B''} = \frac{[(\rho_1-\rho_2)u_2]_0 + [(\rho_3-\rho_2)u_2 - (\rho_3-\rho_1)u_1]_A}{2} \qquad (4.6.5)$$

$$\Delta\rho u_{1B} = \frac{[(\rho_3-\rho_1)u_1]_0 + [(\rho_3-\rho_1)u_1]_A}{2} \qquad (4.5.6)$$

By defining the mass fluxes in the above manner, mass is conserved since $\Delta\rho u_{2B'} = \Delta\rho u_{2B''} + \Delta\rho u_{1B}$. The value of u_1 at A can be arbitrarily specified, and mass will still be conserved. It will be shown that the choice $u_1=u_2$ at A will also ensure the conservation of momentum. Thus, making this choice $\Delta\rho u_{2B''}$ may be written as:

$$\Delta\rho u_{2B''} = \frac{[(\rho_1-\rho_2)u_2]_0 + [(\rho_1-\rho_2)u_2]_A}{2} \qquad (4.6.7)$$

The same flux calculation and wind extrapolation procedure is applied to the Δpv term as well.

Following the same procedure, the form of the $(\overline{\Delta\rho u}^x \overline{u}^x)$ fluxes in the Δpu momentum equation can also be determined. Again viewing figures 4.1 and 4.2 and considering only the $(\overline{\Delta\rho u}^x \overline{u}^x)$ term of the Δpu momentum equation (3.5.1), the equations have the following form:

$$\frac{\partial}{\partial t}[(\rho_3-\rho_2)u_2]_A = -\frac{(\overline{\Delta\rho u}^x \overline{u}^x)_{2B'} - (\overline{\Delta\rho u}^x \overline{u}^x)_{2C}}{\Delta x} \qquad (4.6.8)$$

$$\frac{\partial}{\partial t}[(\rho_1-\rho_2)u_2]_0 = -\frac{(\overline{\Delta\rho u}^x \overline{u}^x)_{2F} - (\overline{\Delta\rho u}^x \overline{u}^x)_{2B''}}{\Delta x} \qquad (4.6.9)$$

$$\frac{\partial}{\partial t}\left[(\rho_s-\rho_1)u_1\right]_0 = -\frac{(\overline{\Delta\rho u}^x\,\bar{u}^x)_{1F}-(\overline{\Delta\rho u}^x\,\bar{u}^x)_{1B}}{\Delta x} \qquad (4.6.10)$$

where the momentum fluxes at 2C, 2F, and 1F have their usual

and at 2B", 1B, and 2B' are:

$$(\overline{\Delta\rho u}^x\,\bar{u}^x)_{2B''} = \frac{\{[(\rho_1-\rho_2)u_2]_0+[(\rho_1-\rho_2)u_2]_A\}(u_{20}+u_{2A})}{4} \qquad (4.6.11)$$

$$(\overline{\Delta\rho u}^x\,\bar{u}^x)_{1B} = \frac{\{[(\rho_s-\rho_1)u_1]_0+[(\rho_s-\rho_1)u_1]_A\}(u_{10}+u_{1A})}{4} \qquad (4.6.12)$$

$$(\overline{\Delta\rho u}^x\,\bar{u}^x)_{2B'} = \frac{\{[(\rho_s-\rho_1)u_1]_0+[(\rho_s-\rho_1)u_1]_A\}(u_{10}+u_{1A})}{4} + \frac{\{[(\rho_1-\rho_2)u_2]_0+[(\rho_1-\rho_2)u_2]_A\}(u_{20}+u_{2A})}{4} \qquad (4.6.13)$$

It can be seen that by setting $u_{1A}=u_{2A}$, the momentum fluxes are consistent with the mass fluxes for the continuity equation. Again, this procedure is applied to the $(\overline{\Delta\rho v}^y\,\bar{u}^y)$ terms for the Δpu momentum equation. The same general procedure is also applied to the Δpv momentum equation.

The thermodynamic equation has similar forms for the heat fluxes. Viewing the $(\overline{\Delta\rho u}^x\,\overline{\bar{\theta}^\theta}^x)$ term, for figures 4.1 and 4.2 the equations are:

$$\frac{\partial}{\partial t}\left[(\rho_s-\rho_2)\bar{\theta}_2^\theta\right]_A = -\frac{(\overline{\Delta\rho u}^x\,\overline{\bar{\theta}^\theta}^x)_{2B'}-(\overline{\Delta\rho u}^x\,\overline{\bar{\theta}^\theta}^x)_{2C}}{\Delta x} \qquad (4.6.14)$$

$$\frac{\partial}{\partial t}\left[(\rho_1-\rho_2)\bar{\theta}_2^{\theta}\right]_0 = -\frac{(\overline{\Delta\rho u}^x\,\overline{\bar{\theta}^{\theta}}^x)_{2F} - (\overline{\Delta\rho u}^x\,\overline{\bar{\theta}^{\theta}}^x)_{2B''}}{\Delta x} \qquad (4.6.15)$$

$$\frac{\partial}{\partial t}\left[(\rho_s-\rho_1)\bar{\theta}_1^{\theta}\right]_0 = -\frac{(\overline{\Delta\rho u}^x\,\overline{\bar{\theta}^{\theta}}^x)_{1F} - (\overline{\Delta\rho u}^x\,\overline{\bar{\theta}^{\theta}}^x)_{1B}}{\Delta x} \qquad (4.6.16)$$

where the heat fluxes at 2C, 2F, and 1F follow the usual form and at 2B", 1B, and 2B' are:

$$(\overline{\Delta\rho u}^x\,\overline{\bar{\theta}^{\theta}}^x)_{2B''} = \frac{\{[(\rho_1-\rho_2)u_2]_0 + [(\rho_1-\rho_2)u_2]_A\}\{[(\theta_1+\theta_2)/2]_0 + [(\theta_1+\theta_2)/2]_A\}}{4} \qquad (4.6.17)$$

$$(\overline{\Delta\rho u}^x\,\overline{\bar{\theta}^{\theta}}^x)_{1B} = \frac{\{[(\rho_s-\rho_1)u_1]_0 + [(\rho_s-\rho_1)u_1]_A\}\{[(\theta_s+\theta_1)/2]_0 + [(\theta_s+\theta_1)/2]_A\}}{4} \qquad (4.6.18)$$

$$(\overline{\Delta\rho u}^x\,\overline{\bar{\theta}^{\theta}}^x)_{2B'} = \frac{\{[(\rho_1-\rho_2)u_2]_0 + [(\rho_1-\rho_2)u_2]_A\}\{[(\theta_1+\theta_2)/2]_0 + [(\theta_1+\theta_2)/2]_A\}}{4}$$

$$+ \frac{\{[(\rho_s-\rho_1)u_1]_0 + [(\rho_s-\rho_1)u_1]_A\}\{[(\theta_s+\theta_1)/2]_0 + [(\theta_s+\theta_1)/2]_A\}}{4} \qquad (4.6.19)$$

Note that since $\theta_{1A} = \theta_{10} \equiv \theta_1$, then $\frac{\partial\bar{\theta}_2^{\theta}}{\partial t} \equiv 0$ for $\theta_1 > \theta_s$ (i.e. the mean potential temperature of a layer above the ground surface does not change). The fields $\bar{\theta}^{\theta}$ (the mean potential temperature of the lowest layer) and $\Delta\rho\bar{\theta}^{\theta}$ are discontinuous accross an intersecting isentrope since θ_v changes. This, however, does not affect the calculation of $\Delta\rho\bar{\theta}^{\theta}$ in any way.

4.7 Treatment of other Discontinuites in Space

The only other variable affected by the intersection of

$\theta = \theta_s$ is $M=\phi+\theta\pi$. The variables p_s, θ_s, and π_s are unaffected by the intersection. In the gradient term $\delta_x \overline{\overline{M}}^{\theta^x}$ of the Δpu momentum equation the values of $\overline{\overline{M}}^{\theta^x}$ near an intersection are computed in the following manner (see figures 4.1 and 4.2):

$$\overline{\overline{M}}^{\theta^x}_{2B''} = \frac{1}{2}\left[\left(\frac{M_2+M_1}{2}\right)_D + \left(\frac{M_2+M_1}{2}\right)_A\right] \qquad (4.7.1)$$

$$\overline{\overline{M}}^{\theta^x}_{1B} = \frac{1}{2}\left[\left(\frac{M_1+M_s}{2}\right)_D + \left(\frac{M_1+M_s}{2}\right)_A\right] \qquad (4.7.2)$$

$$\overline{\overline{M}}^{\theta^x}_{2B'} = \frac{1}{2}\left[\left(\frac{M_2+M_s}{2}\right)_D + \left(\frac{M_2+M_s}{2}\right)_A\right] \qquad (4.7.3)$$

The averages away from the intersection have their usual meaning. The same procedure applies to the $\overline{\overline{M}}^{\theta^y}$ calculations for the Δpv momentum equation. The values of M below the ground are obtained by using the hydrostatic equation and the values of θ and π defined in their usual manner.

4.8 Treatment of Discontinuites in Time

A time scheme of the form:

for each time step n

$$\begin{cases} \Delta y_n = F(\Delta y_{n-1}, y'(y_{n-1})) \\ y_n = y_{n-1} + \Delta y_n \end{cases}$$

where F is the scheme function

$y'(y)$ is the time derivative

will be referred as a multi-time level scheme. The N-cycle

scheme used in the present model and the Adams-Bashfort method are examples of this type of scheme. Whenever interpolations or extrapolations are performed altering time dependent fields, y_n, in the model (such as θ_s and p_s), the time increment, Δy_n, must be adjusted to be consistent with the altered fields. In some cases the layers or levels involved have been altered or the time increment did not exist at the previous time step (case 3). This problem is solved by taking the value, y_{n-1}, from the previous time step and subtracting it from the modified value, y_n, for the present time step. This difference is the new value of the time increment, Δy_n. Cases 1, 2, and 3 require this procedure. See appendix for a list of the necessary modifications.

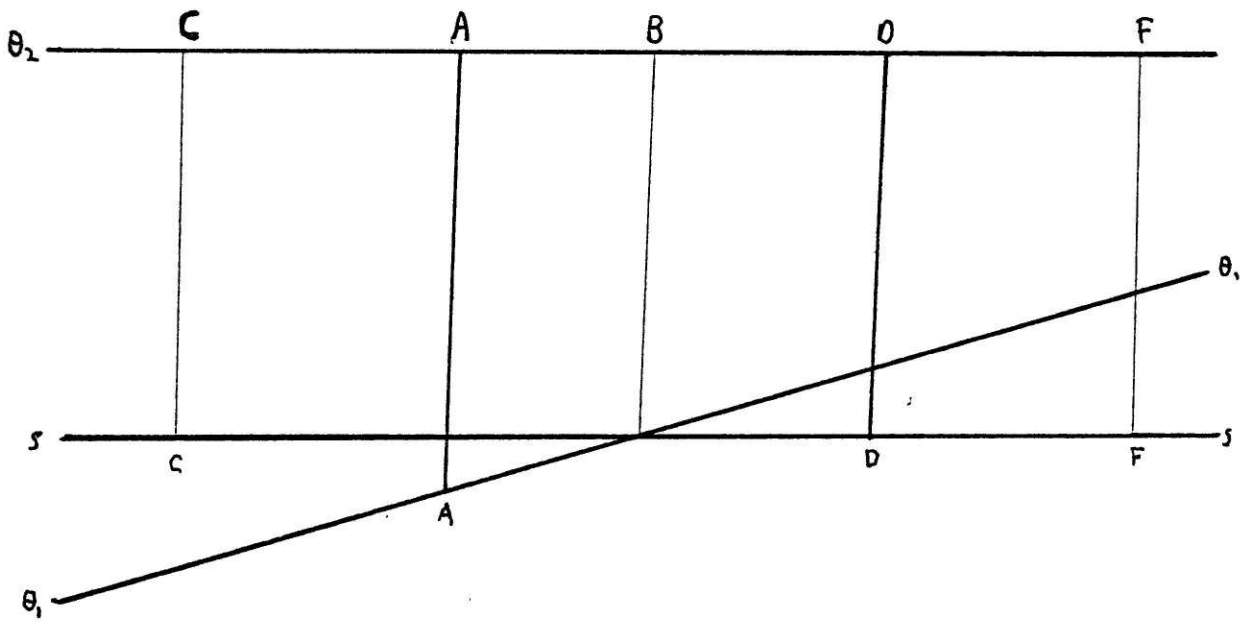

Figure 4.1 Diagram of intersecting isentrope with grid points A and D, and "box walls" at C, B, and F.

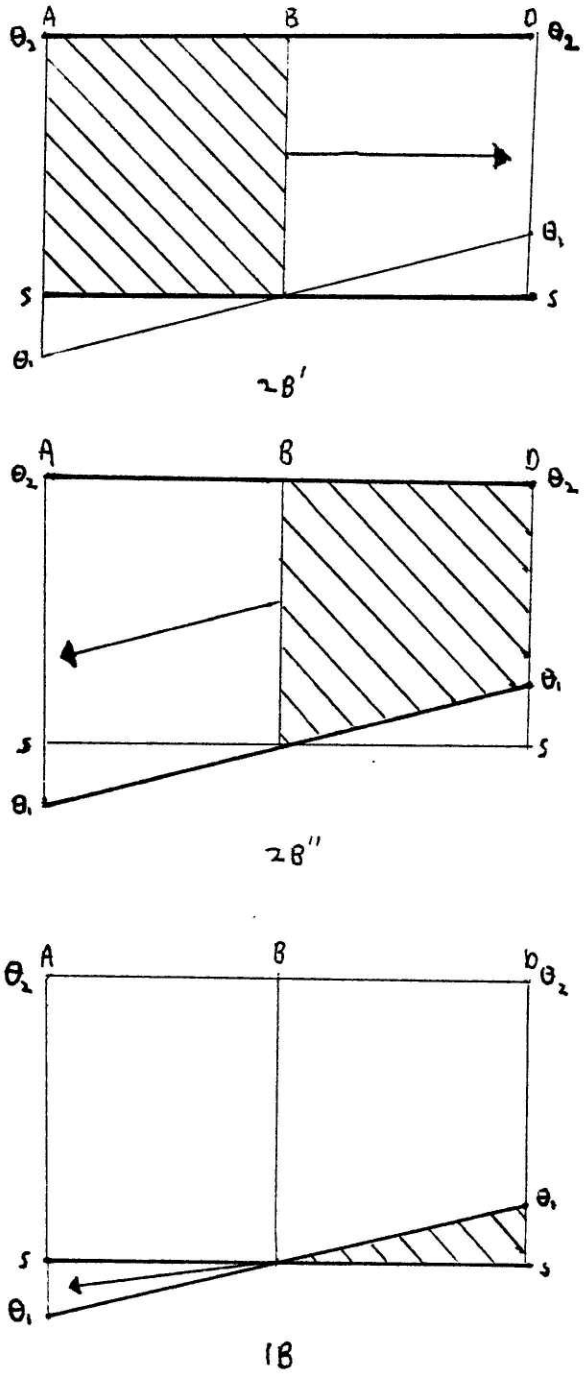

Figure 4.2 Schematic of the computation of the horizontal fluxes coming out of a box (shaded) near the intersection. Bold lines indicate vertical boundaries.

CHAPTER 5

FILTERING, VERTICAL DIFFUSION, AND HEATING

5.1 Filtering

To reduce energy build-up in the small waves (wavelength $\lesssim 3\Delta y$), the pressure and potential temperature fields at the ground are filtered every four time steps, at the time in which the model output is most accurate (see section 3.11). The filter used is a high order filter (Shapiro, 1970 and Kálnay-Rivas, 1977a). The form of the filter is:

$$\overline{g} = \{1 - (h_x^2)^8\}\{1 - (h_y^2)^8\} g \qquad (5.1.1)$$

where

$$h_x^2 (g_{ij}) = (g_{i+1,j} - 2g_{ij} + g_{i-1,j})/4 \qquad (5.1.2)$$

$$h_y^2 (g_{ij}) = (g_{i,j+1} - 2g_{ij} + g_{i,j-1})/4 \qquad (5.1.3)$$

The order of the filter in the y direction is reduced near the y boundaries: $(1-h_y^2)$ is applied one grid point away from the boundaries, $(1+(h_y^2)^2)$ is applied two grid points away, etc. Except for the high order filter, there is no horizontal diffusion. As shown by Kálnay-Rivas (1977b), the use of this filter on an energy conserving model replaces sucessfully the use of an enstrophy conserving scheme.

5.2 Vertical Diffusion of Momentum

Turbulent diffusion cannot be neglected in a long numerical

integration of an atmospheric model. Turbulent diffusion of momentum in the vertical has been included using the simple parameterization originally developed by Palmén (1955). In the Δpu momentum equation the friction term is computed as:

$$F_{x_k} = \left(\frac{\partial \tau_x}{\partial z}\right)_k \approx \frac{\Delta \tau_{x_k}}{\Delta z_k} \qquad (5.2.1)$$

where the internal stress between two layers is defined by:

$$\tau_{x_k} = \mu \frac{\partial u}{\partial z} \approx \mu \frac{u_{k+1} - u_k}{\left(\frac{z_{k+1}+z_k}{2}\right) - \left(\frac{z_k + z_{k-1}}{2}\right)} \qquad (5.2.2)$$

where μ is the coefficent of eddy viscosity. The stress at the ground is given by:

$$\tau_{x_s} = -c_D \rho \sqrt{u_v^2 + v_v^2}\, u_v \qquad (5.2.3)$$

where C_D is the drag coefficent. Similar formulas hold for the Δpv momentum equation.

5.3 Heating and Vertical Diffusion of Heat

Contrary to previous models, the diabatic terms in the various equations are included. This allows the model to be forced so that time integrations can be carried out beyond the three or four days of adiabatic runs. The diabatic terms require the specification of $\dot{\theta}$. In this model $\dot{\theta}$ is determined by newtonian cooling and diffusion and has the form:

$$\dot{\theta}_k = \frac{c_p (T_e - T_k)}{\pi_k \tau} + \frac{\Delta H_k}{\left(\frac{z_{k+1}+z_k}{2}\right) - \left(\frac{z_k + z_{k-1}}{2}\right)} \qquad (5.3.1)$$

where T_k is the actual temperature at level k.

T_e is the equilibrium temperature at level k.

where τ is the radiative relaxation time constant

H_k is given by:

$$H_k = \mu \frac{\Delta \theta_k}{\Delta z_k} \qquad (5.3.2)$$

The value of T_k is $\theta_k \pi_k / c_p$. τ has a value of around 18 days. The equilibrium temperature, T_e, in the two layer is specified in a manner similar to Roads (1977). First the equilibrium temperature at the ground, T_G, is defined by:

$$T_G = T_o + \left\langle \overline{\frac{\partial T_G}{\partial y}} \right\rangle \left(\frac{3y^2}{B} - \frac{2y^3}{B^2} \right) \qquad (5.3.3)$$

where T_o is the ground temperature at y=0

$\left\langle \overline{\frac{\partial T_G}{\partial y}} \right\rangle$ is the equilibrium ground temperature gradient between y=0 and y=B.

$\frac{\partial T_G}{\partial y}$ vanishes at y=0 and y=B and is maximum at $y=\frac{B}{2}$. The value of T_e at higher levels is determined by:

$$T_e = T_G + \left\langle \overline{\frac{\partial T_e}{\partial z}} \right\rangle \cdot Z \qquad (5.3.4)$$

where $\left\langle \overline{\frac{\partial T_e}{\partial z}} \right\rangle$ is the vertical equilibrium temperature gradient This is allowed to vary linearly witn y by:

$$\left\langle \overline{\frac{\partial T_e}{\partial z}} \right\rangle = \gamma_o + \left\langle \overline{\frac{\partial \gamma}{\partial y}} \right\rangle y \qquad (5.3.5)$$

where γ_o is the vertical equilibrium temperature gradient at y=0. and $\left\langle \overline{\frac{\partial \gamma}{\partial y}} \right\rangle$ is the y gradient of the vertical equilibrium temperature gradient. This allows for heating in the southern boundary and cooling at the northern boundary while maintaining a proper density stratification.

CHAPTER 6

INTEGRATION EXPERIMENTS

6.1 Introduction

Five runs (experiments) with the two layer version of the model are presented here. The first three can be compared with the Eliassen and Raustein (1968) model. The first run is adiabatic with no high order filtering and no vertical diffusion. The second run includes filtering, and the third run includes both filtering and vertical diffusion. All three have the isentrope nearest the ground set to 290°K. The fourth run is identical to the first run, except that the isentrope nearest the ground is set to 315°K. This is sufficently large to prevent any intersection of this isentrope with the ground. The fifth run is diabatic with filtering, vertical diffusion, and a 315°K isentrope. For each run and for each day where useful the fields of surface pressure, p_s, surface potential temperature, θ_s, and upper layer Montgomery potential, $\overline{M_2}^{\theta}$, are presented. The interpretation of these fields is shown in figure 6.6.1.

6.2 Initial Conditions and Model Constants for Puns 1,2, and 3

The initial conditions have the same form as Eliassen and Raustein (1968). The pressure and potential temperature at the ground are determined by:

$$p_s = \overline{p_s} - \Delta p_s \left(\tanh^2 2 - \tanh^2 \left[4 \left(\frac{y}{\beta} - \frac{1}{2} \right) \right] \right) \sin \left(2\pi \frac{x}{L} \right) \qquad (6,2,1)$$

$$\theta_s = \overline{\theta}_s - \Delta\theta_s \tanh\left[2\left(\frac{y}{B}-\frac{1}{2}\right)\right] / \tanh 1 \qquad (6.2.2)$$

where $\overline{p}_s$, $\overline{\theta}_s$, Δp_s, $\Delta\theta_s$ are constants

The constant tanh 1 was not in the original Eliassen and Raustein formula but is included as a normalizing constant since the Eliassen and Raustein results show that without the constant, the resulting field does not conform to their θ_s field. The value of the Exner function, π , for the middle isentrope is determined by linear interpolation since it is known at the top and at the ground. Thus, π_1 is given by:

$$\pi_1 = (\pi_s - \pi_2)\,\frac{\theta_2-\theta_1}{\theta_2-\theta_s} + \pi_2 \qquad (6.2.3)$$

The wind components are determined by geostrophic balence, and since p_s, θ_s, and π are specified, all other variables are directly determined.

The values of the parameters and constants used in runs 1, 2, and 3 are:

θ_1=290°k	$p_2=2\times10^4$ Pascals
θ_2=350°K	$p_s=10^5$ Pascals
$\overline{\theta}_s$=285°K	$p_s=3\times10^3$ Pascals
$\Delta\theta_s$=20°K	R=287 Joules kg^{-1}
g=9.8 m s^{-2}	C_p=1003 Joules kg^{-1}
$f_o=.913\times10^{-4}$ s^{-1}	μ=20 m^2 s^{-1}
$\beta=3.67\times10^{-12}$ m^{-1} s^{-1}	$C_D=1.0\times10^{-3}$ kg m^2
$L=8\times10^6$ m	$\Delta x=4\times10^5$ m
$B=5.6\times10^6$ m	$\Delta y=4\times10^5$ m

δt=integration time step=10 min.

The initial fields of the pressure at the ground, p_s, the potential temperature at the ground, θ_s, and the layer average Montgomery potential, $\overline{M}_2^{\theta}$ for runs 1-3 are shown in figures 6.0.1-6.0.3 respectively.

6.3 Run 1: Adiabatic, Unfiltered, with no Vertical Diffusion, Using an Intersecting Isentrope

Figures 6.1.1-6.1.3 show the resulting fields of p_s, θ_s, and $\overline{M}_1^{\theta}$ after one day of model time. Despite the fact that no filtering or diffusion is used, the fields remain quite smooth. When compared to the results of Eliassen and Paustein (1968), the fields are not as well developed. This can be expected from the fact that the present model uses winds defined at only two layers, whereas Eliassen and Raustein use three levels of winds. Thus, better information on the developement of the low and front will be obtained by the Eliassen and Raustein model.

After two days the fields shown in figures 6.1.4-6.1.6 remain generally quite smooth. The abruptness of the Montgomery potential is caused by the sudden change of slope between the ground and the isentrope. Comparing these results to the Eliassen and Raustein results with linear diffusion after 48 hours, the results are quite similar. Here even the general intensites are the same.

After three days short waves manifest themselves in both the surface pressure and potential temperature fields as can be

seen in figures 6.1.7 and 6.1.8. The resulting Montgomery potential field as shown in figure 6.1.9 is extremely noisy as it depends on both f these fields. When compared to the nonlinear diffusion run of Eliassen and Raustein, the fields are about the same, except that the low is more intense than in Eliassen and Raustein. This is to be expected from the lack of filtering or vertical diffusion. Figure 6.1.10 shows the surface pressure field after four days. It is clear that the short waves are unacceptably large and must be suppressed for futher integration.

For comparison it should be noted that Eliassen and Raustein had integration breakdown after 32 hours with no diffusion and 56 hours with linear diffusion. The present model can be integrated to 72 hours without serious error with no filtering or diffusion.

6.4 Run 2: Adiabatic with a High Order Filter

The first two days with filtering were nearly identical to those without filtering and are not shown. After three days of integration figures 6.2.1-6.2.3 show somewhat smoother fields as compared with figures 6.1.7-6.1.9. The short waves have been smoothed out, but it can be seen that the warm front is unrealistically strong. The difficulty of an excessively strong warm front has been observed in all past isentropic models. A sharp kink just south of the warm front and in reality associated with the intersecting isentrope can also be seen. Figures 6.2.4-

6.2.6 show that after four days the warm front and kink have become unacceptably sharp. Shortly after this, excessive winds developed along the southern boundary due to the squeezing of the air by the 290°K isentrope colliding with the southern boundary. This indicates the necessity of including friction.

6.5 Run 3: Adiabatic with Filtering and Vertical Diffusion

Figures 6.3.1-6.3.3 show that after one day with vertical diffusion the low and high are somewhat less developed. Figures 6.3.4-6.3.12 show the same tendency. The winds near the southern boundary are reduced enough so that integration can continue to five days (figures 6.3.13-6.3.15). Integration could be continued beyond five days, but the results were not realistic in that pockets of cold and warm air began to show. The results seem reasonable for five days, except that the excessively sharp warm front and the sharp kink south of the front were not greatly reduced. In the next section it will be shown that the presence of the sharp kink is due to the intersection of the isentrope with the ground.

6.6 Run 4: Adiabatic, Unfiltered, with no Vertical Diffusion and no Intersecting Isentrope

Run 4 is identical to run 1, except that the presence of an intersecting isentrope is avoided by defining $\theta_1 = 315°K$ which is too warm to intersect the ground. Figure 6.4.1 shows the slightly modified initial Montgomery potential field for the upper

layer.

Figures 6.4.2-6.4.7 show the results of the numerical integration after one, two, and three days. The first two days are quite similar to those of run 1, except that the low and the high are shallower. For three days the main differences are that the fields remain smoother and that the spurious kink south of the warm front is not present. Figures 6.4.8-6.4.10 show that after four days, short waves become apparent. The excessively strong warm front is still present.

This run indicates that the treatment of the intersection of the isentrope and the ground needs futher improvement in this model. The appearence of the spurious kink south of the intersecting isentrope after two or three days could probably be alleviated by a more frequent application of the high order Shapiro filter (it was applied only once every 2 2/3 hours), and by applying it also to the wind field (it was only applied to the pressure and potential temperature fields at the ground). The fact that two or three days are required to see the kink suggests the problem is not a basic one with the model but can be corrected with minor modifications.

6.7 Run 5: Diabatic with Filtering and Vertical Diffusion

In this run the same non-intersecting isentrope is chosen as in the previous section because for the two layer model the heating is not properly calculated with an intersecting isentrope. This is because the model forecasts the product of the pressure thickness of the lower layer, Δp_L, times the mean

potential temperature of the lower layer, $\bar{\theta}^{\theta}$. Therefore, heating appears in two terms: the first, $\Delta(\overline{(\frac{\Delta p}{\Delta \theta})^{\theta}}\dot{\theta}\prec\theta)$, represents basically the loss of mass of the lower layer that occurs when it is warmed. The second, $\Delta p\,\overline{\dot{\theta}}^{\theta}$, represents the increase in temperature of the layer due to heating. For a two layer model the first term is an order of magnitude larger than the second. Since the first term does not appear south of the intersection of an isentrope with the ground, the heating that occurs will apply to the entire top to bottom layer. Thus, the effective warming at the ground will be misrepresented. Better specification of the heating could be achieved by increasing the vertical resolution or modifying the finite difference form of the diabatic terms.

The parameterization of radiative heating was introduced into the model, as indicated in section 5.3, in the form of newtonian cooling. The constants determining the radiative equilibrium temperature are (c.f. section 5.3):

$T_o = 310\,°K$

$\langle \frac{\partial T_s}{\partial y} \rangle = -8.035714 \times 10^{-6}\ °K\ m^{-1}$

$\gamma_0 = -7.0 \times 10^{-3}\ °K\ m^{-1}$

$\langle \overline{\frac{\partial \gamma}{\partial y}} \rangle = 6.25 \times 10^{-10}\ °K\ m^{-2} = 3.5\ °K/km/B$

$\tau = 1.6 \times 10^{6}\ s \approx 18$ days

While this specifies an overly stable lapse rate compared with the atmosphere, the fact that no tropopause exists for the model and that only two layers are used requires such a lapse rate to be imposed for realistic heating and cooling.

Days two, four, and six are shown in figures 6.5.1-6.5.9. It can be seen that the low and high are becoming weaker, and that by the sixth day occlusion has nearly completed. It should be noted that the low is a warm core low rather than the cold core low found in the atmosphere. This tendency to generate warm core lows has been observed in all previous isentropic coordinate models without heating. This tendency can be observed even in the numerical forecasts starting with observed initial data performed by Bleck (1974). The present results suggest that this difficulty still occurs when radiative heating and cooling are included.

The secondary wave that is observed on the cold front by the fourth day developes very quickly, and by the seventh day the second low is stronger than the first one. The cyclogenesis continues, and by the tenth day the first low has nearly vanished and the low is extremely strong (with a pressure center of 97.6 kPa.).and has drifted north. After 13 days the numerical integration breaks down at which time strong winds develope near the northern boundary, and the layer pressure thickness becomes excessively small. This problem seems related to the boundary conditions ($v=0$ at two contiguous grid points) and not to the numerical scheme itself.

6.8 Other Numerical Experiments

A numerical integration with the heating function increased by reducing the relaxation time constant to 1.5 days was integrated for 40 days with realistic results at which time strong

winds of 50 m s^{-1} were starting to build up near the northern boundary, and the integration was discontinued.

A multilayer version of the model was developed. The results were similar to those of Eliassen and Raustein (1970). However, the integration was not continued beyond four days because of the same difficultes near the boundaries listed in the previous section were already apparent at this time.

A comparison of the two layer version of the model with a two layer version of a σ-coordinate model developed by Cardelino (1977, private communication) was performed. Preliminary results indicate that with similar initial conditions and horizontal resolution the process of cyclogenesis was much better represented in the isentrope model.

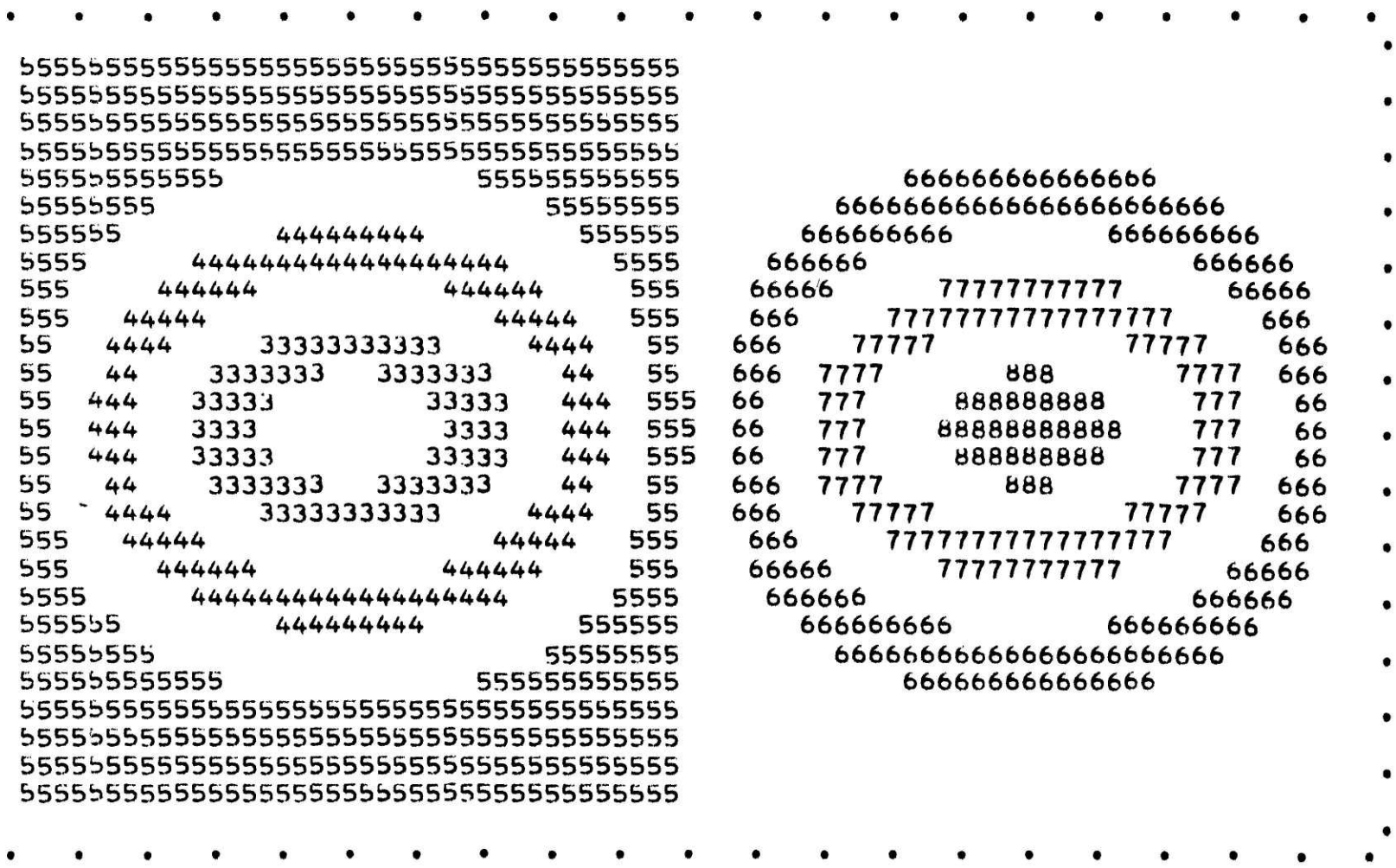

Figure 6.0.1 Initial p_s for all runs.

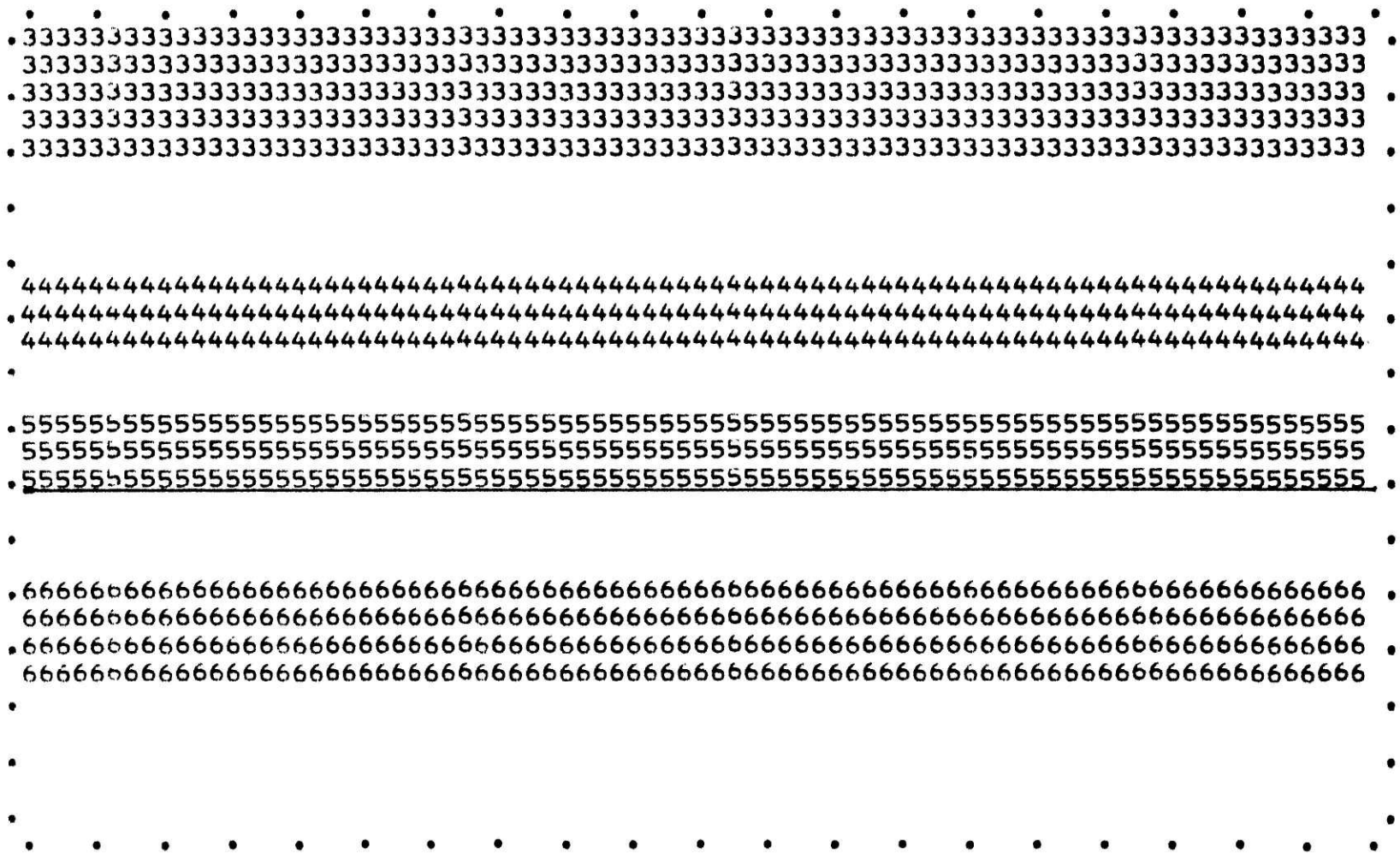

Figure 6.0.2 Initial θ_s for all runs.

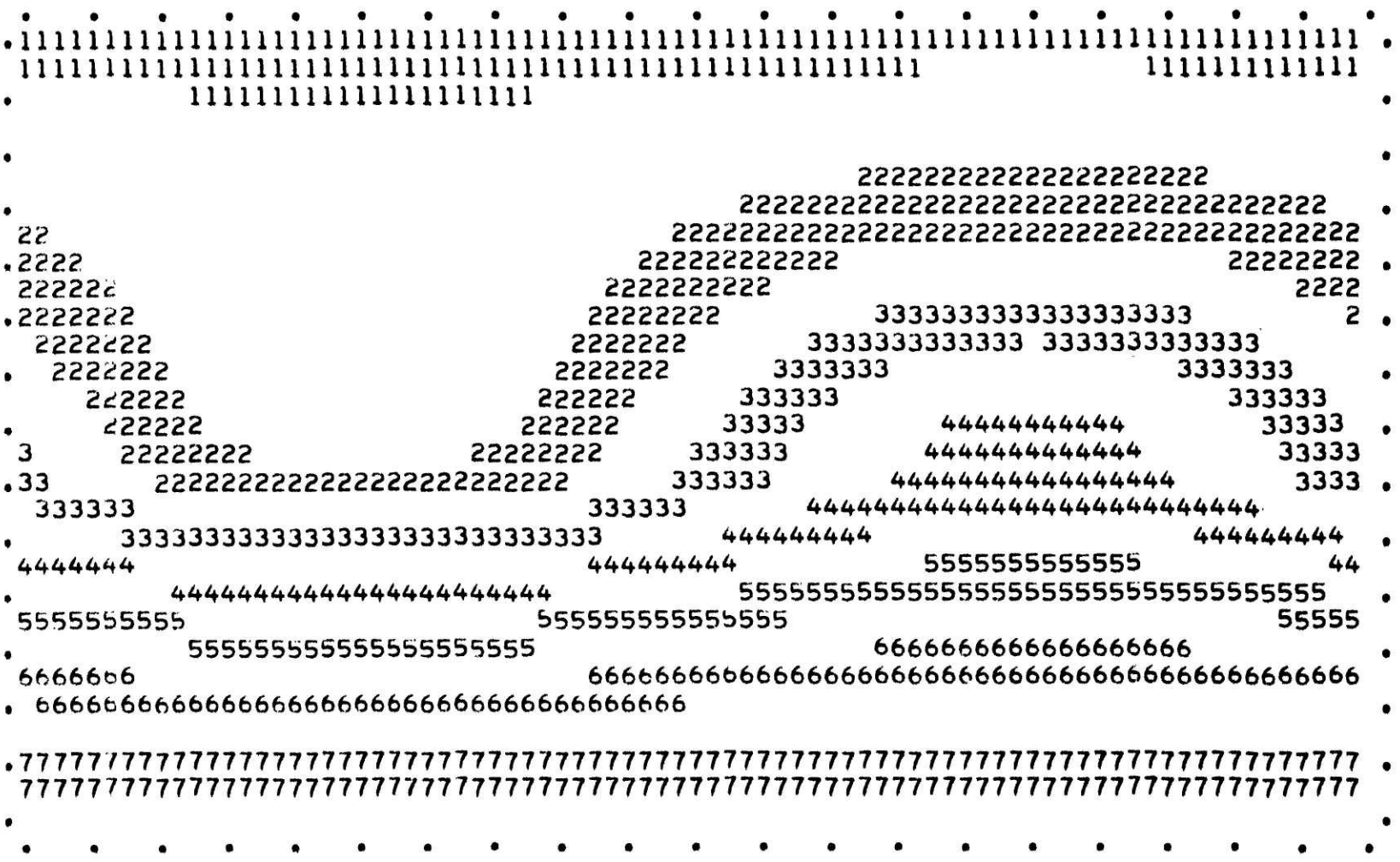

Figure 6.0.3 Initial $\widetilde{M}_2^{\theta}$ for runs 1,2, and 3.

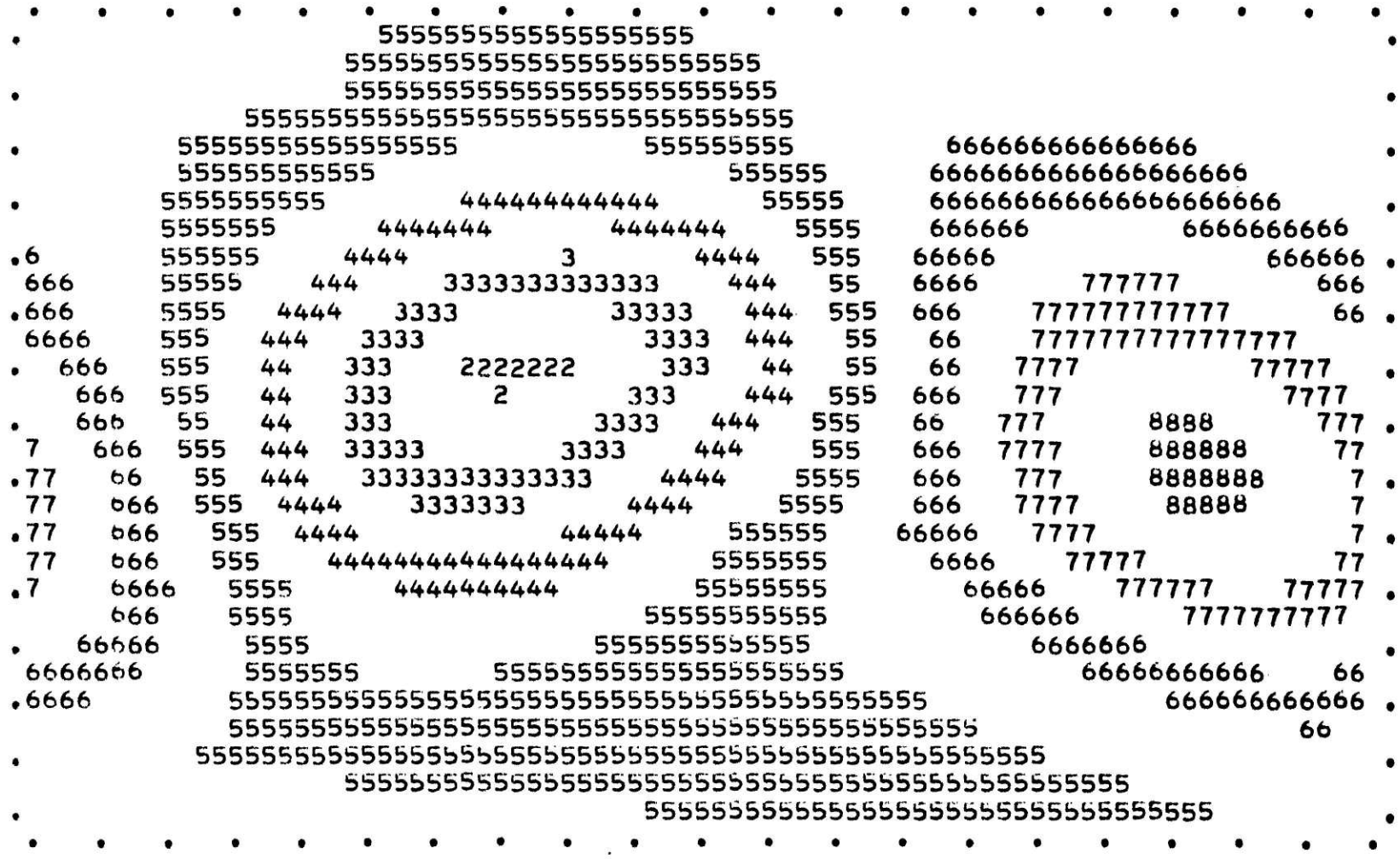

Figure 6.1.1 run 1 p_s after 1 day.

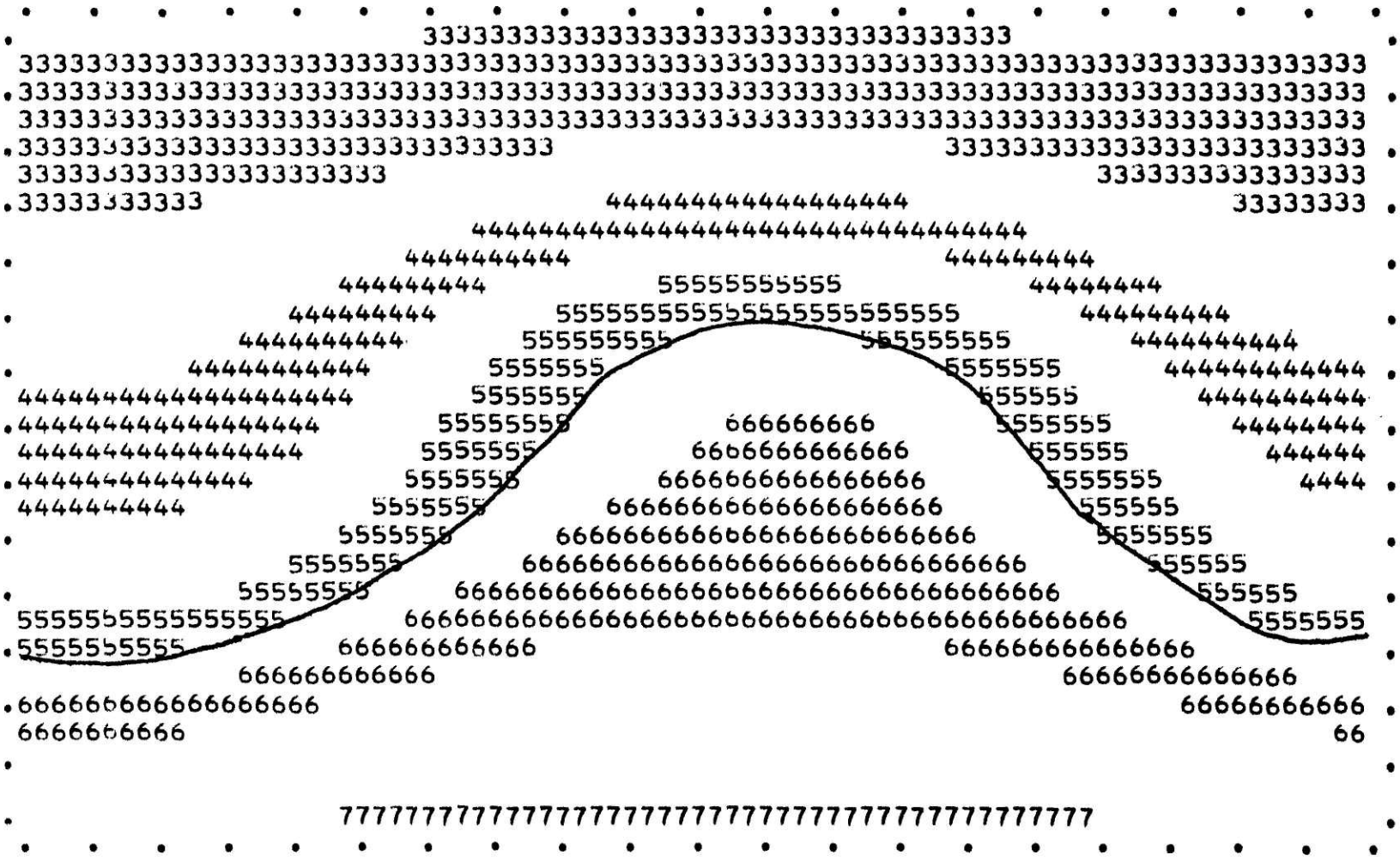

Figure 6.1.2 runl ϑ_f after 1 day.

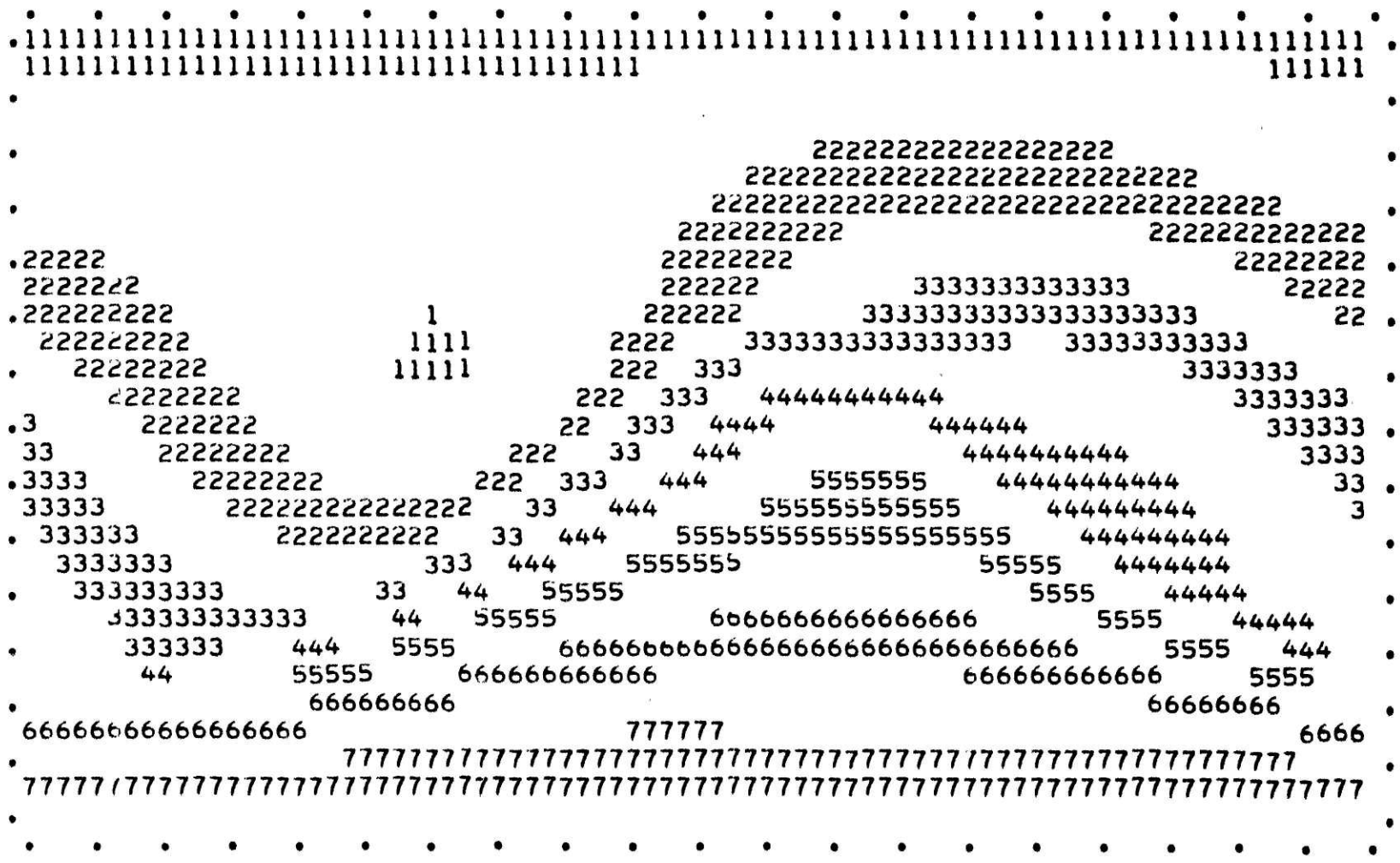

Figure 6.1.3 run 1 $\bar{M}_2^{\theta}$ after 1 day.

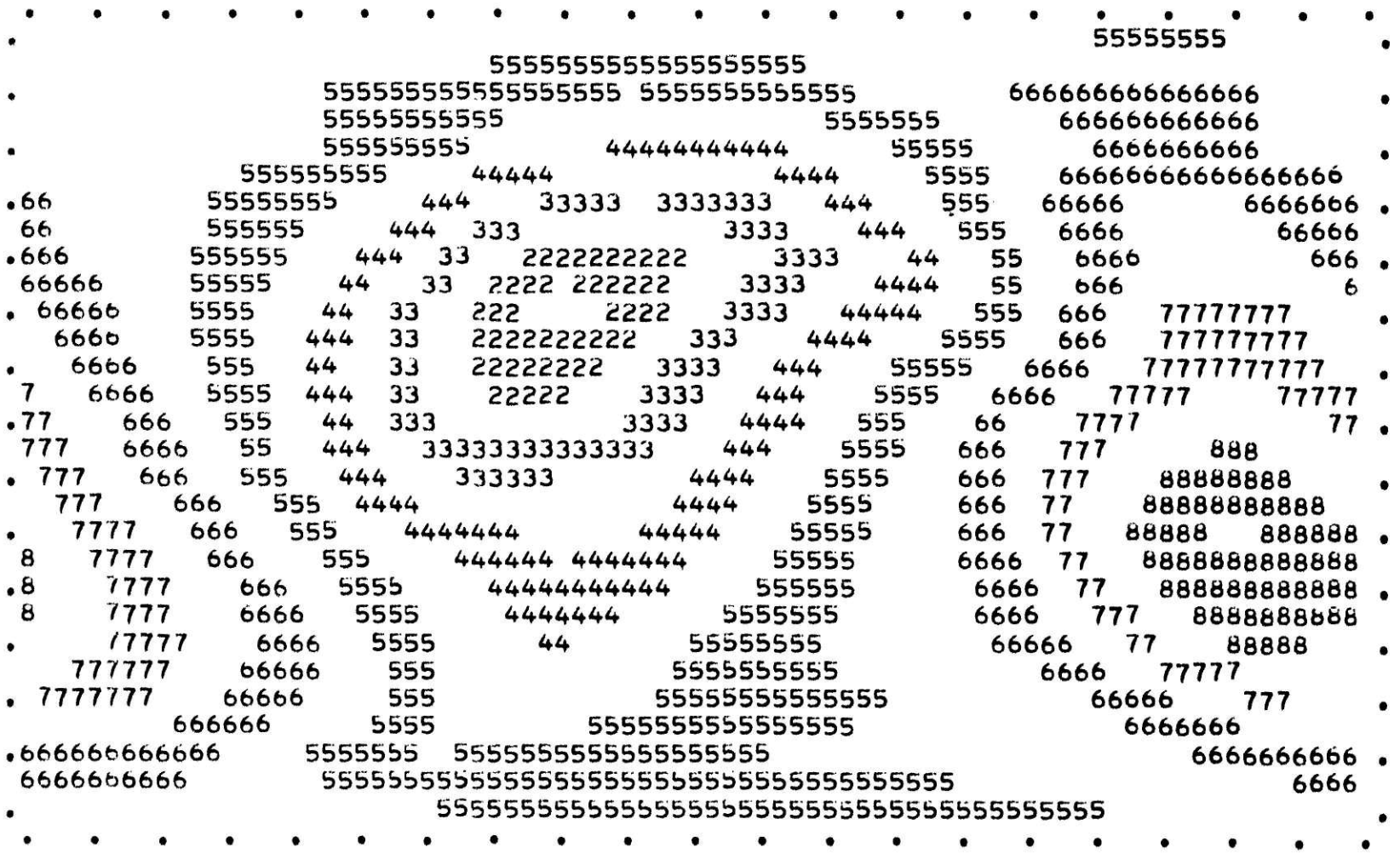

Figure 6.1.4 run 1 p_s after 2 days.

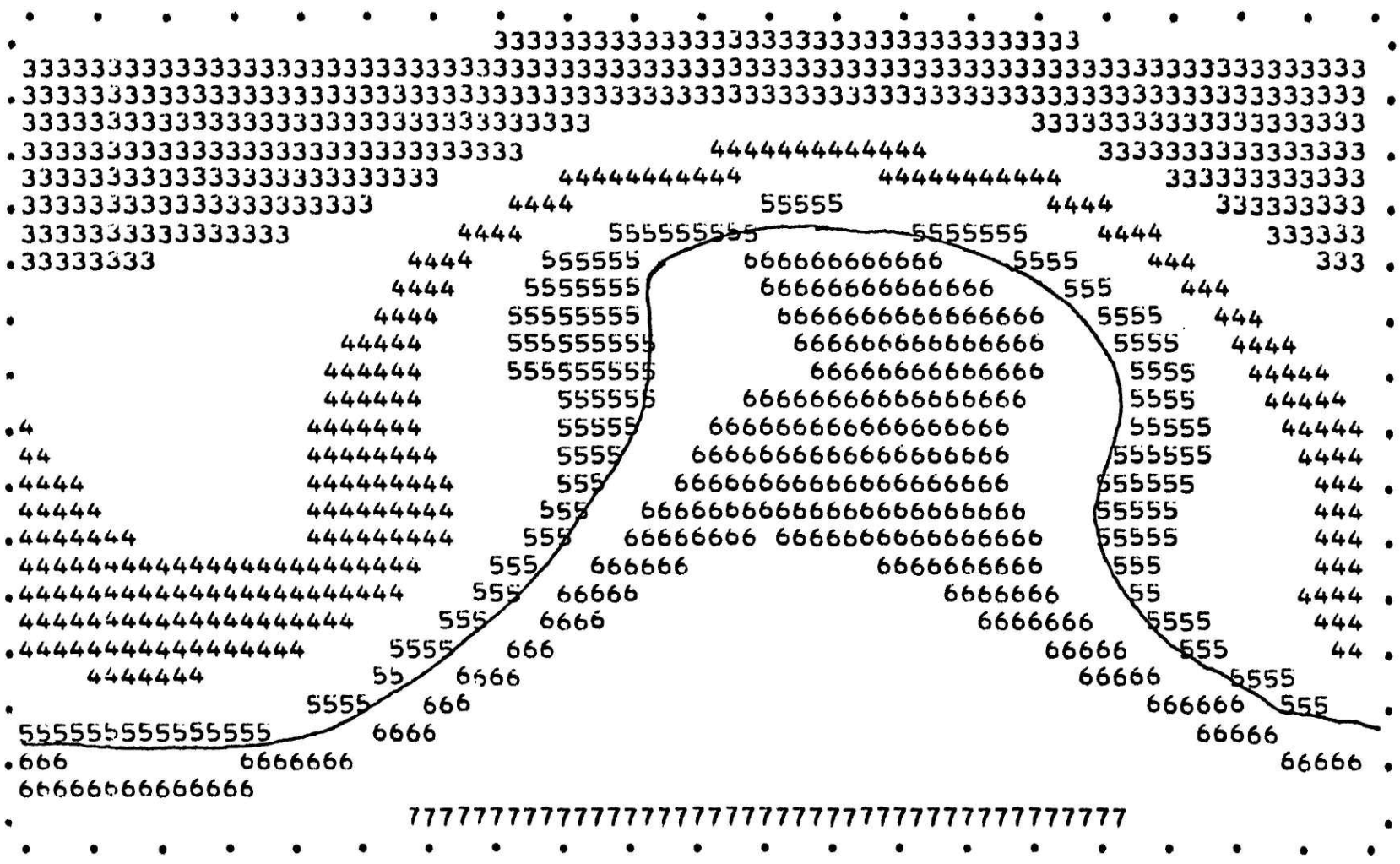

Figure 6.1.5 run 1 θ_3 after 2 days.

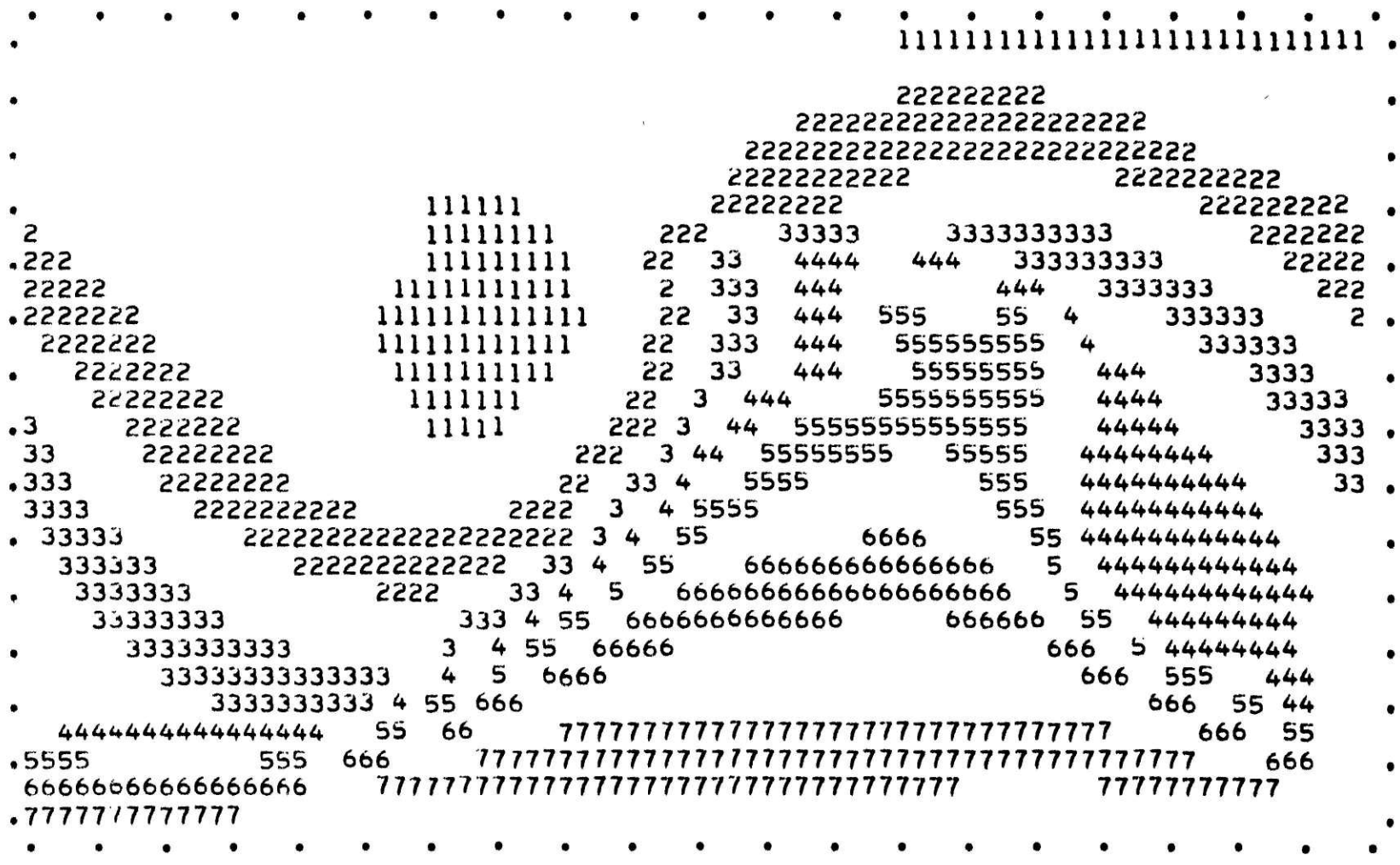

Figure 6.1.6 run 1 $\overline{M}_2^0$ after 2 days.

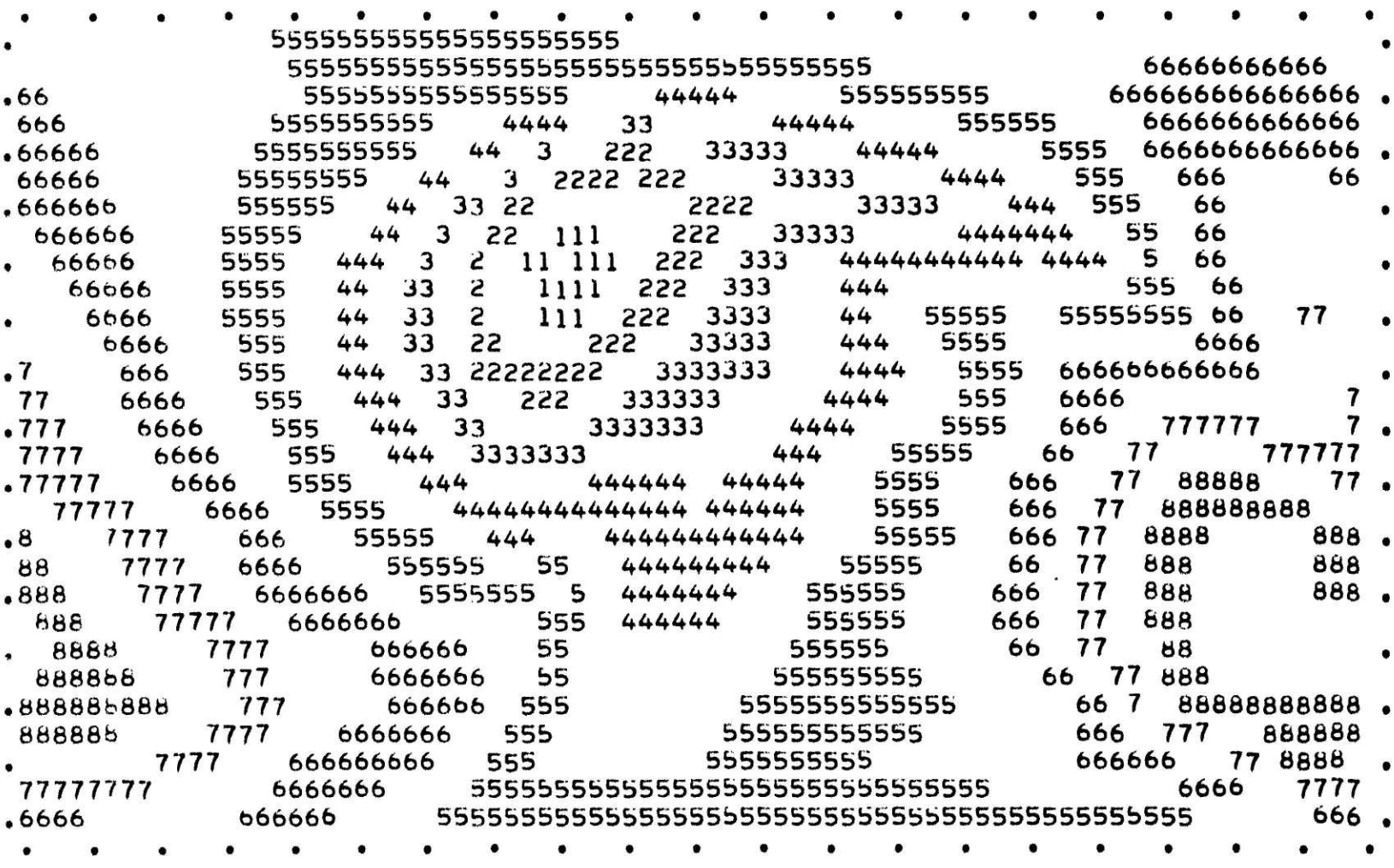

Figure 6.1.7 run 1 p_s after 3 days.

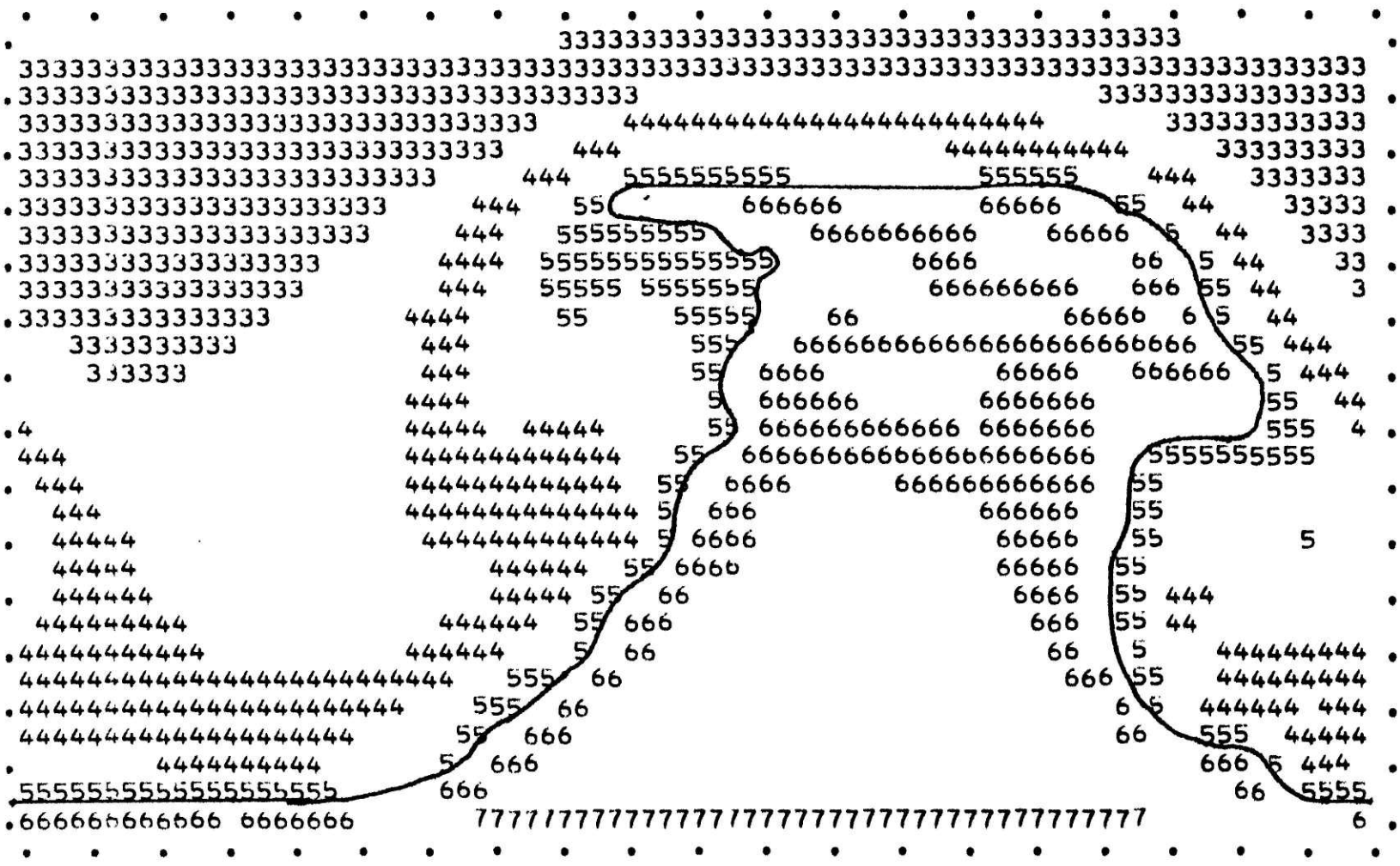

Figure 6.1.8 run 1 ∂_5 after 3 days.

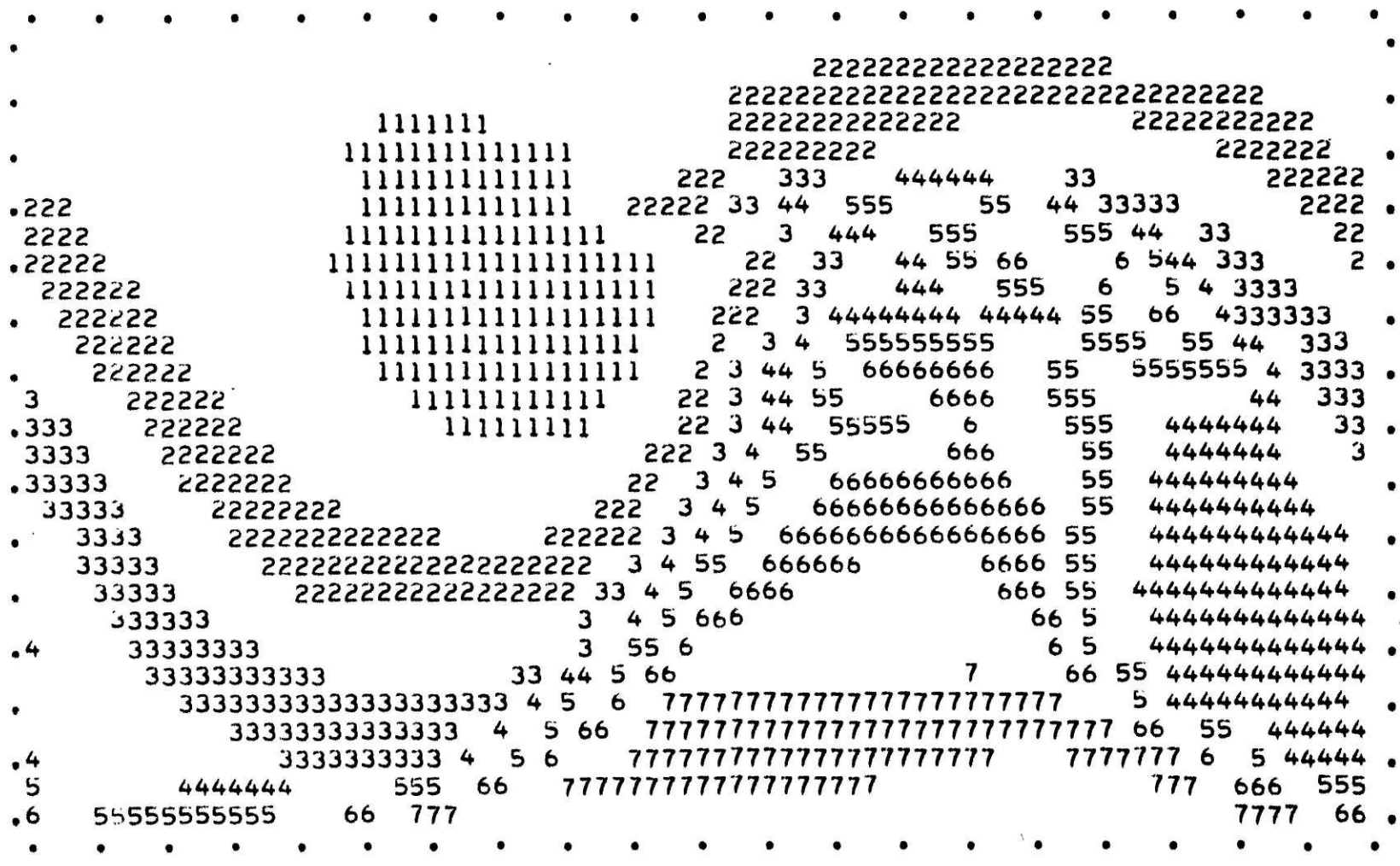

Figure 6.1.9 run 1 $\overline{M}_2^b$ after 3 days.

Figure 6.1.10 run 1 p_s after 4 days.

Figure 6.2.1 run 2 p_s after 3 days.

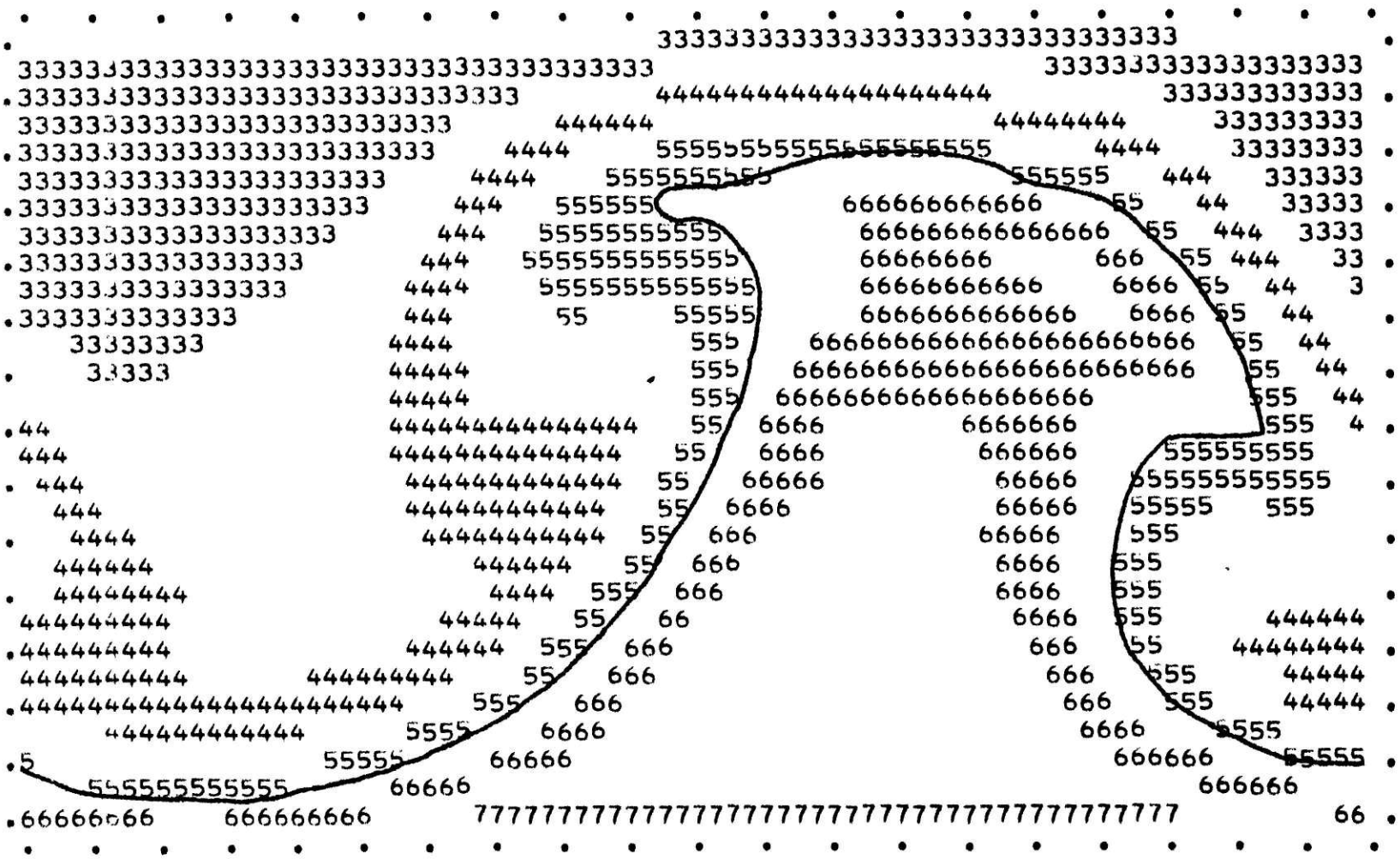

Figure 6.2.2 run 2 ϑ_S after 3 days.

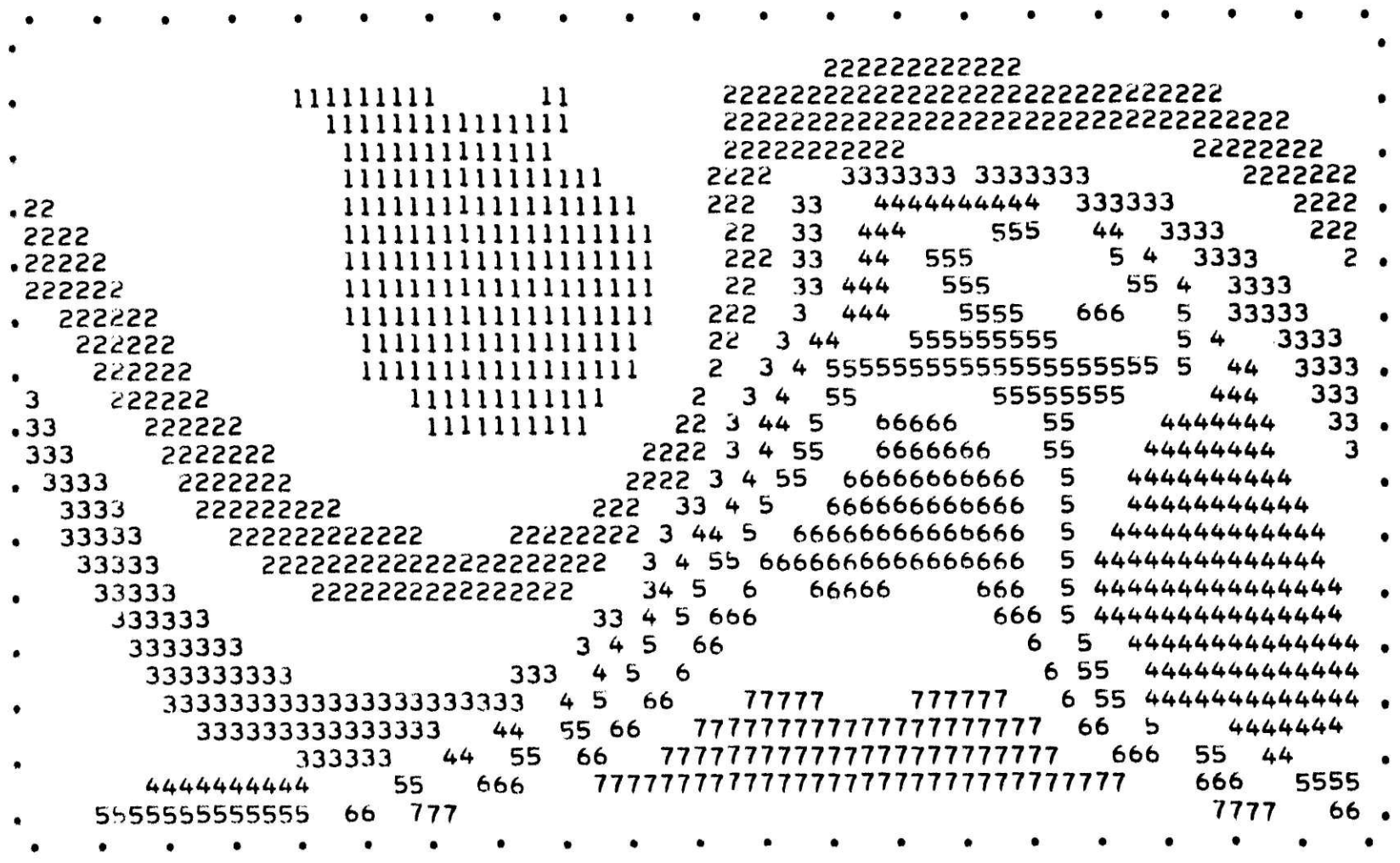

Figure 6.2.3 run 2 $\overline{M}_2^{\theta}$ after 3 days.

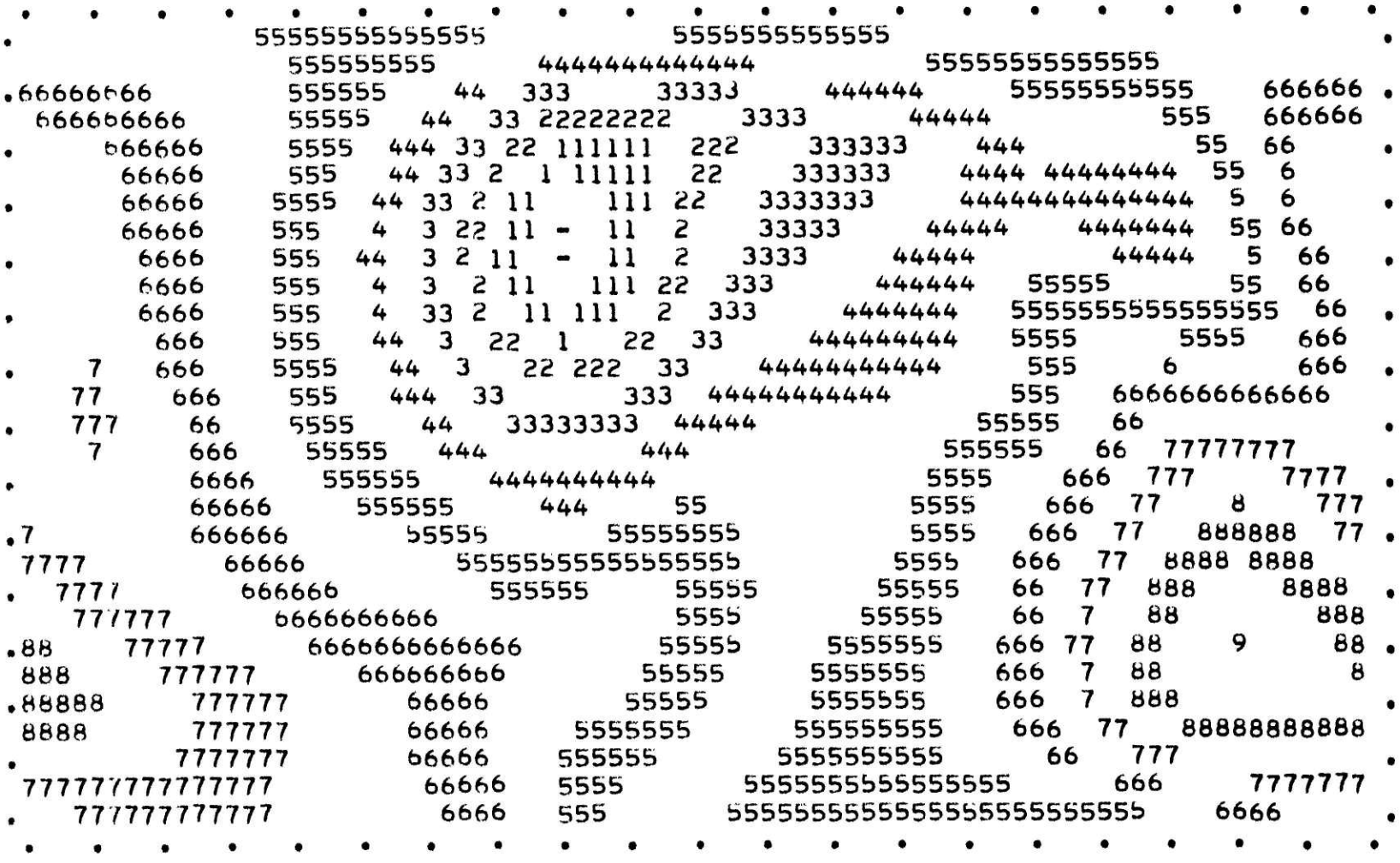

Figure 6.2.4 run 2 p_s after 4 days.

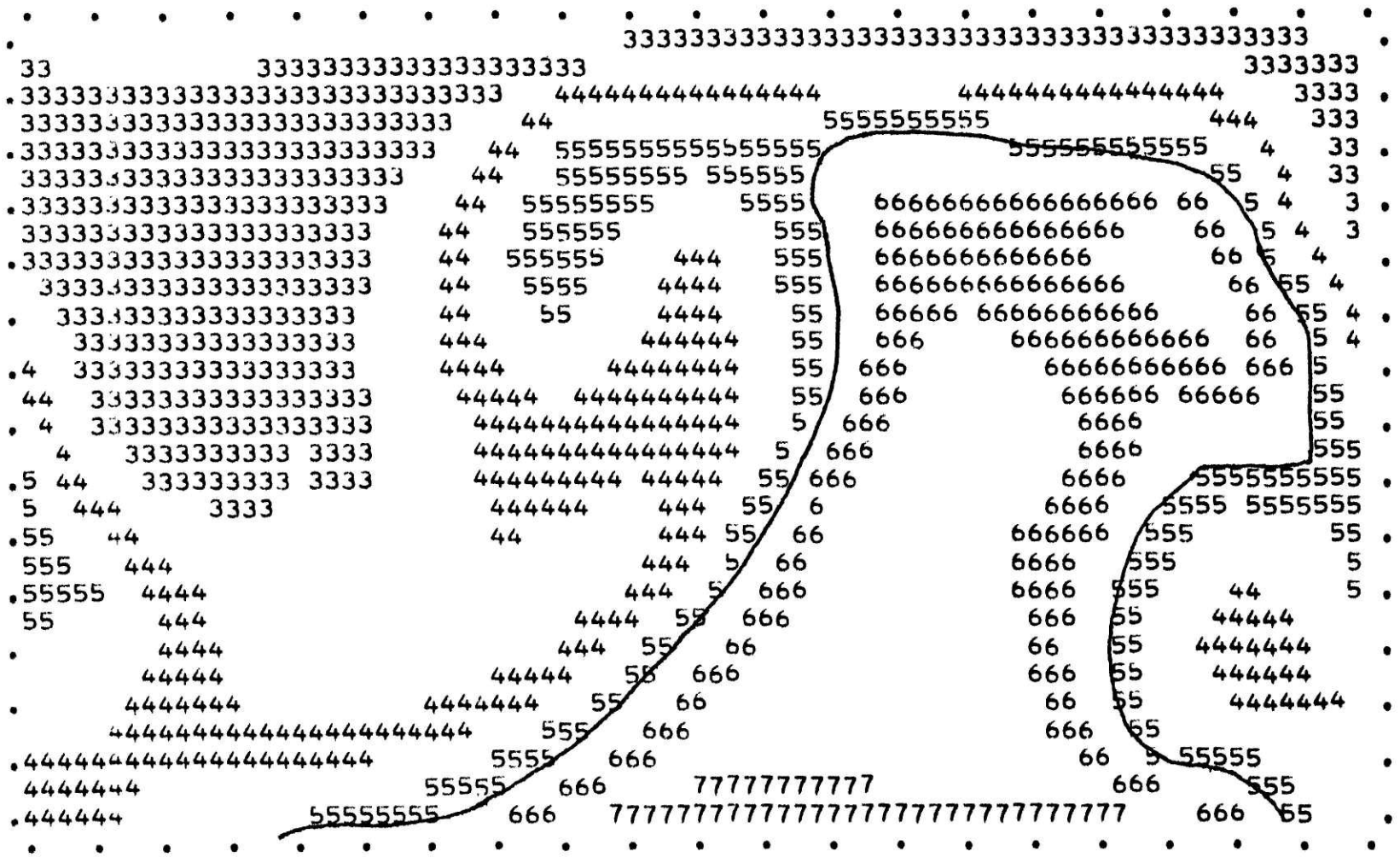

Figure 6.2.5 run 2 θ_5 after 4 days.

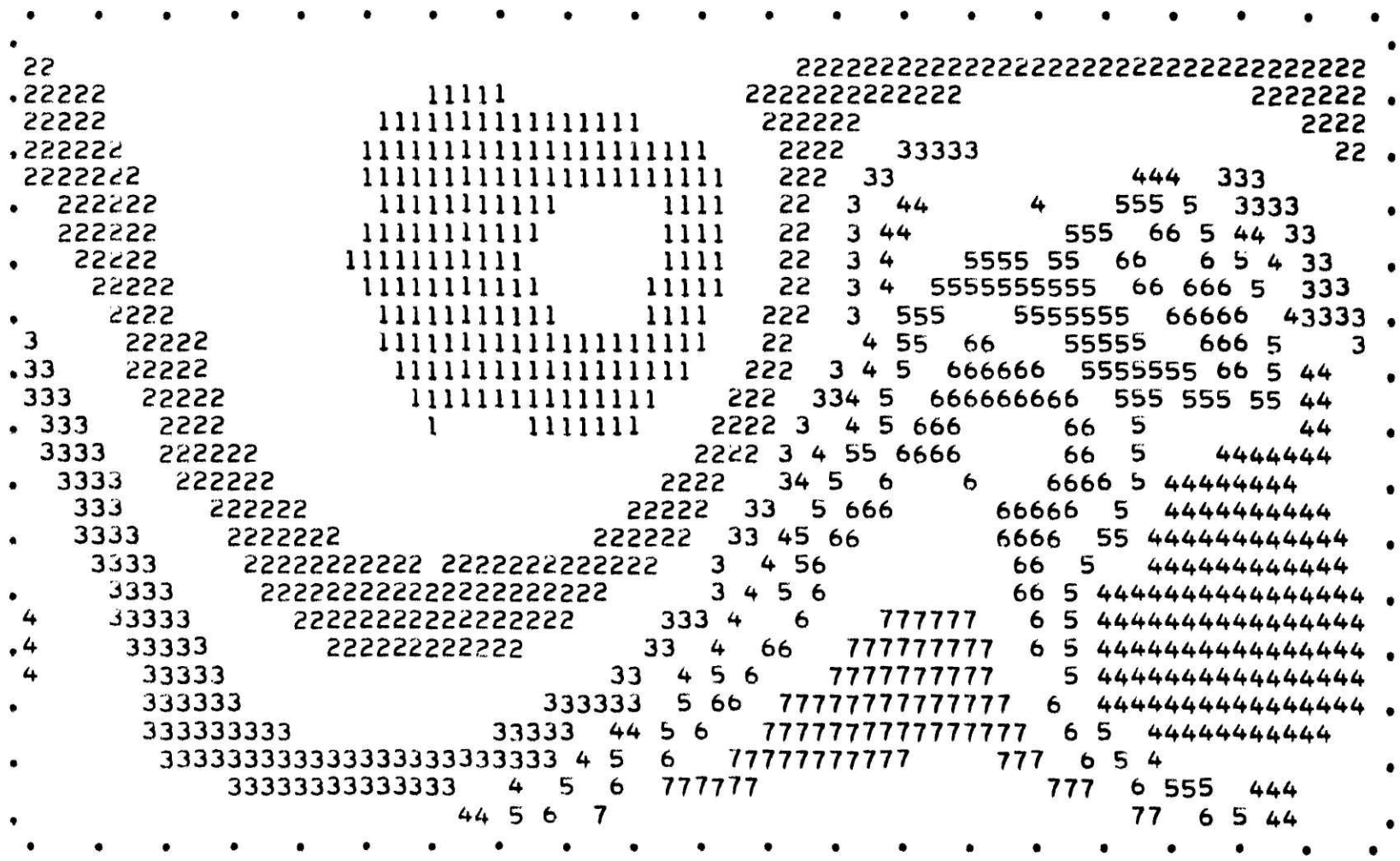

Figure 6.2.6 run 2 M_2 after 4 days.

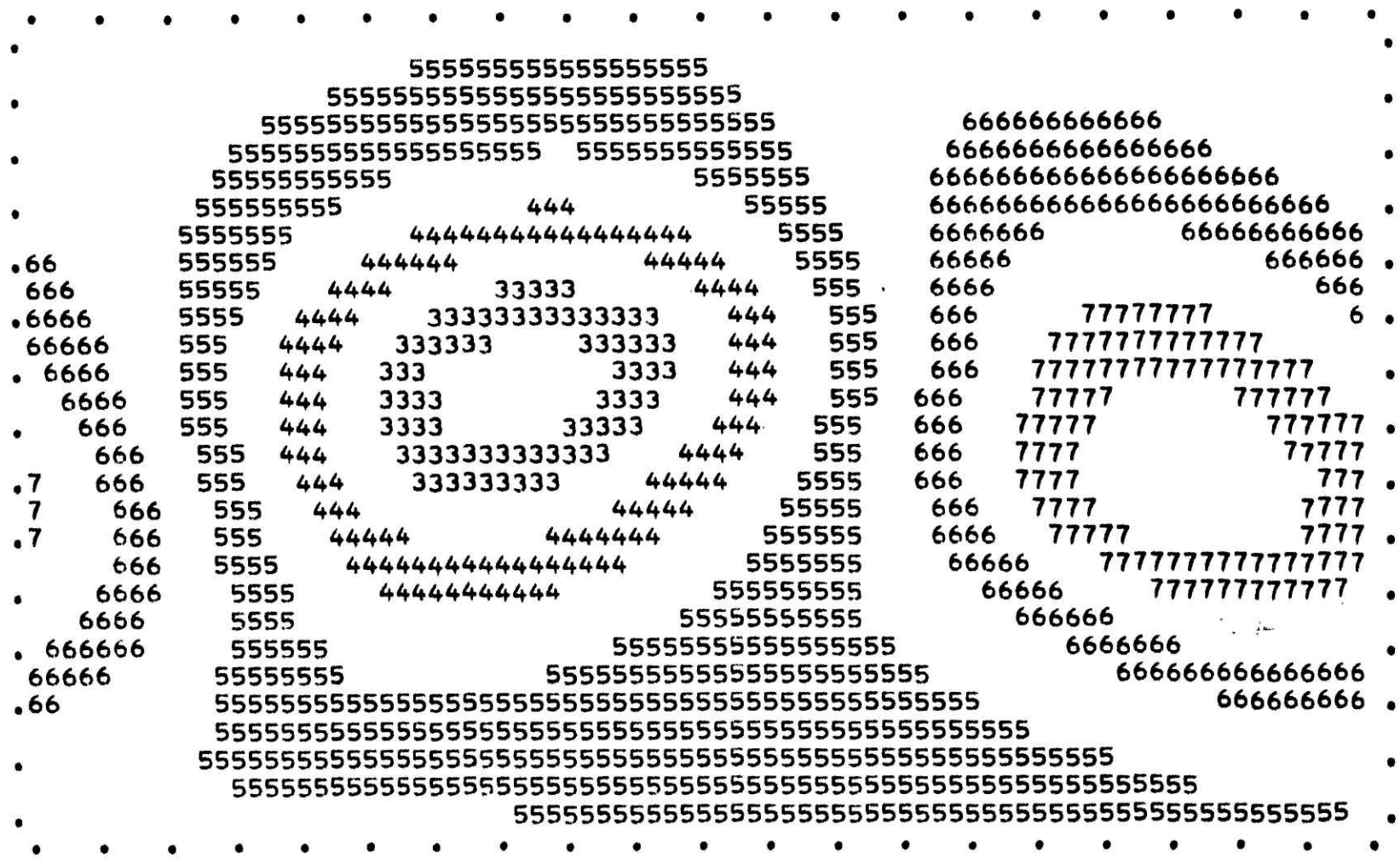

Figure 6.3.1 fun 3 p_s after 1 day.

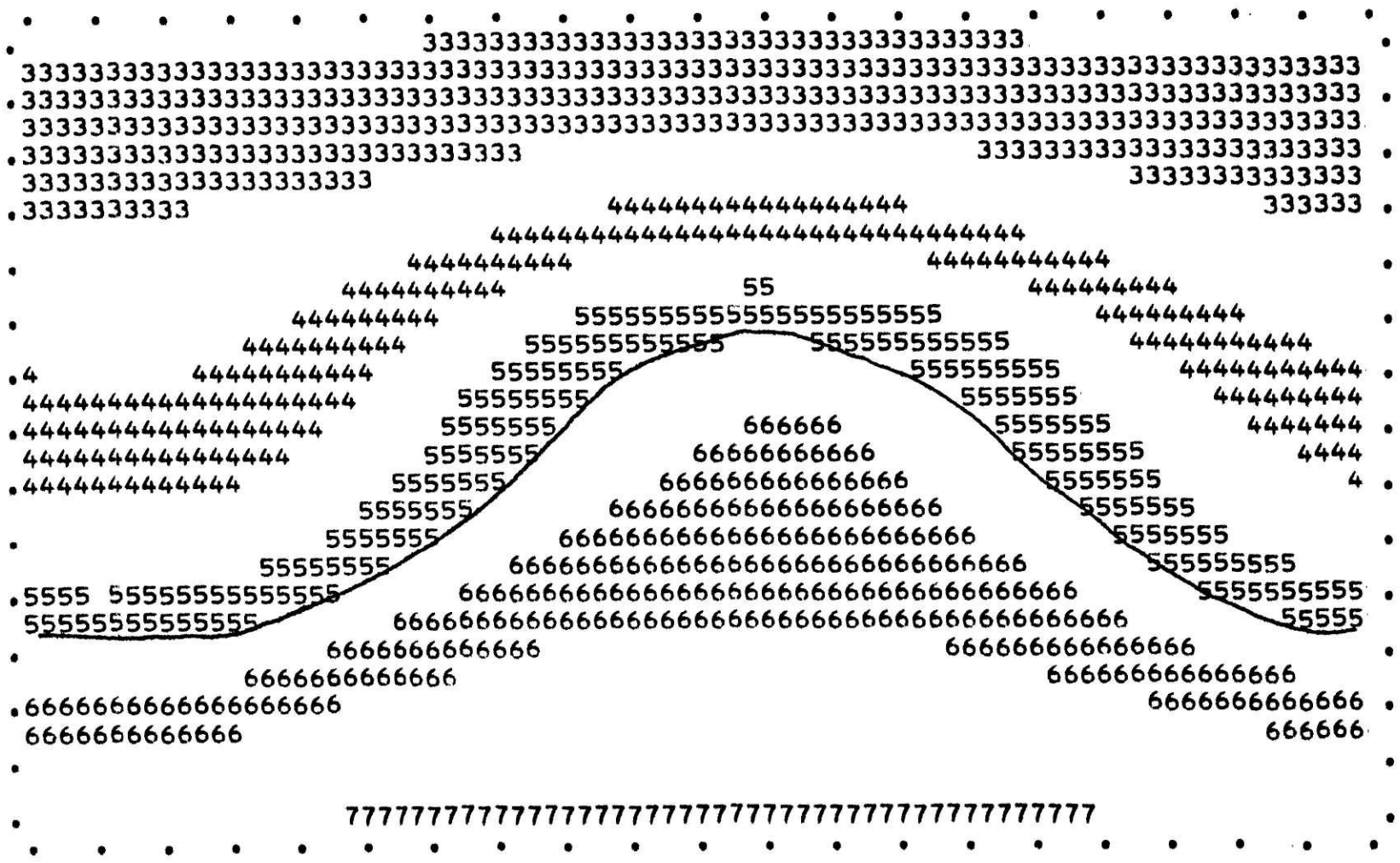

Figure 6.3.2 run 3 θ_S after 1 day.

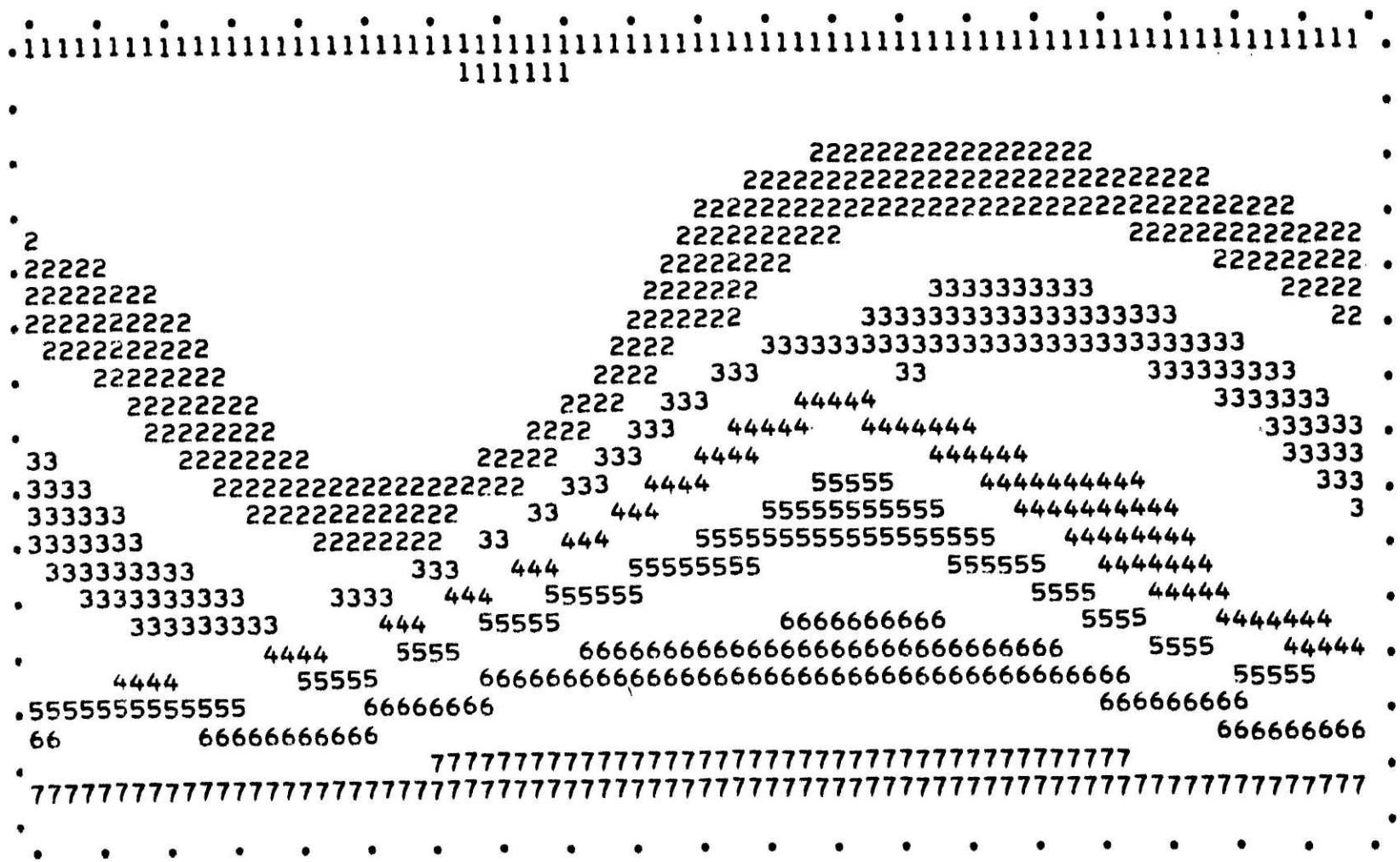

Figure 6.3.3 run 3 $\overline{M}_2^B$ after 1 day.

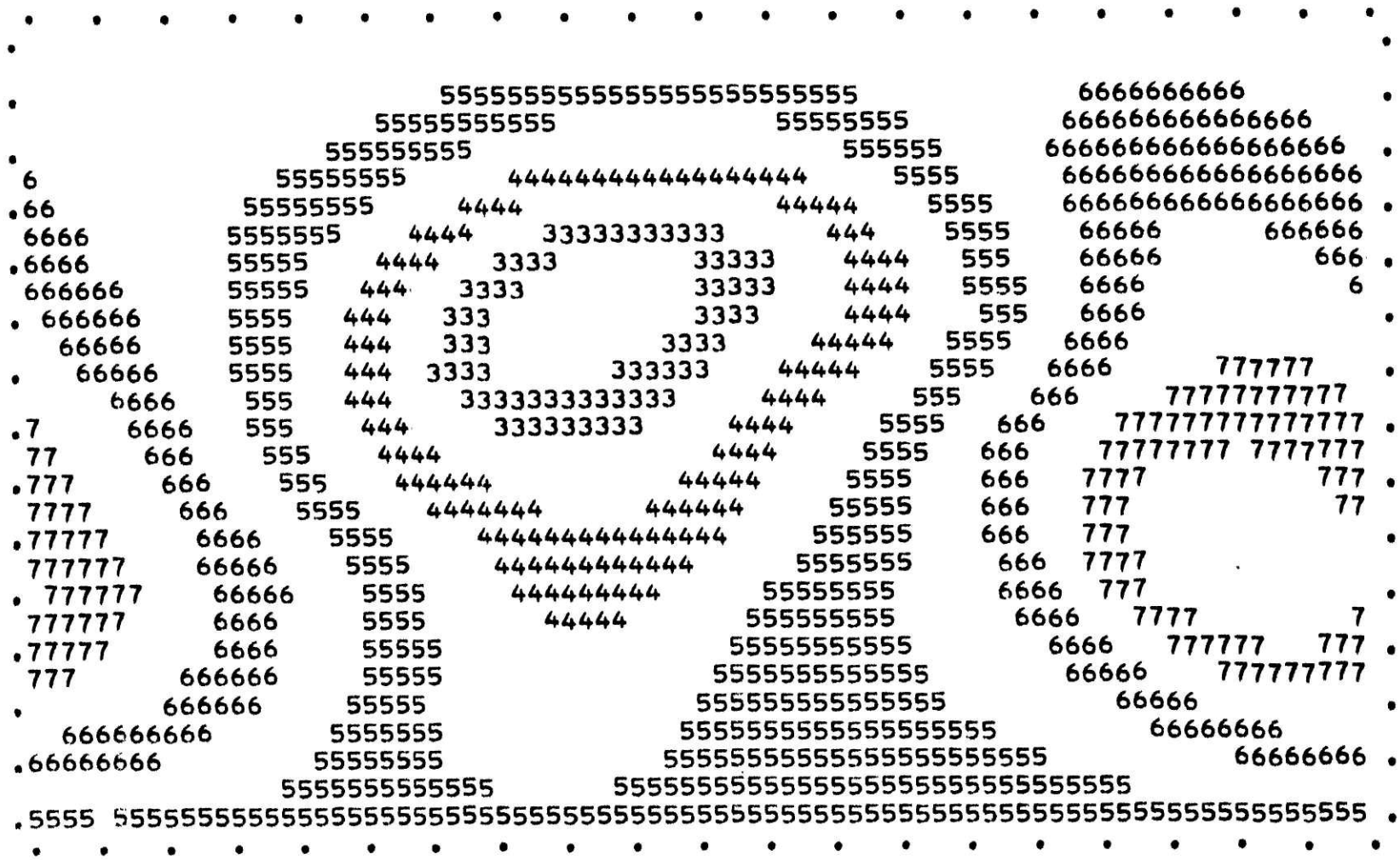

Figure 6.3.4 run 3 p_s after 2 days.

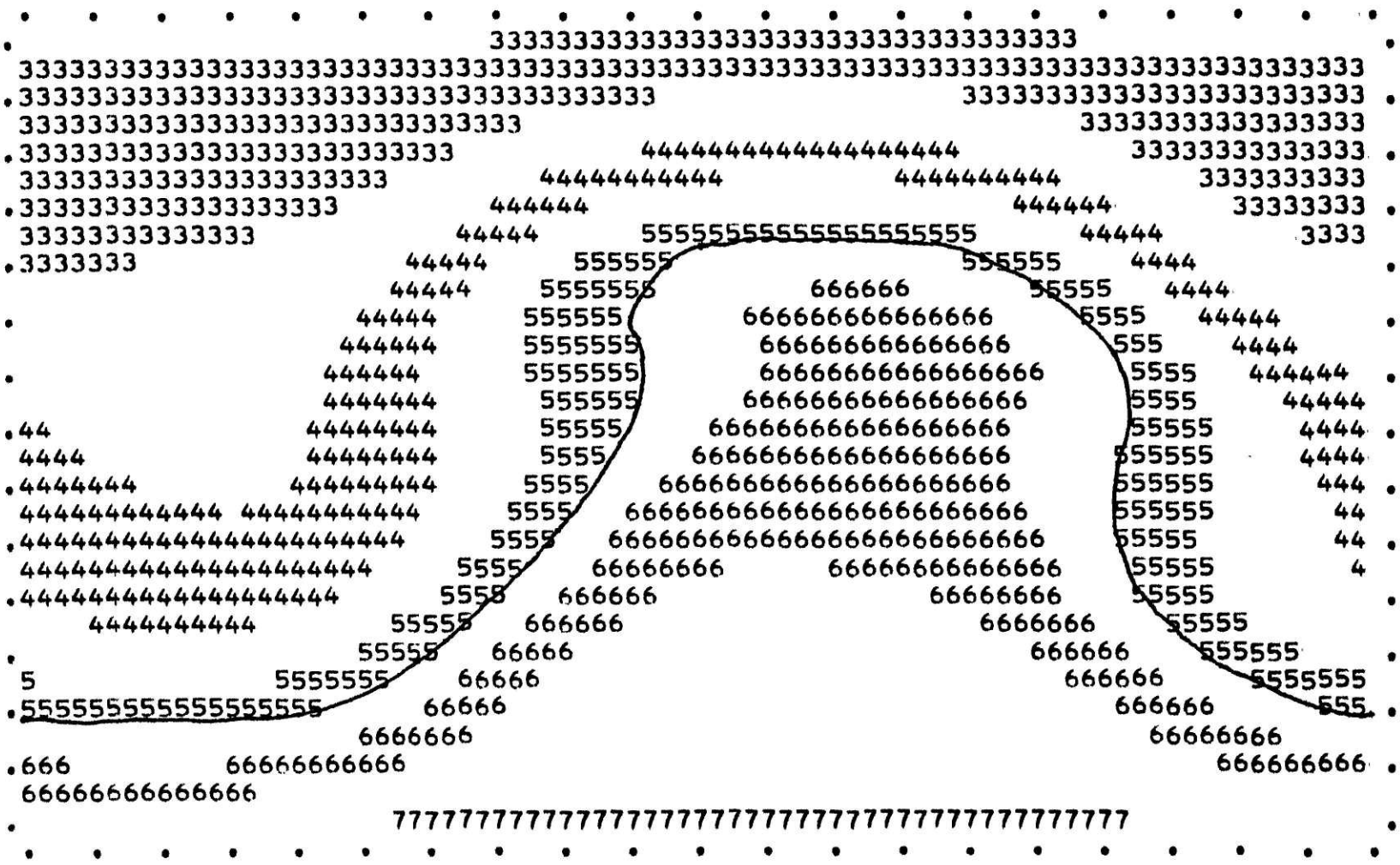

Figure 6.3.5 run 3 θ_5 after 2 days.

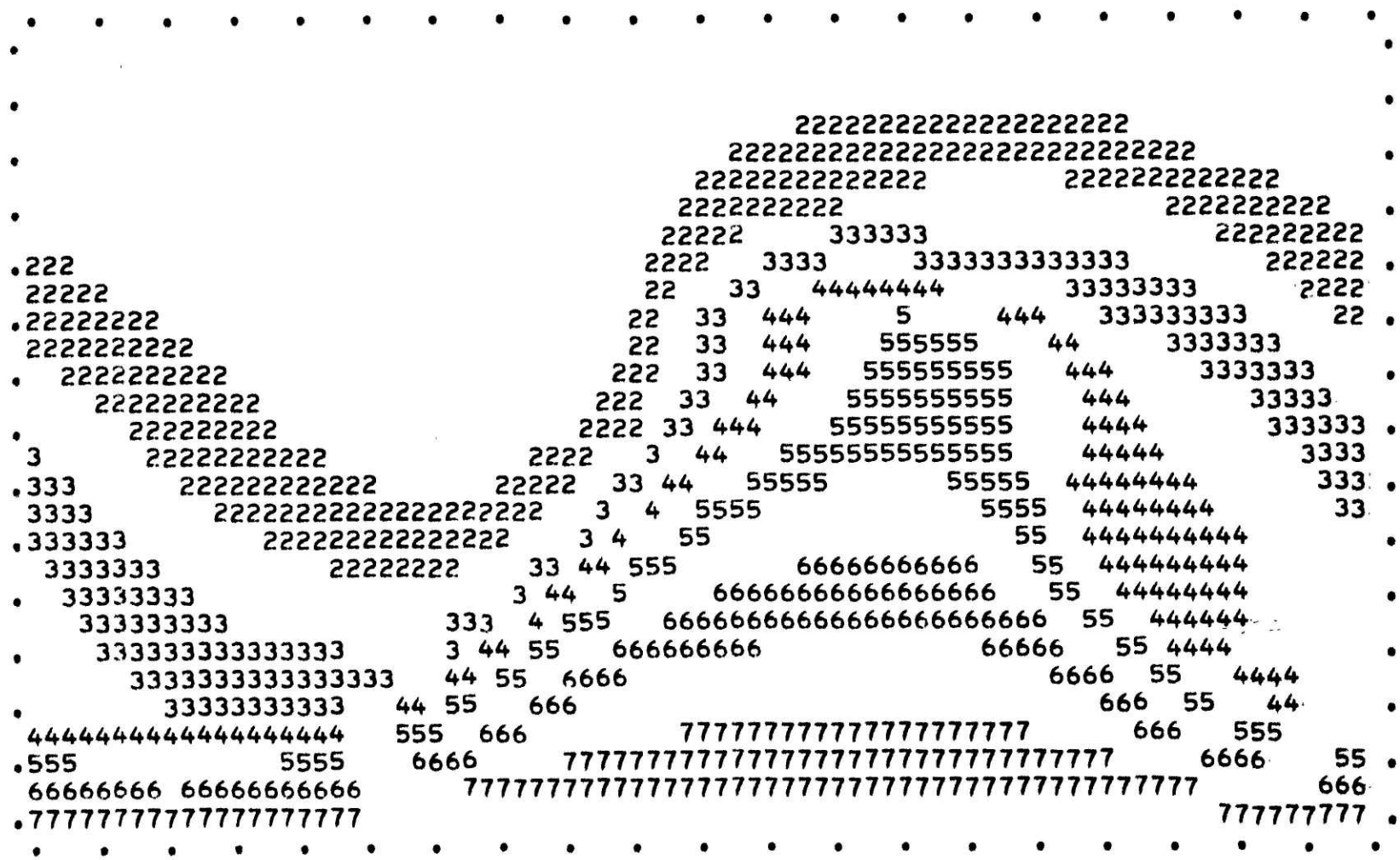

Figure 6.3.6 run 3 $\overline{M}_2^{\theta}$ after 2 days.

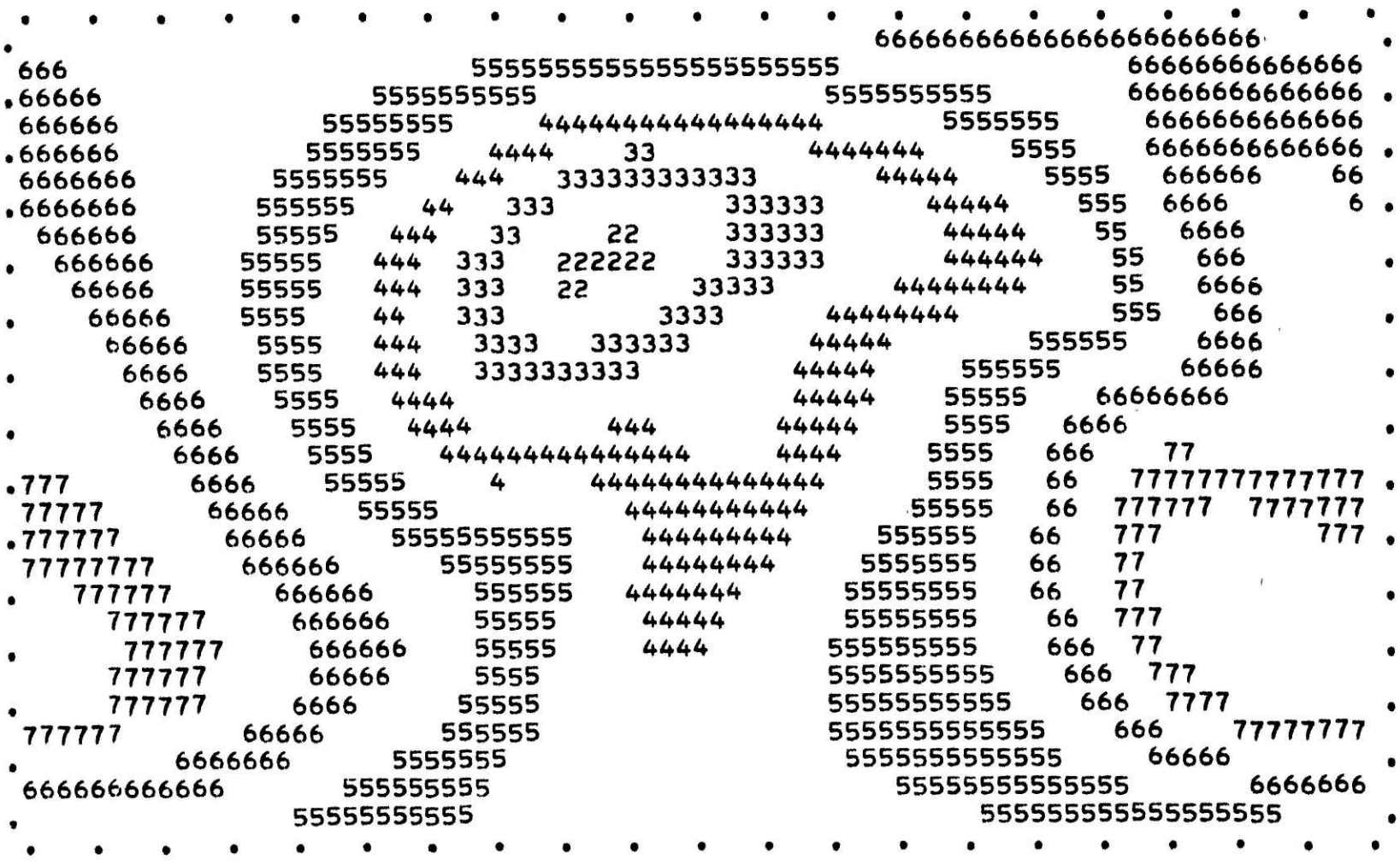

Figure 6.3.7 run 3 p_s after 3 days.

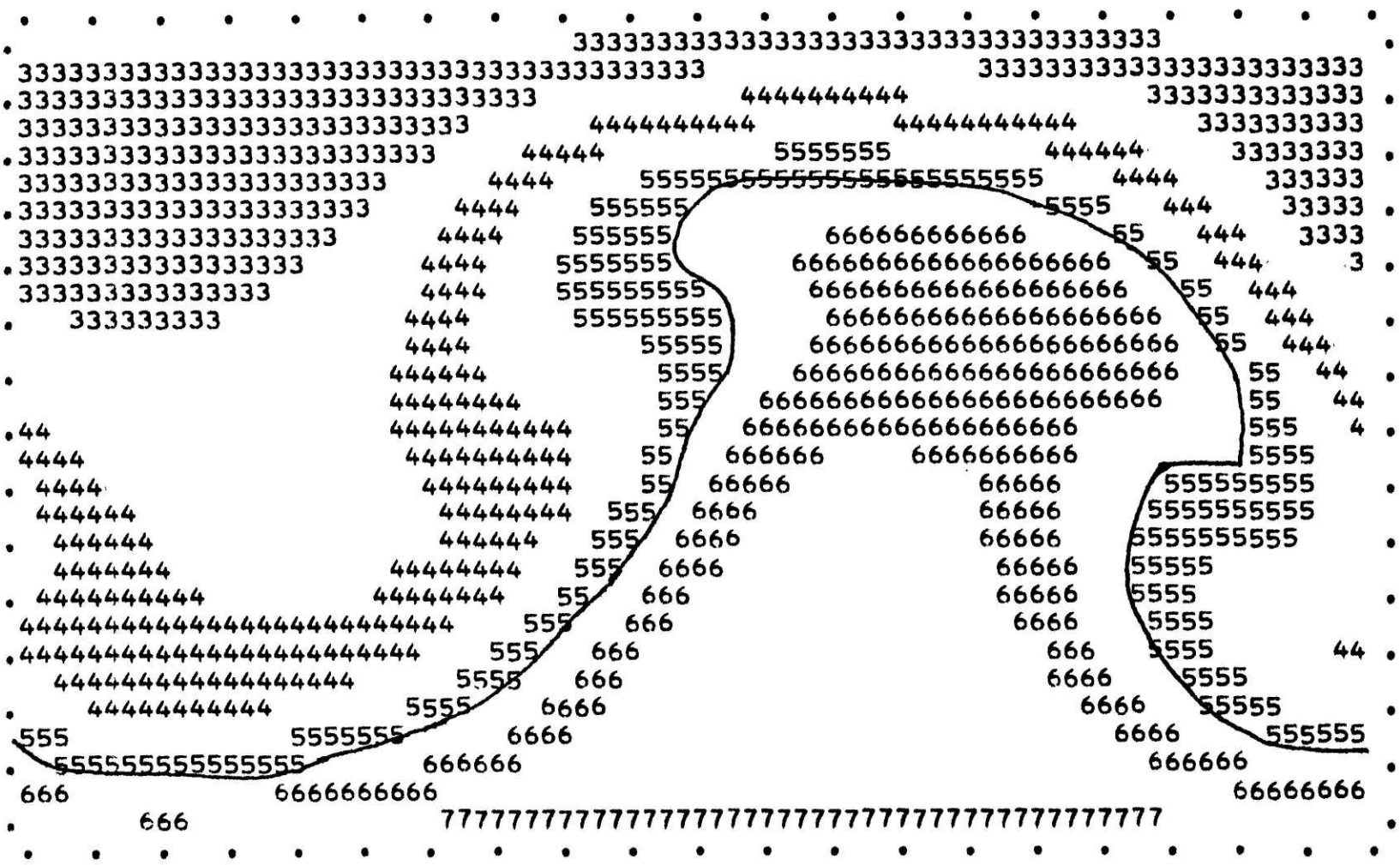

Figure 6.3.8 run 3 $\hat{D}_S$ after 3 days.

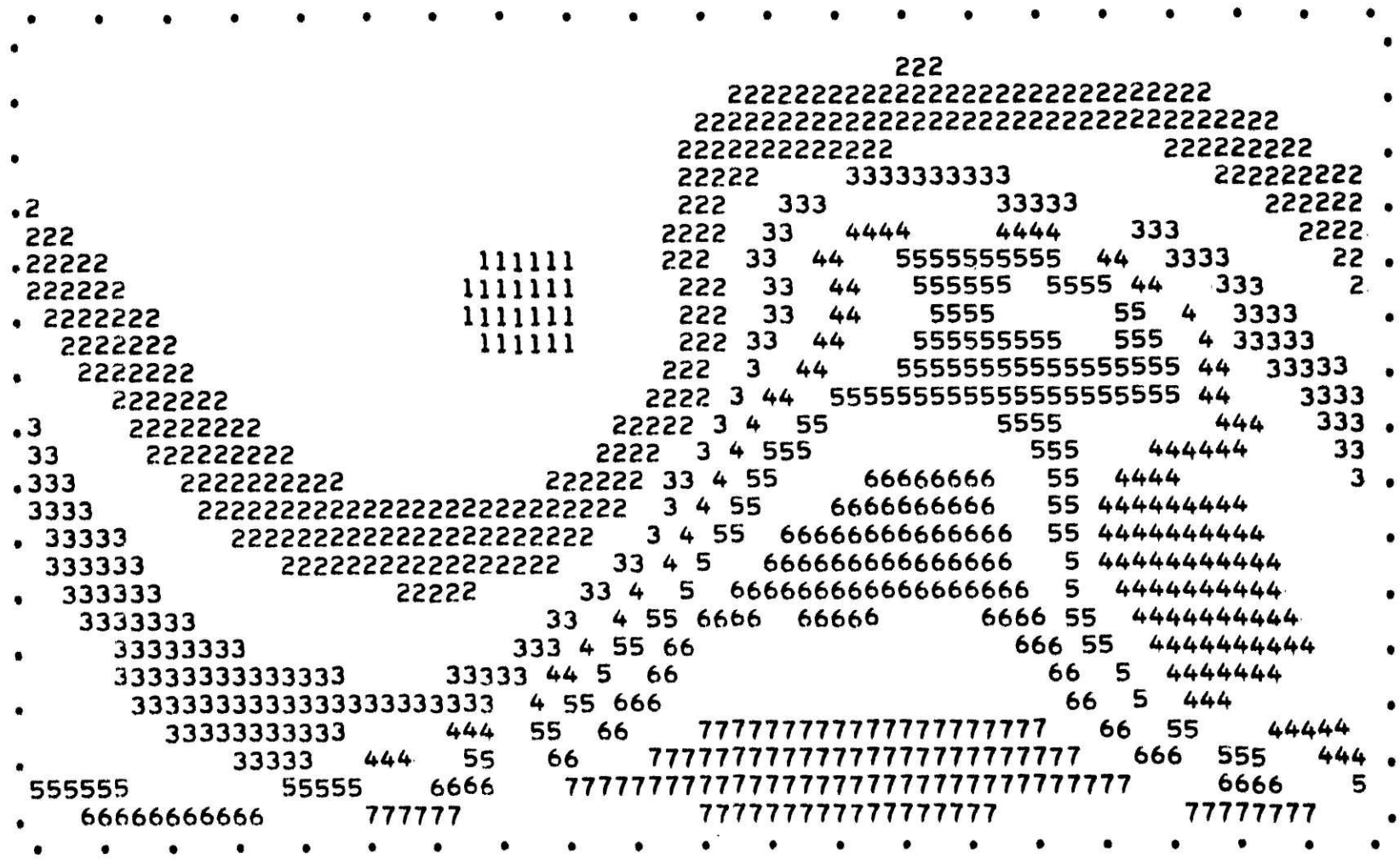

Figure 6.3.9 run 3 $\overline{M}_2^{\theta}$ after 3 days.

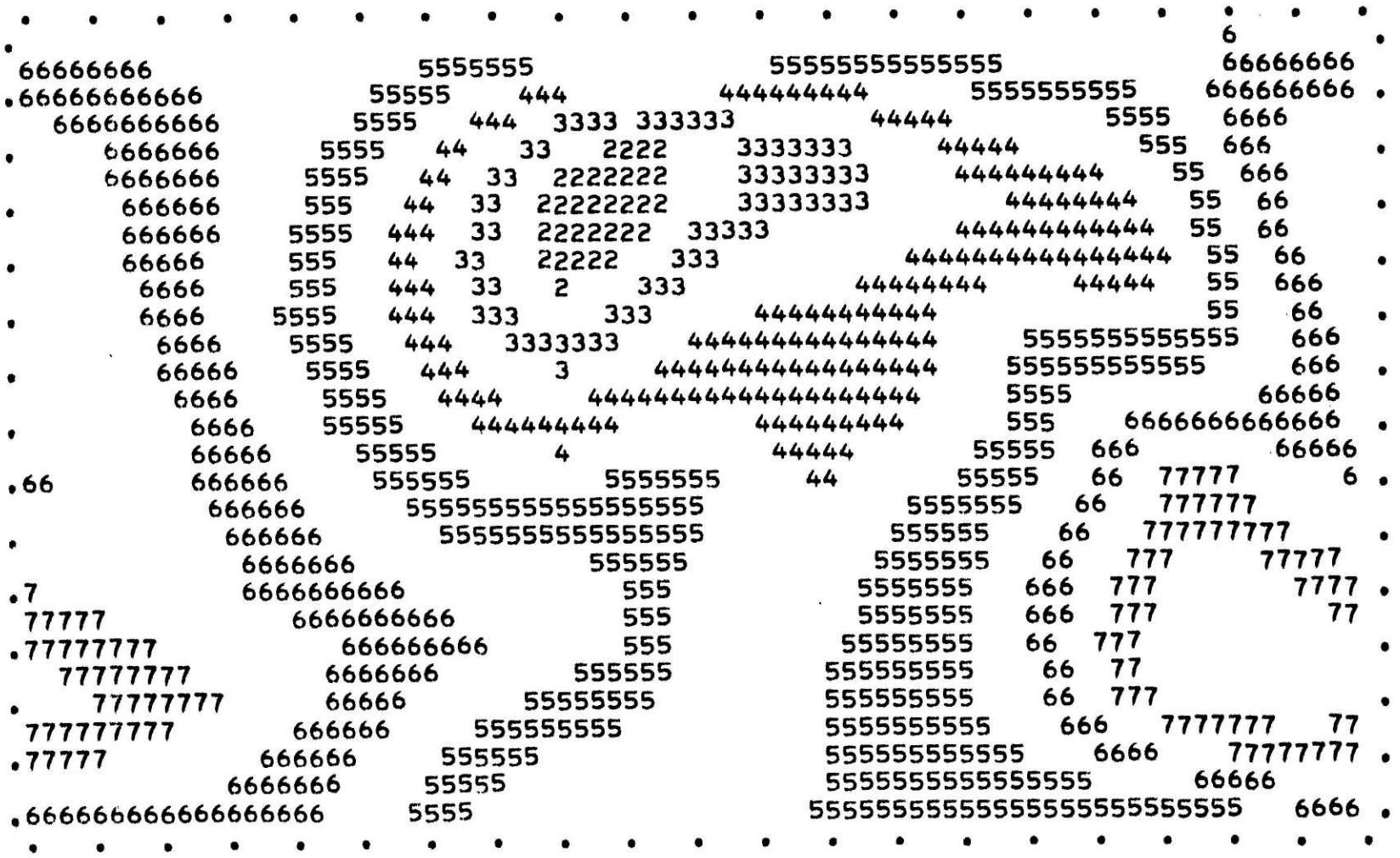

Figure 6.3.10 run 3 p_s after 4 days.

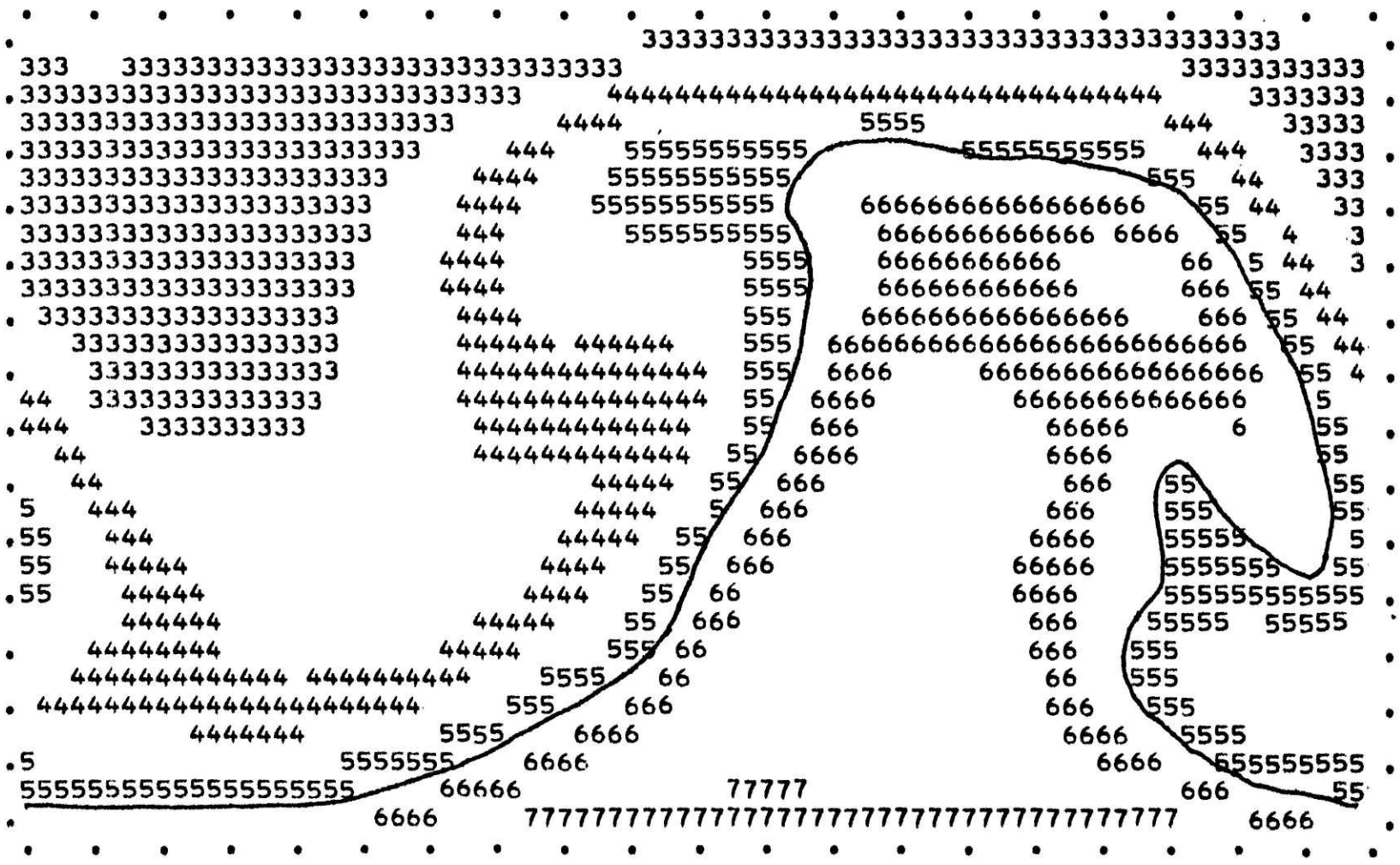

Figure 6.3.11 run 3 θ_f after 4 days.

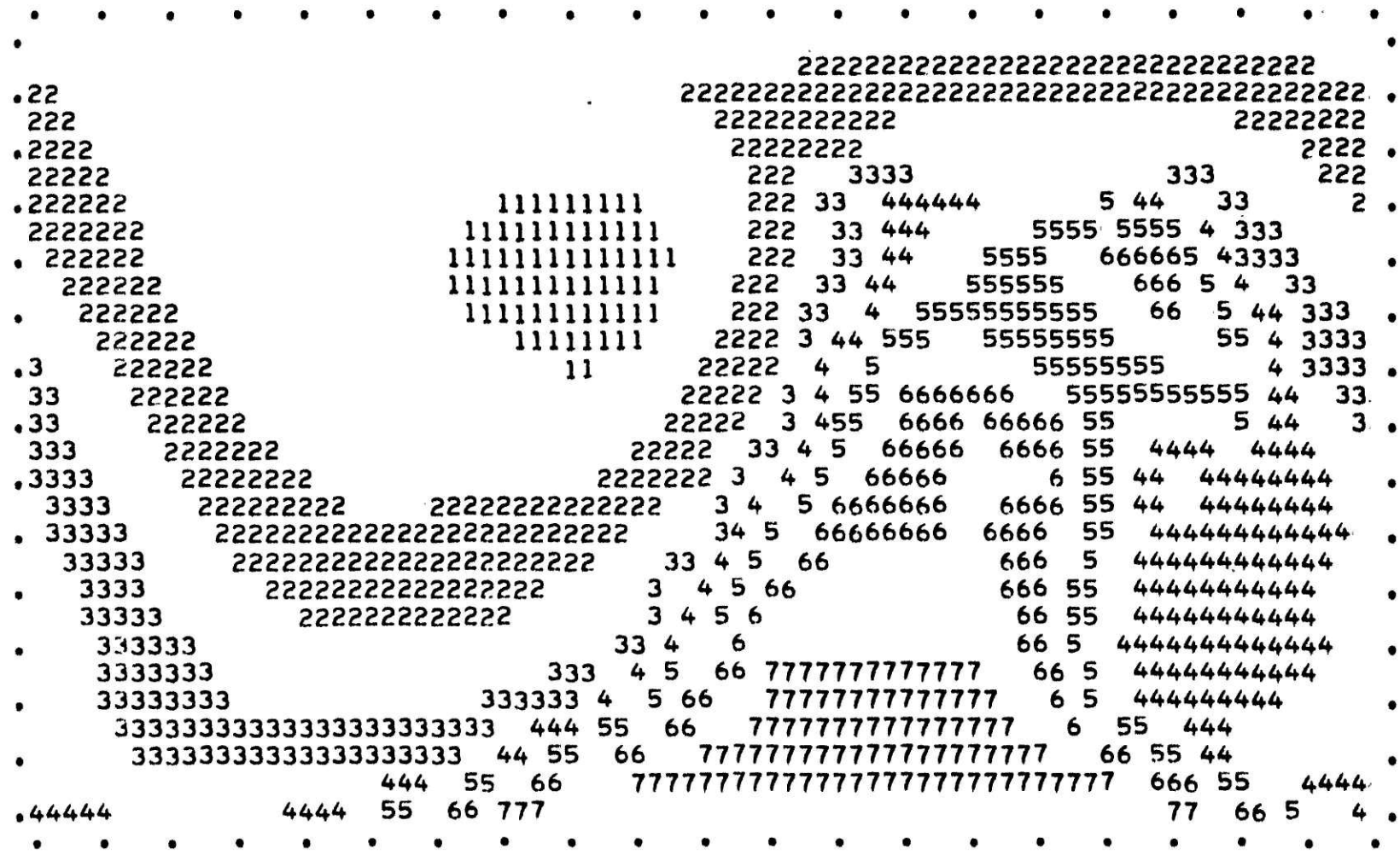

Figure 6.3.12 run 3 $\overline{M_2}^{\theta}$ after 4 days.

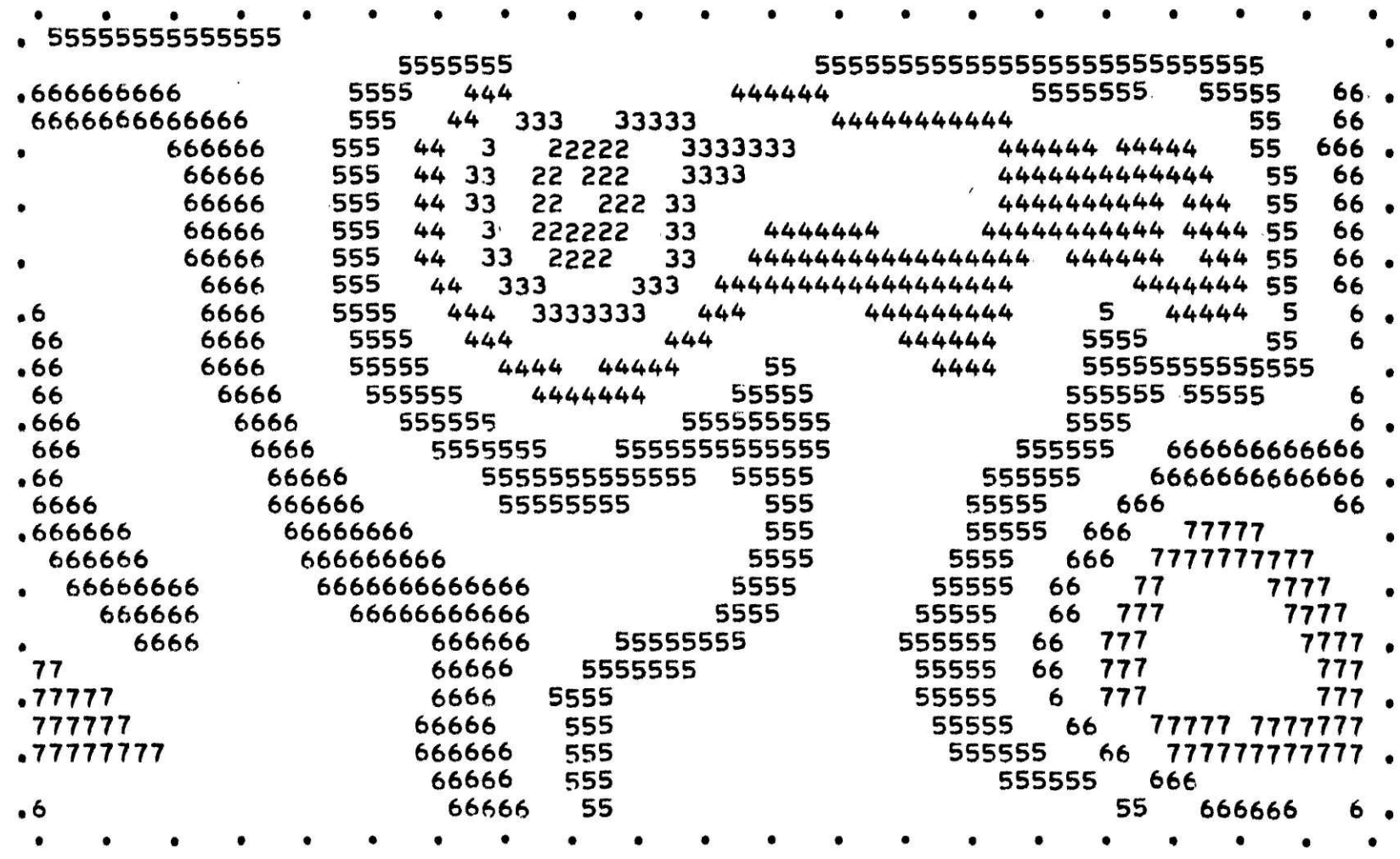

Figure 6.3.13 run 3 p_s after 5 days.

Figure 6.3.14 run 3 θ_s after 5 days.

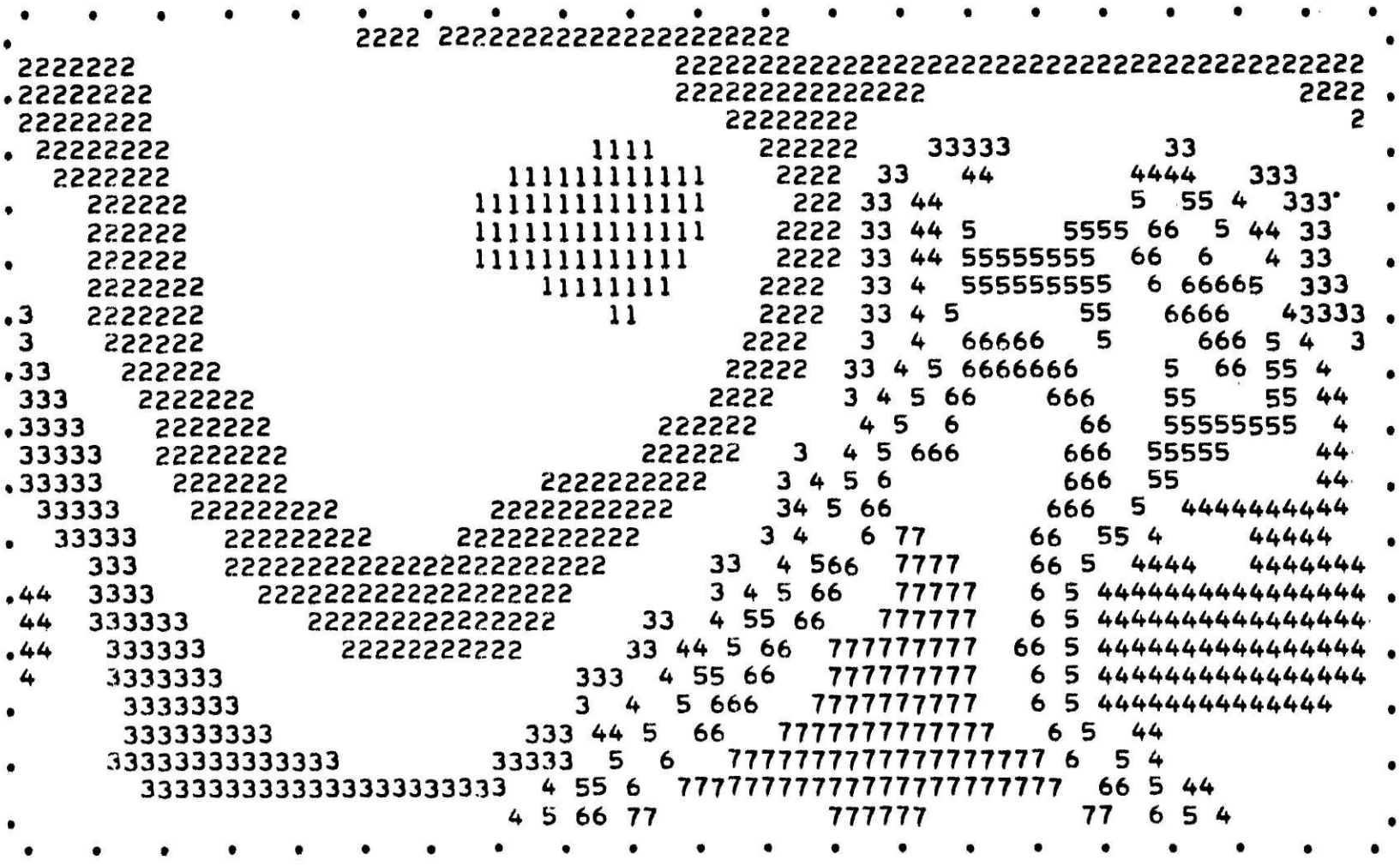

Figure 6.3.15 run 3 $\overline{M_2^{\theta}}$ after 5 days.

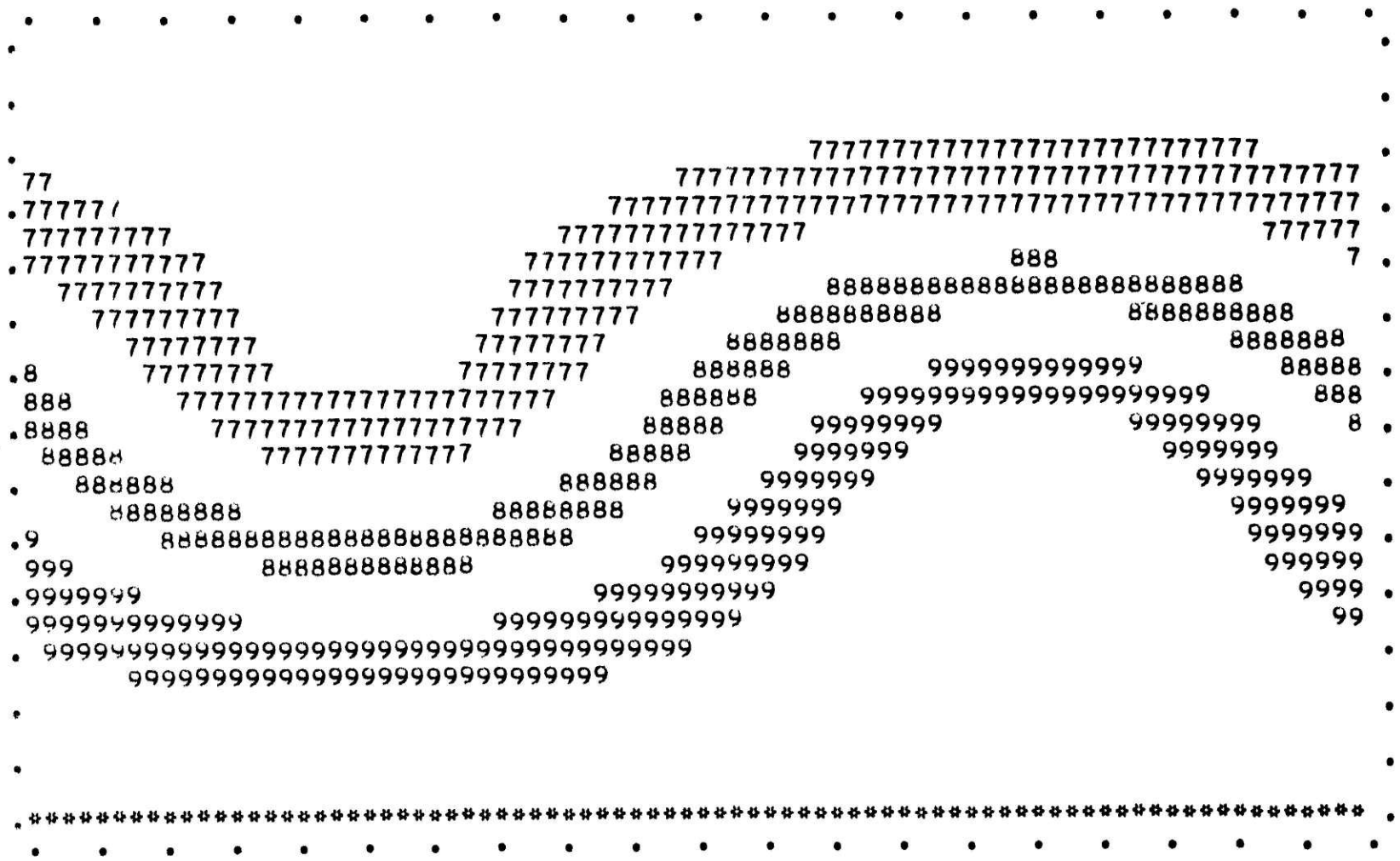

Figure 6.4.1 Initial $\overline{M}_2^0$ for runs 4 and 5.

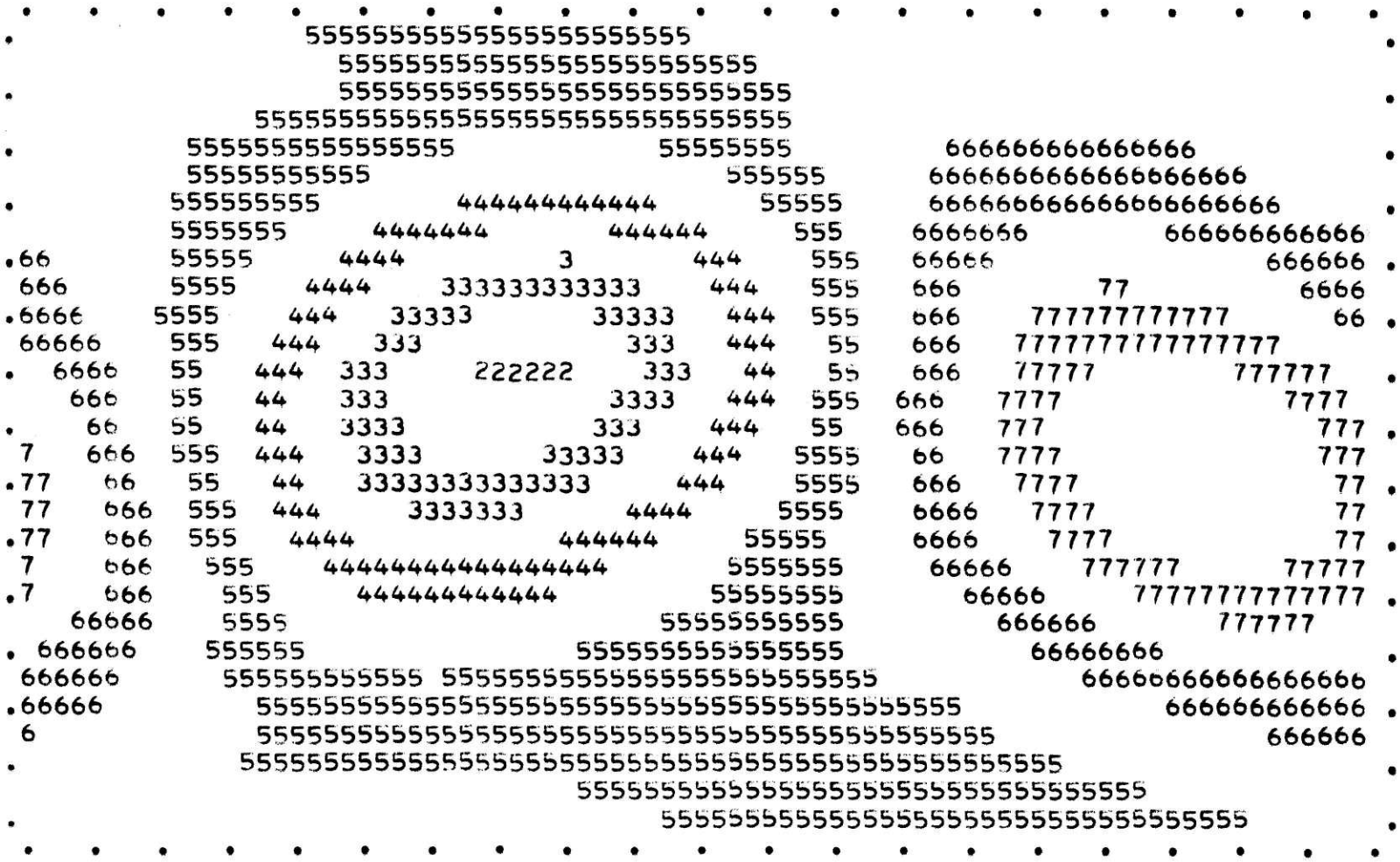

Figure 6.4.2 run 4 p_s after 1 day.

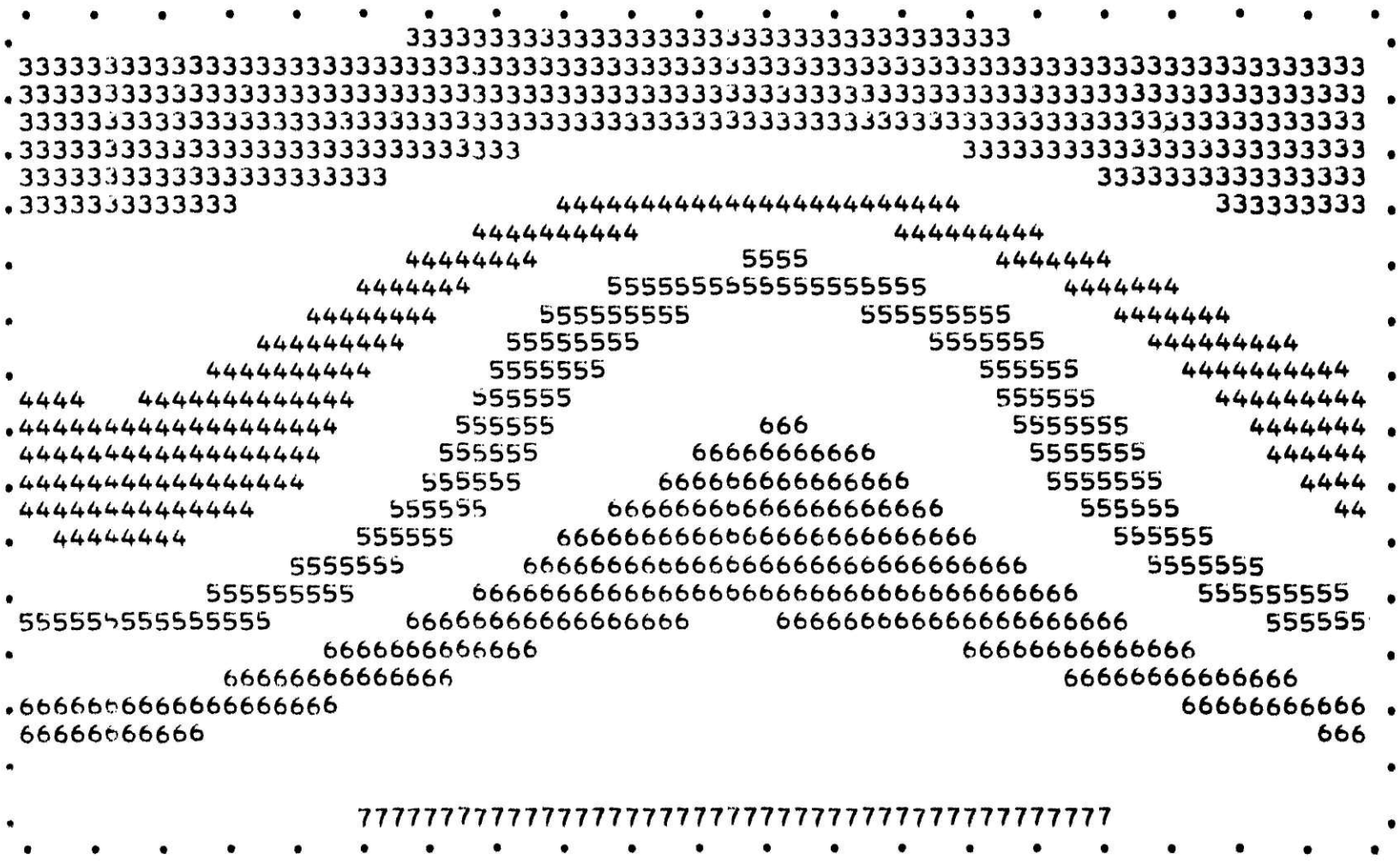

Figure 6.4.3 run 4 θ_J after 1 day.

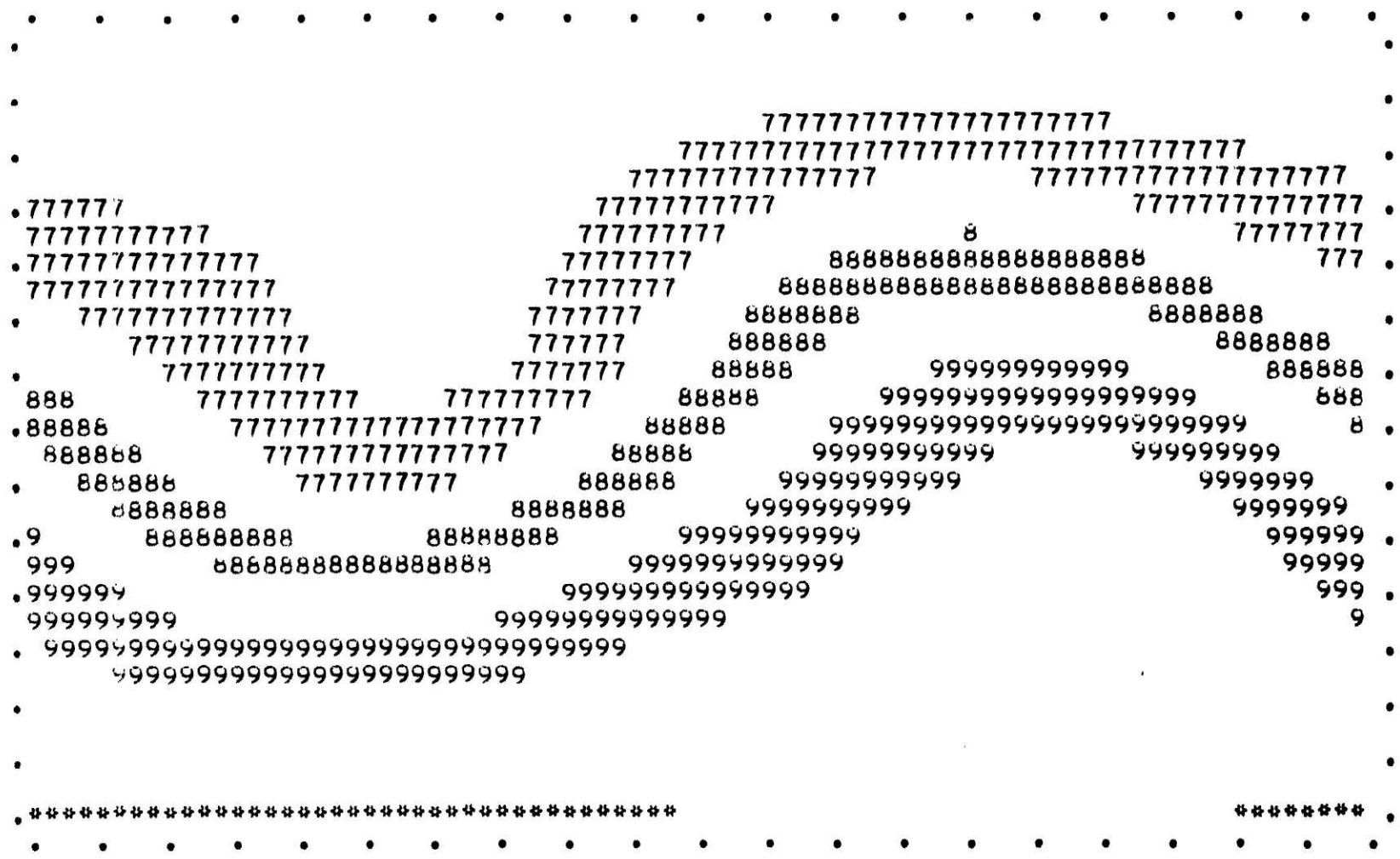

Figure 6.4.4 run 4 $\overline{M}_2^{\theta}$ after 1 day.

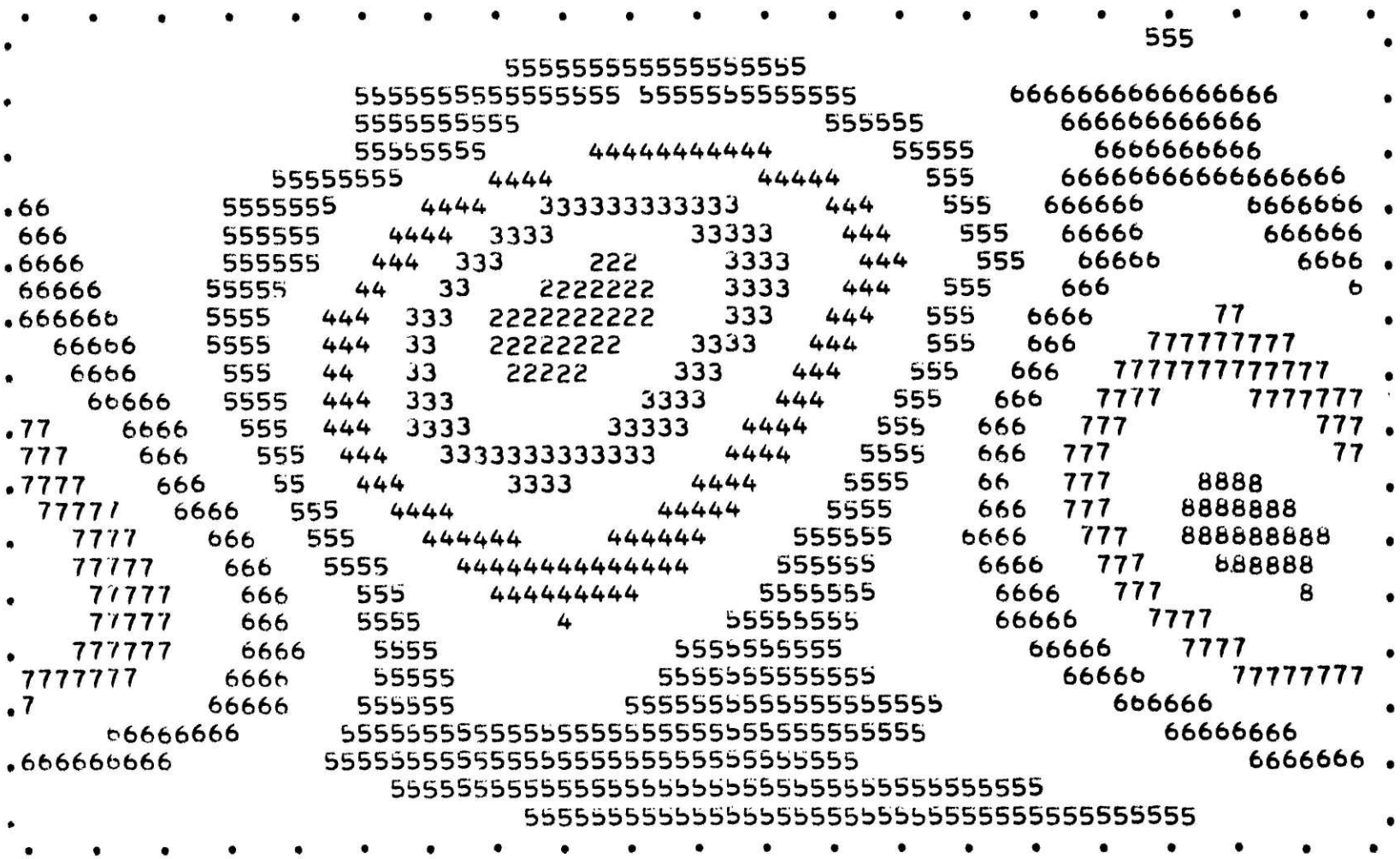

Figure 6.4.5 run 4 p_s after 2 days.

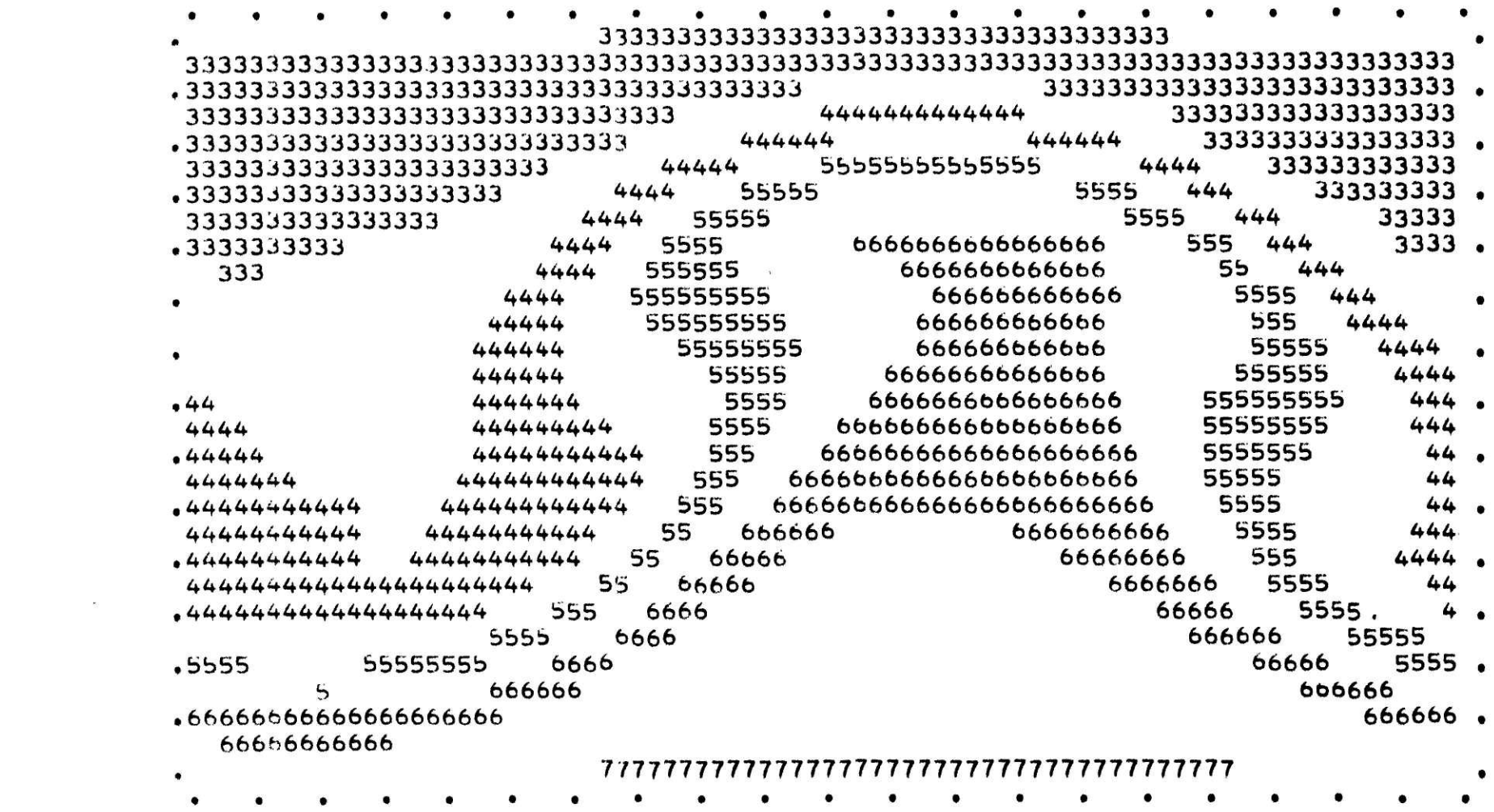

Figure 6.4.6 run 4 θ_s after 2 days.

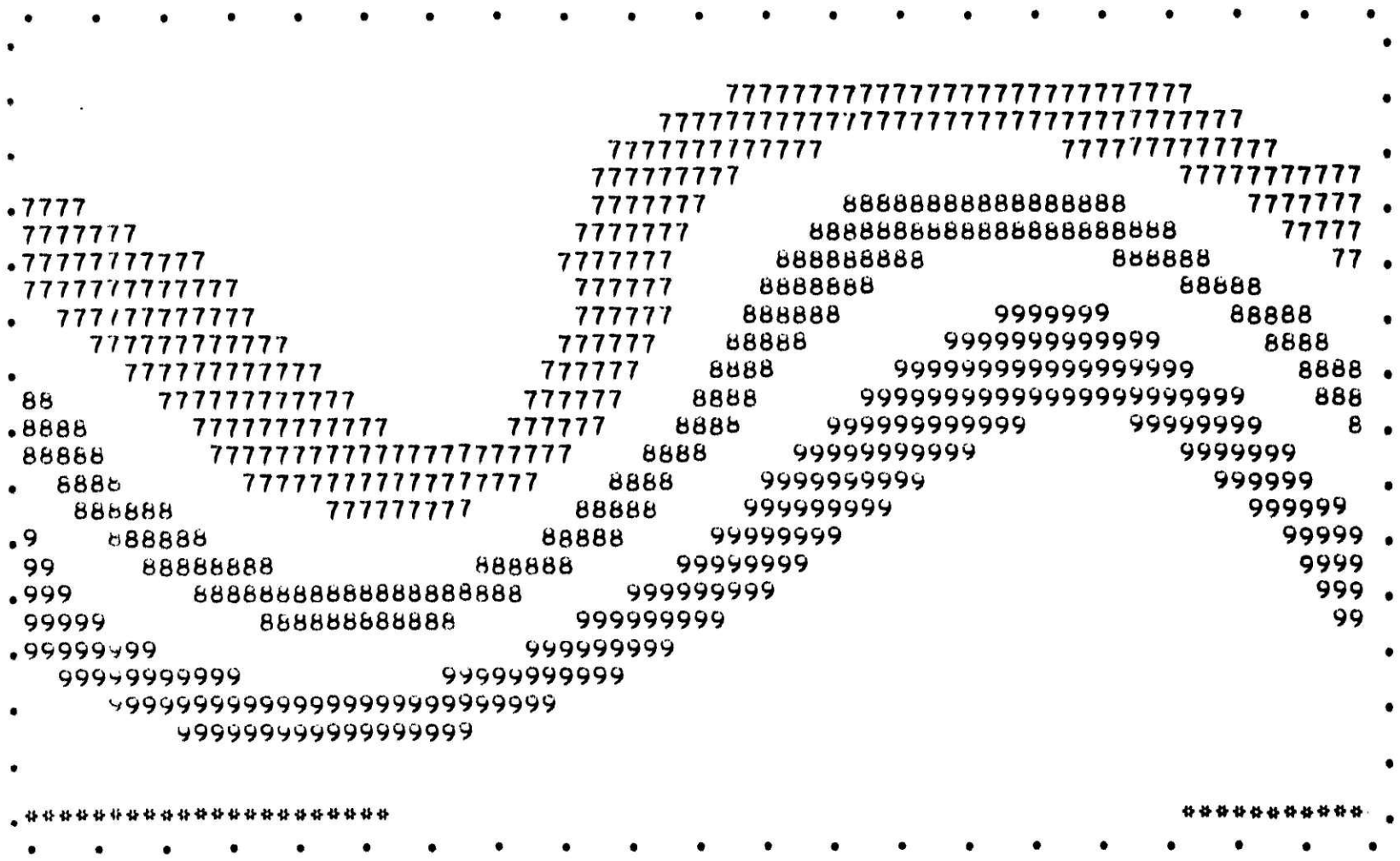

Figure 6.4.7 run 4 $\overline{M}_2^{\theta}$ after 2 days.

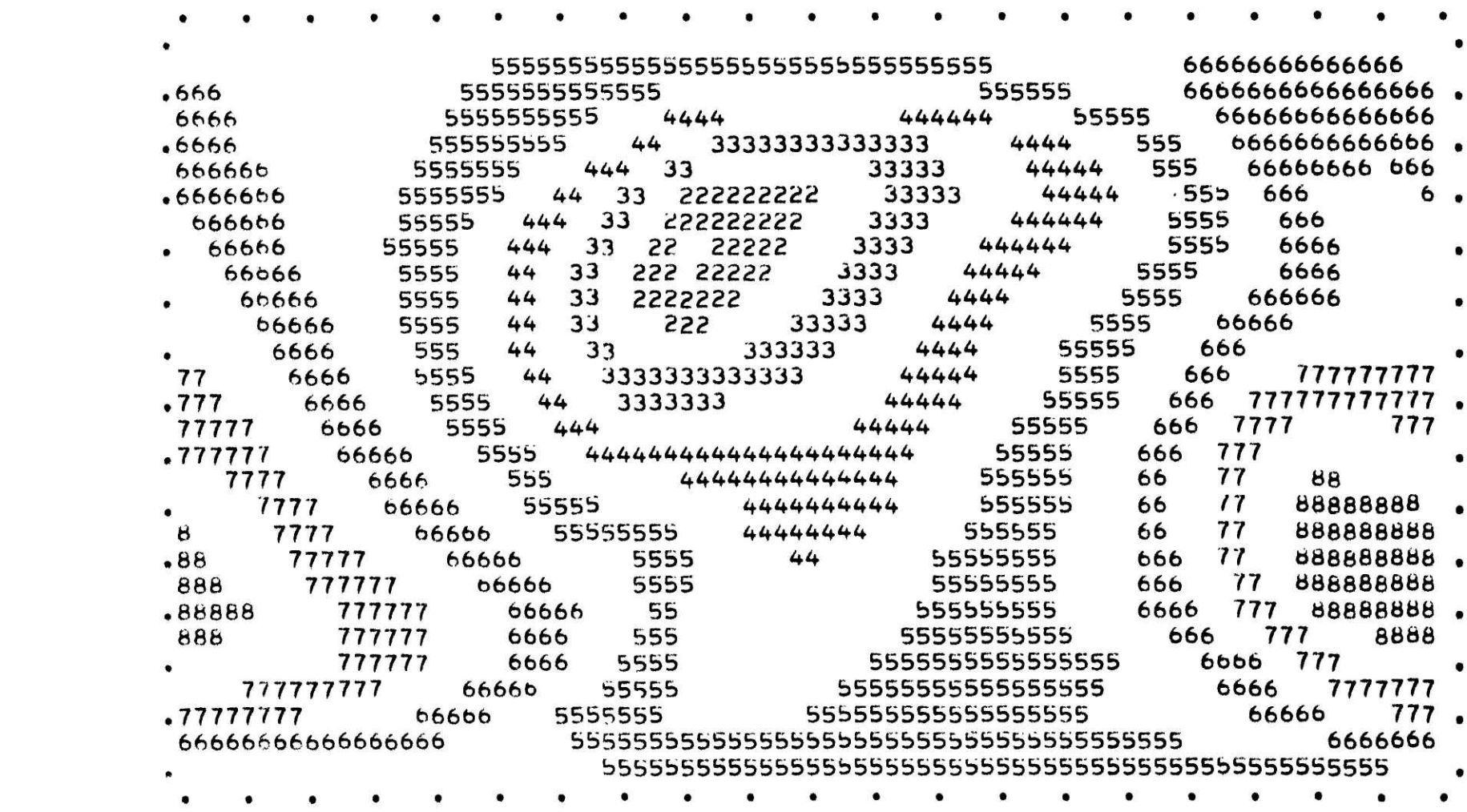

Figure 6.4.8 run 4 p_s after 3 days.

Figure 6.4.9 run 4 θ_5 after 3 days.

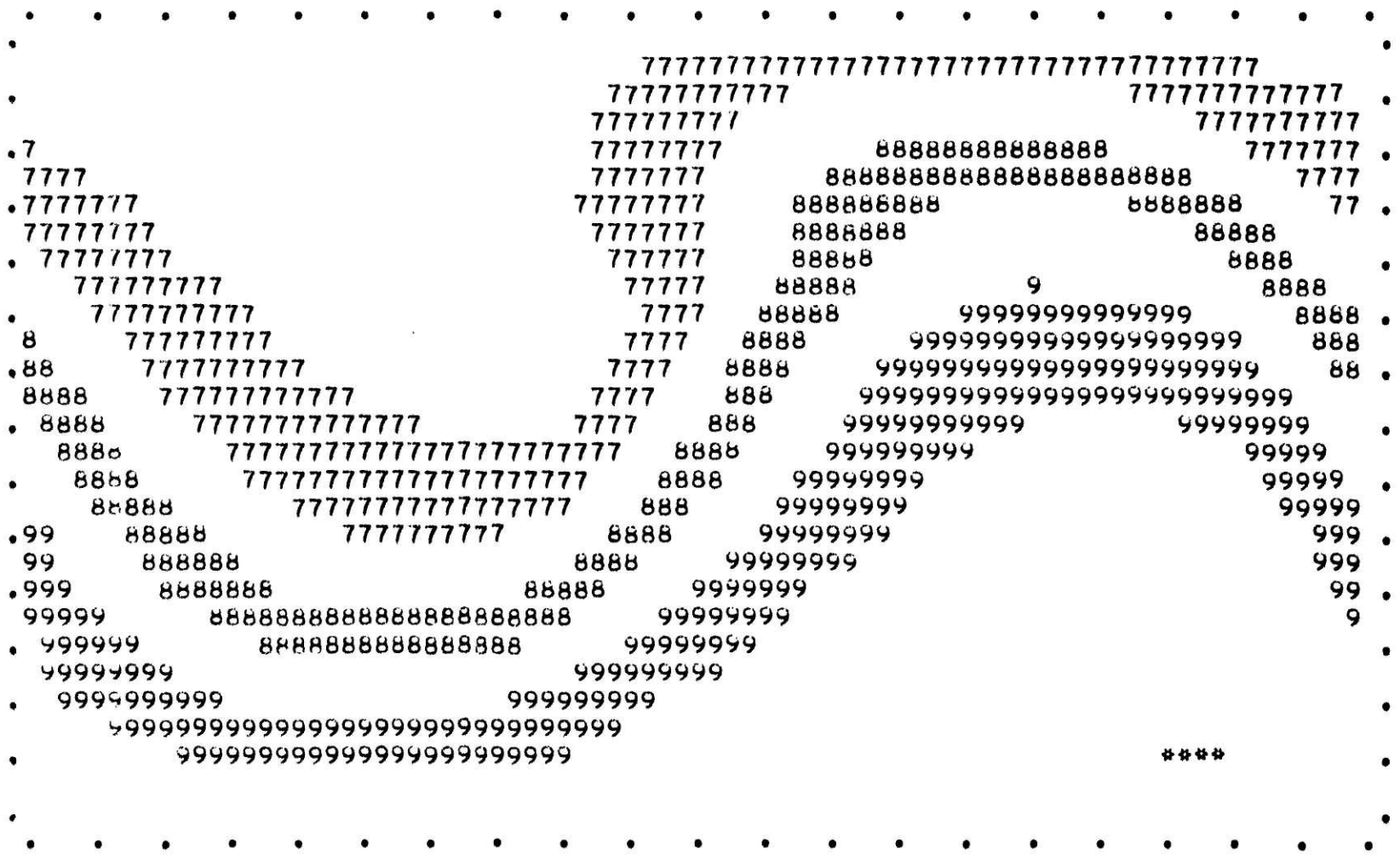

Figure 6.4.10 run 4 $\bar{M}_2^{\theta}$ after 3 days.

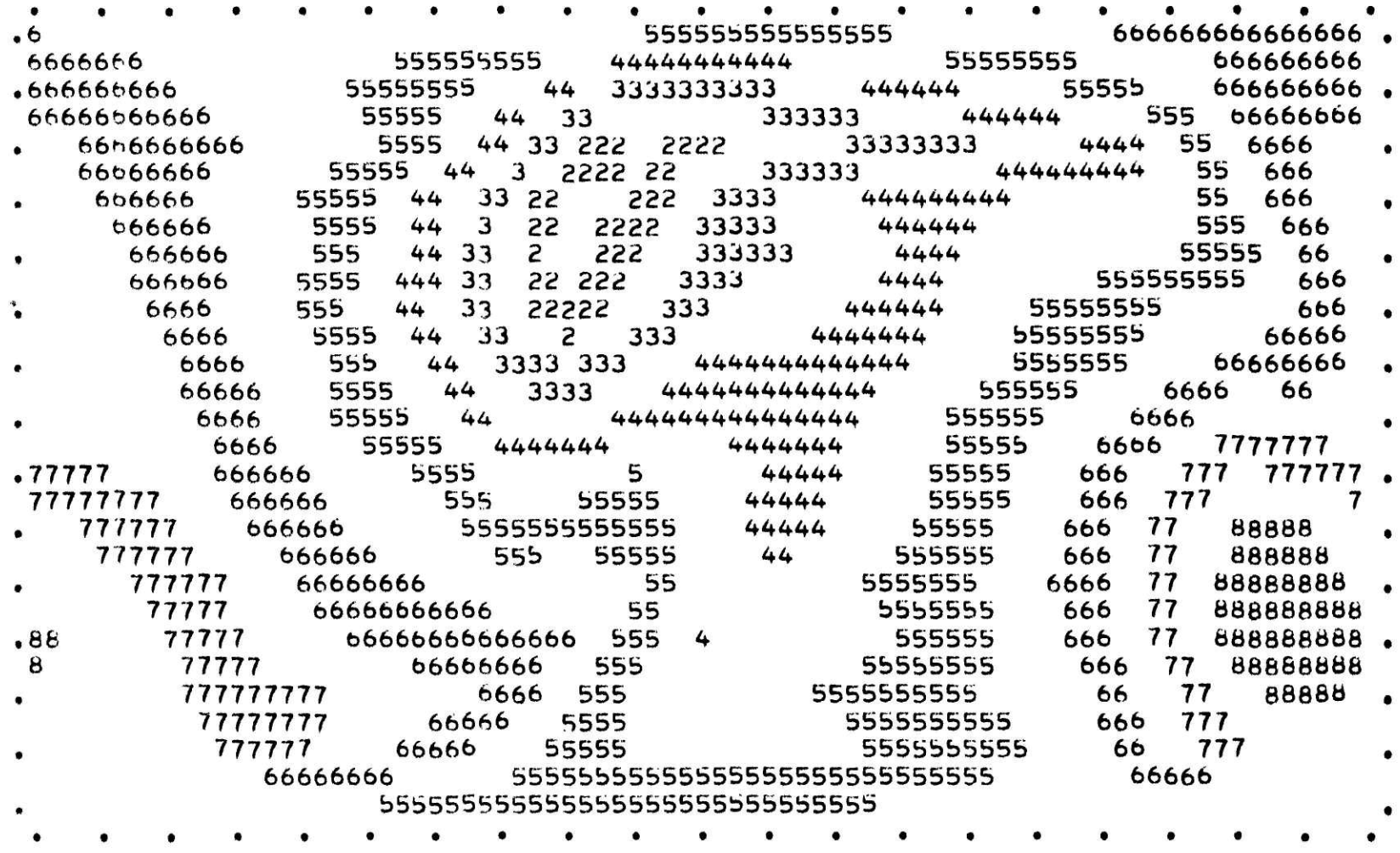

Figure 6.4.11 run 4 p_s after 4 days.

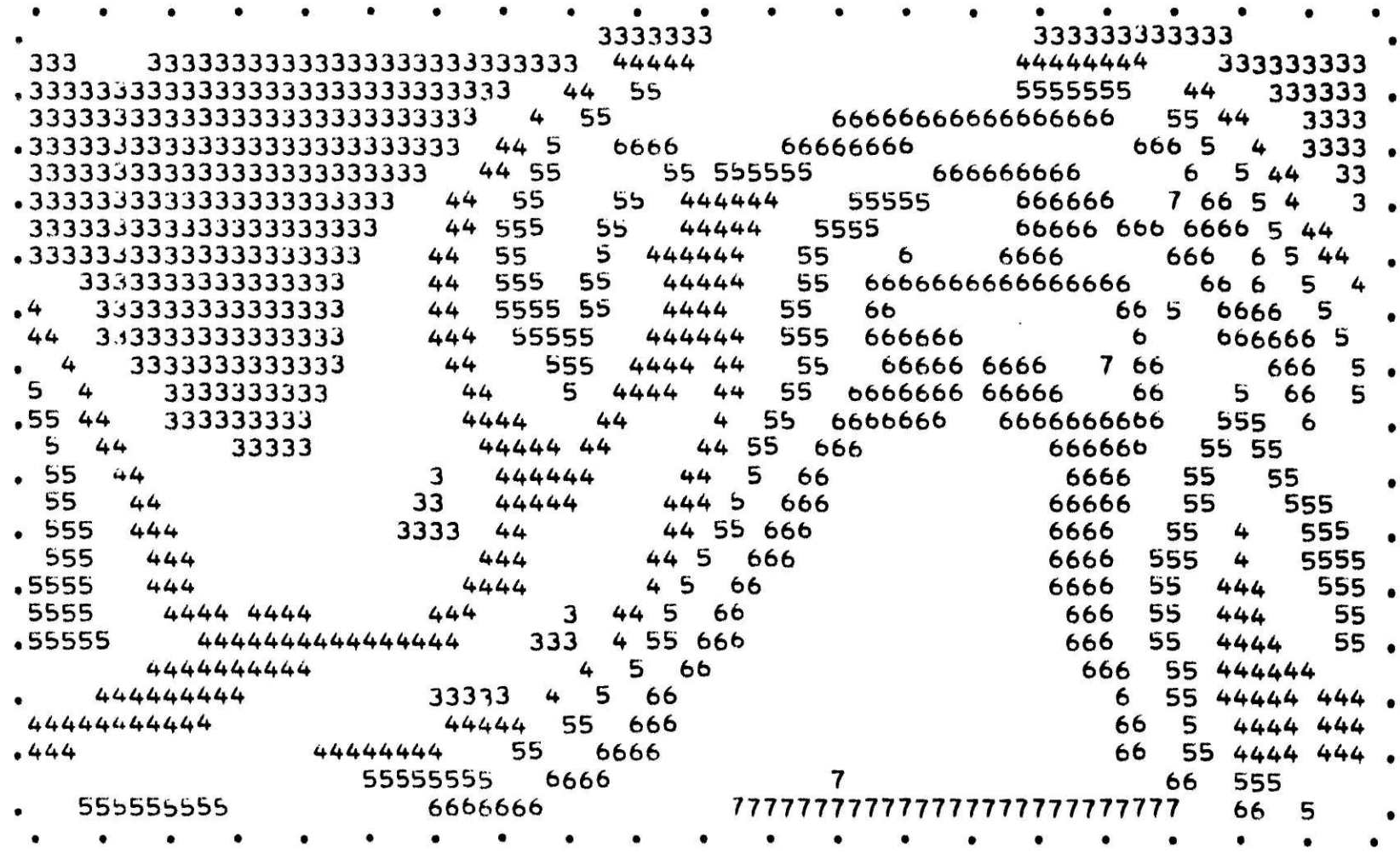

Figure 6.4.12 run 4 θ_S after 4 days.

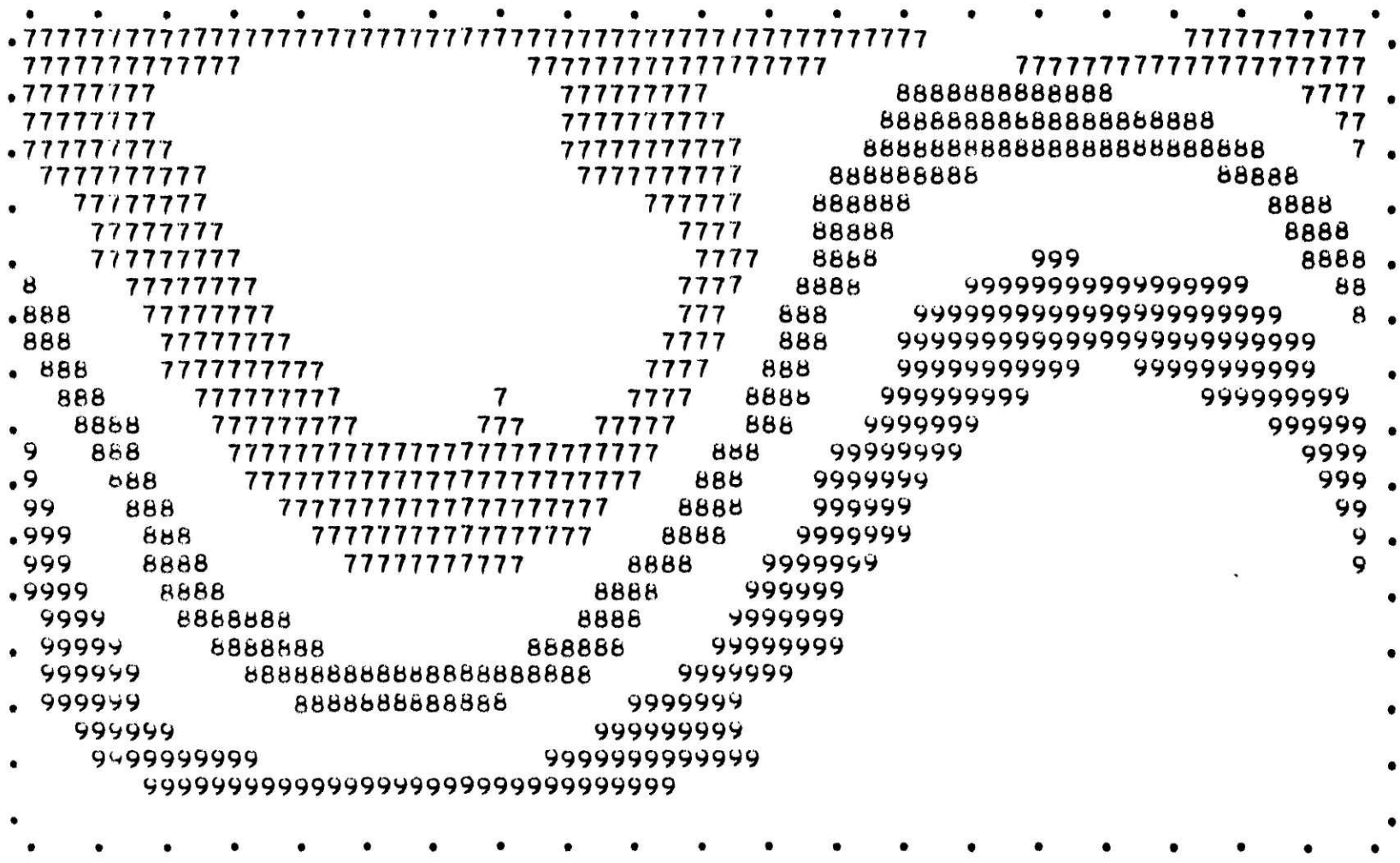

Figure 6.4.13 run 4 $\bar{M}_2^{\theta}$ after 4 days.

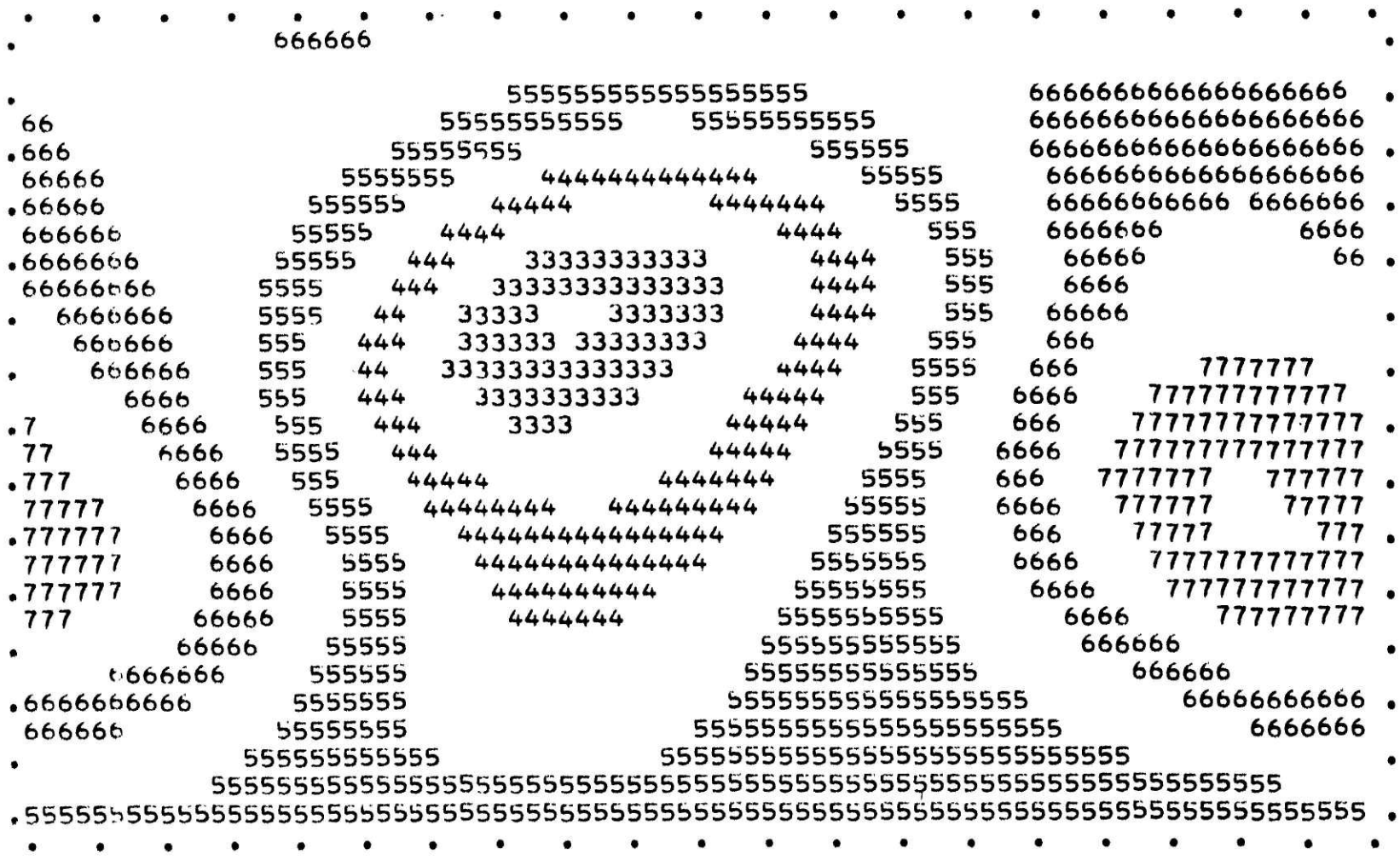

Figure 6.5.1 run 5 p_s after 2 days.

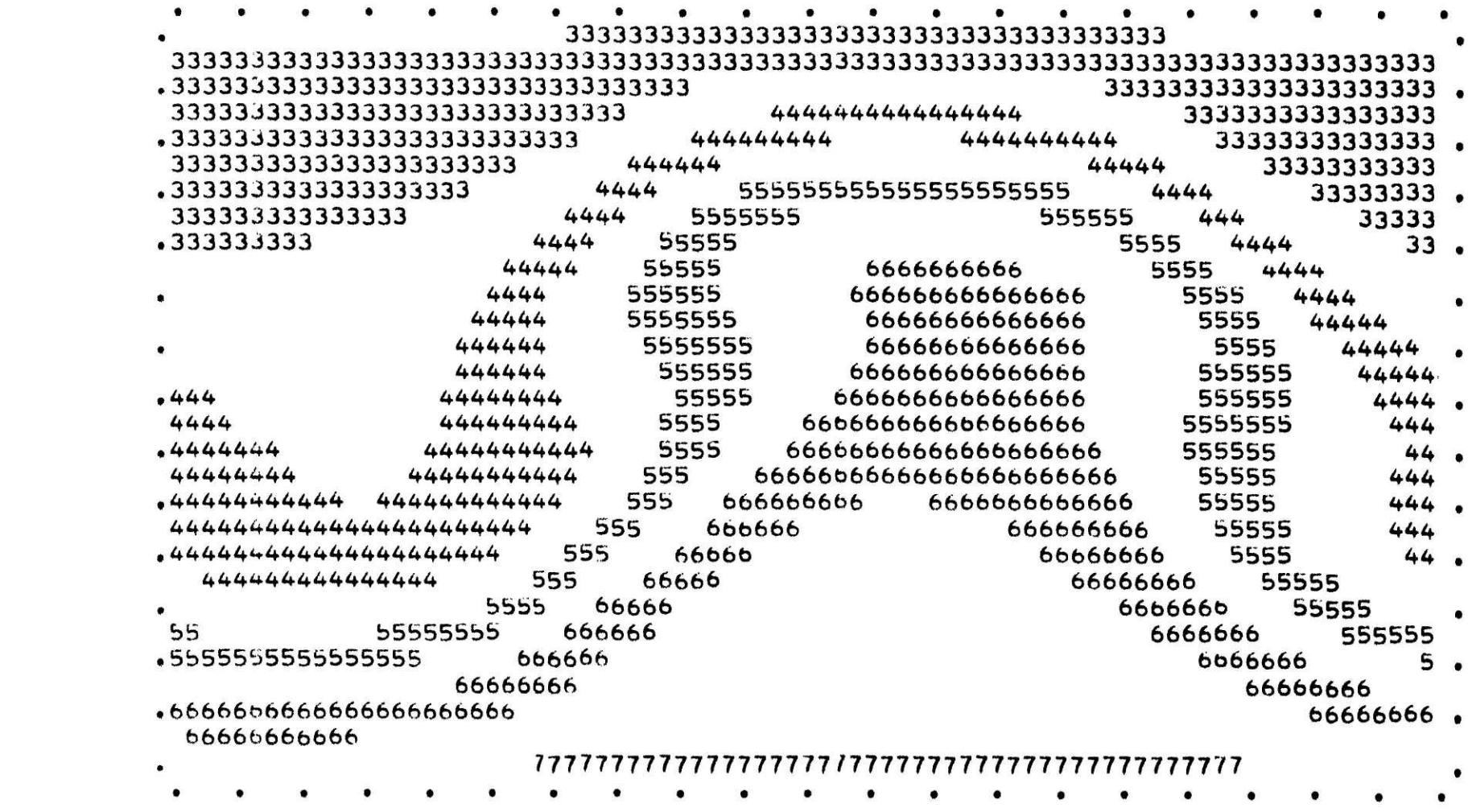

Figure 6.5.2 run 5 θ_s after 2 days.

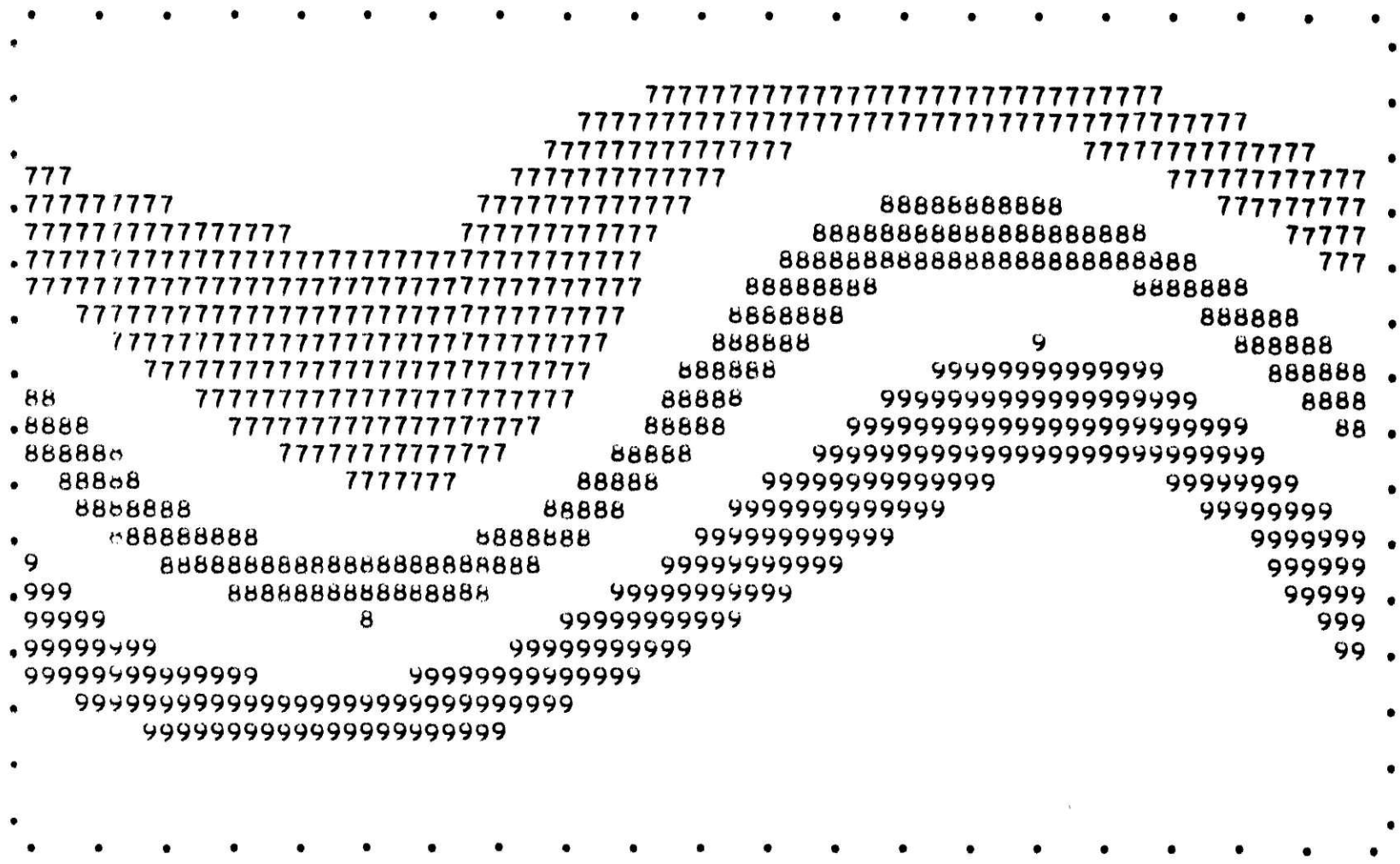

Figure 6.5.3 run 5 $\overline{M}_2^{\theta}$ after 2 days.

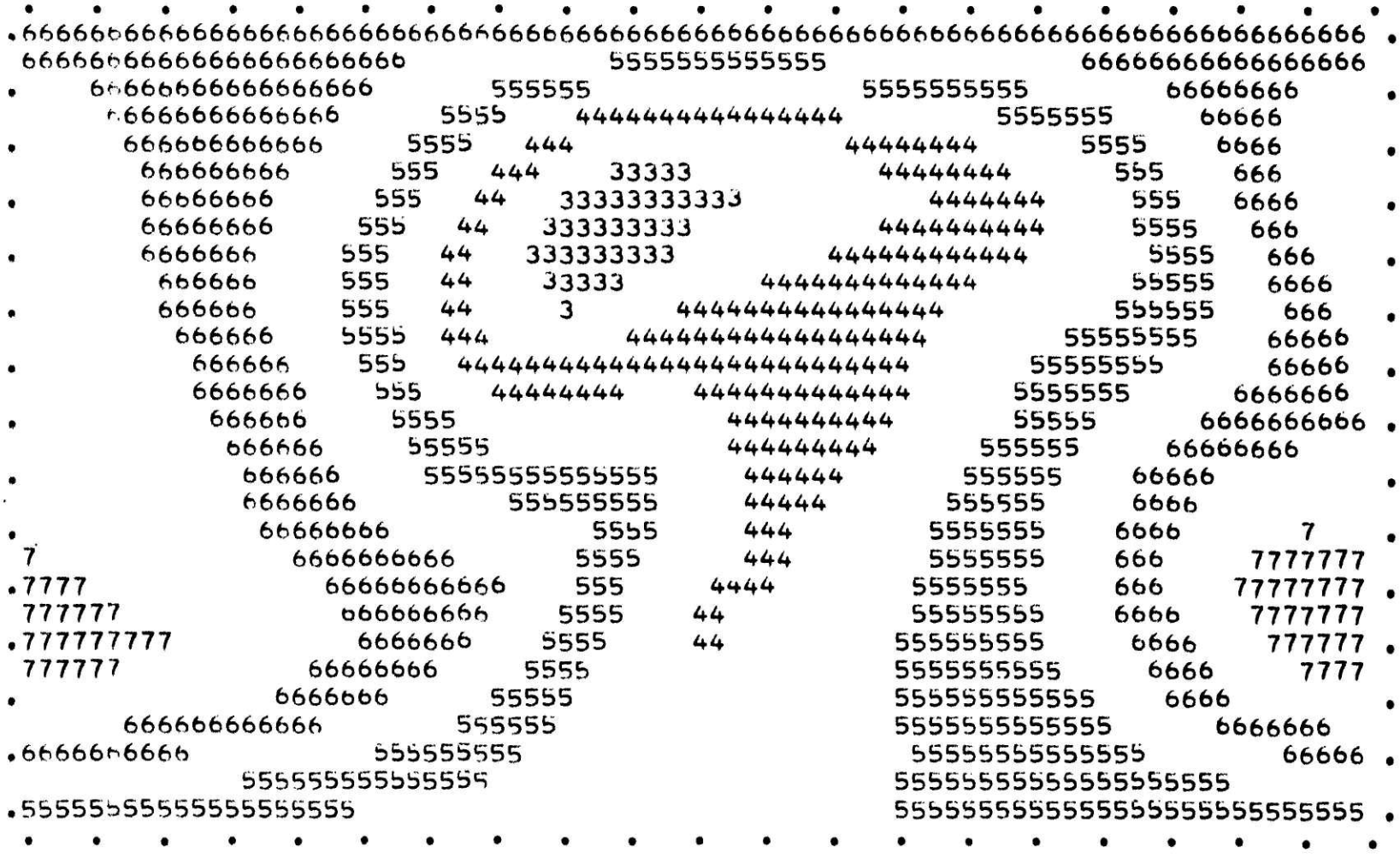

Figure 6.5.4 run 5 p_s after 4 days.

Figure 6.5.5 run 5 θ_S after 4 days.

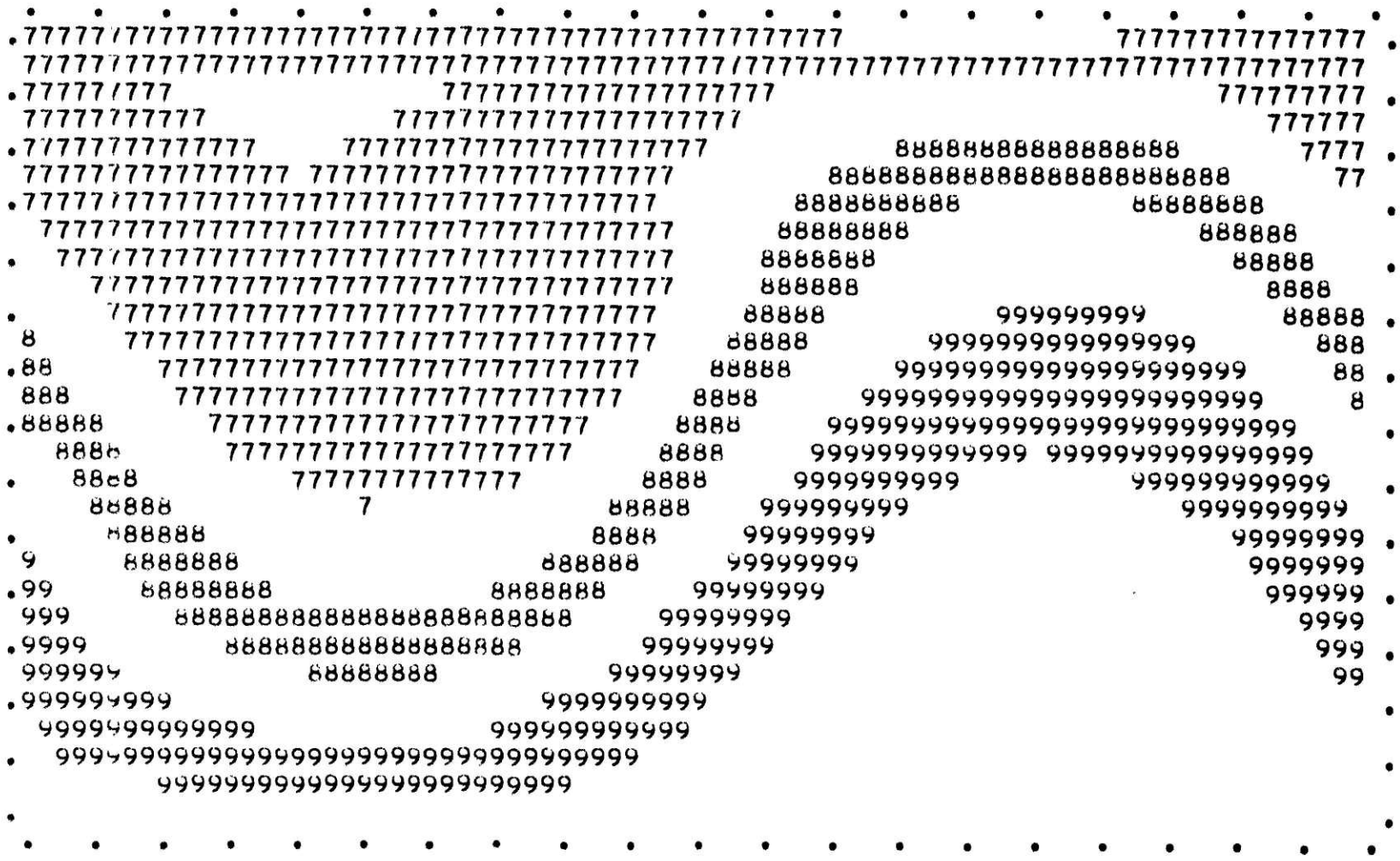

Figure 6.5.6 run 5 $\tilde{M}_2^{\theta}$ after 4 days.

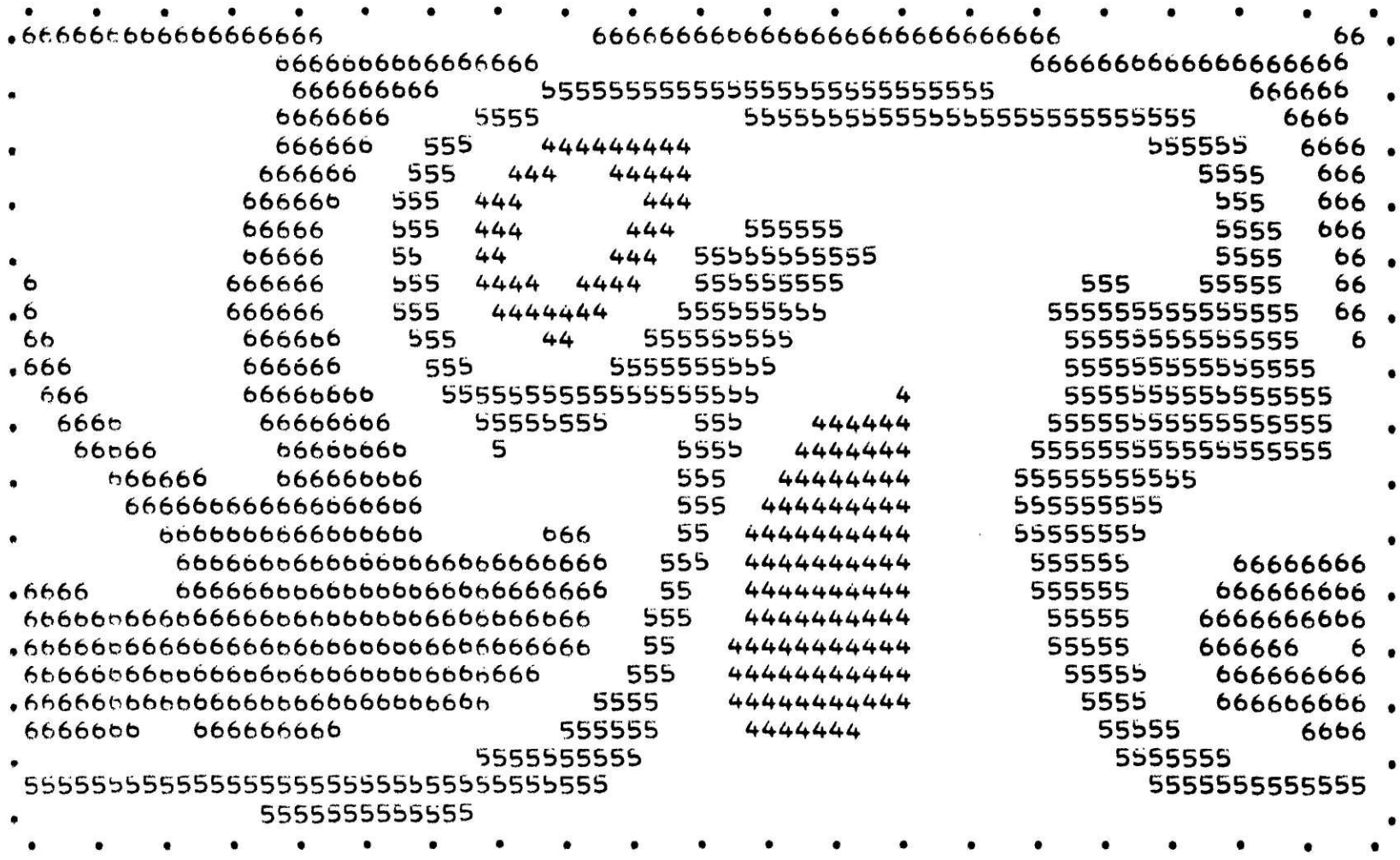

Figure 6.5.7 run 5 p_s after 6 days.

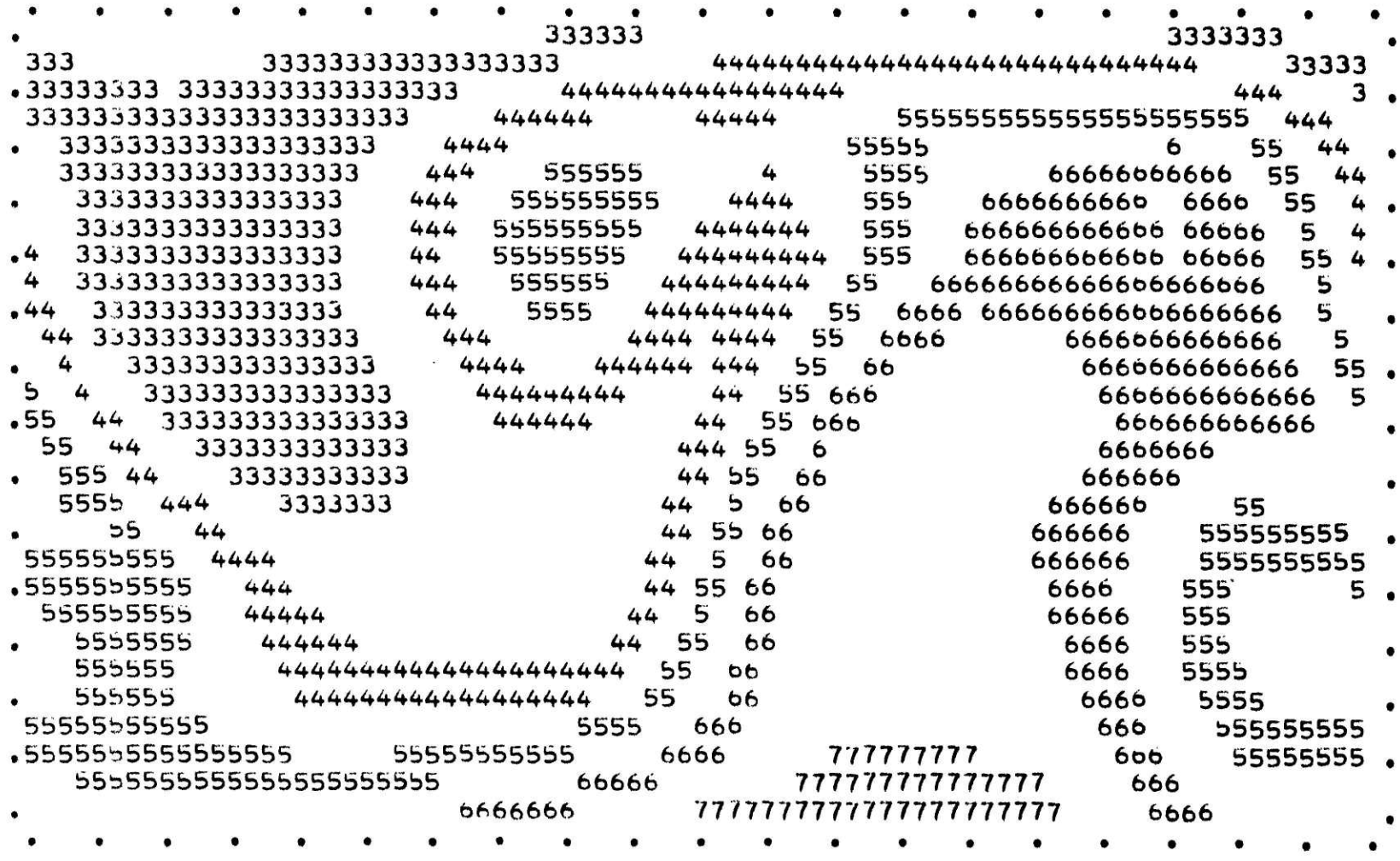

Figure 6.5.8 run 5 θ_5 after 6 days.

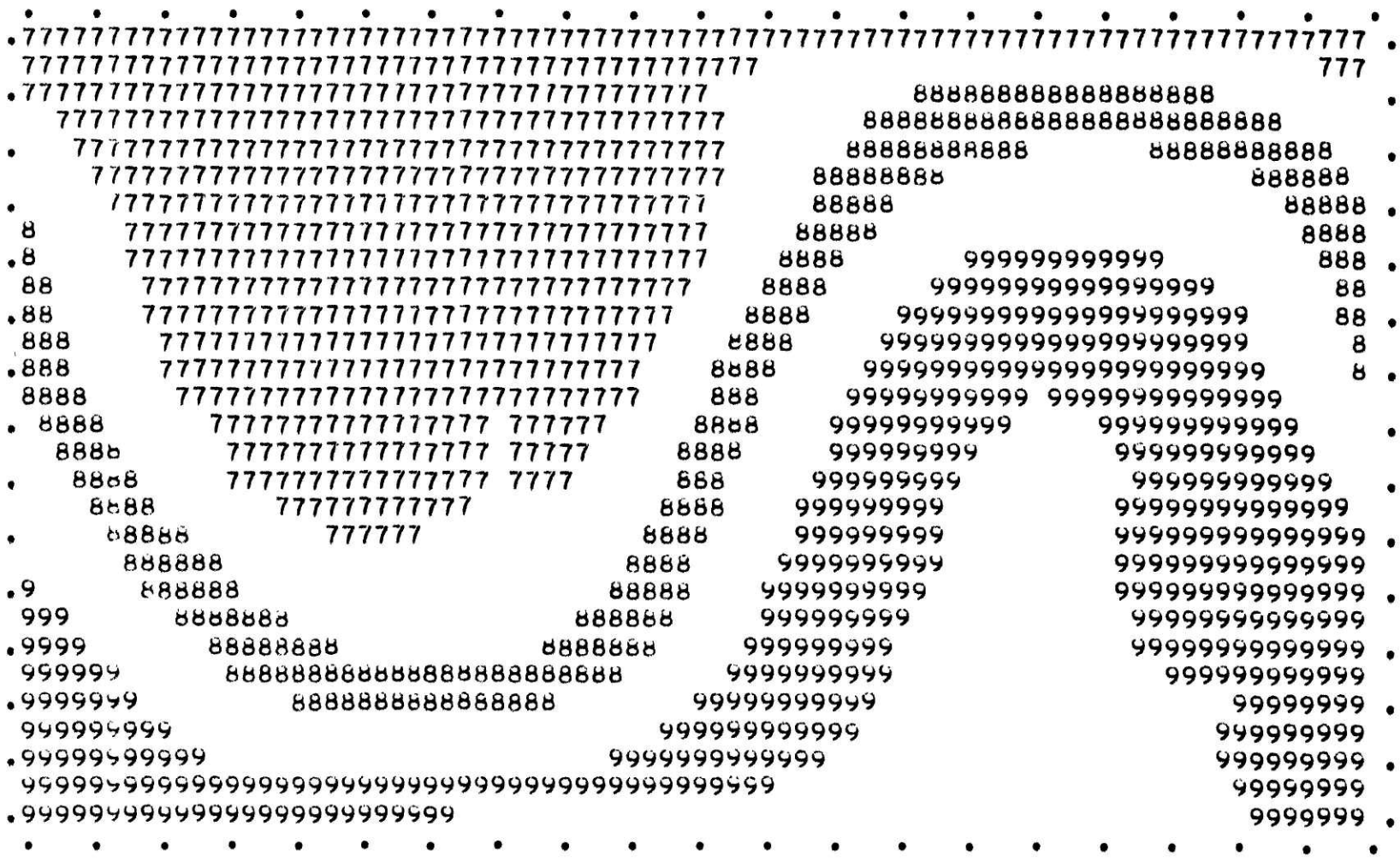

Figure 6.5.9 run 5 $\overline{M}_2^{\theta}$ after 6 days.

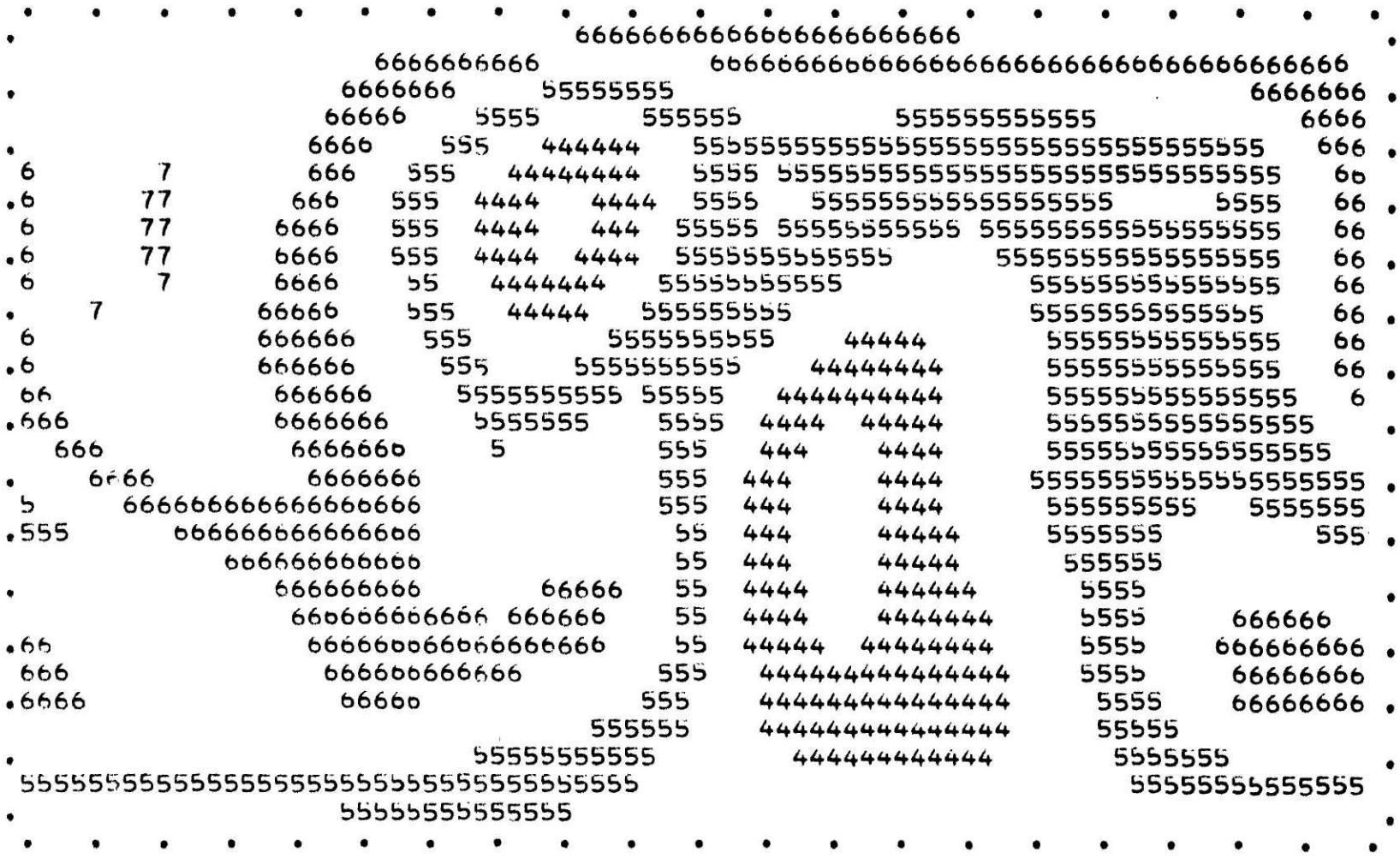

Figure 6.5.10 run 5 p_s after 7 days.

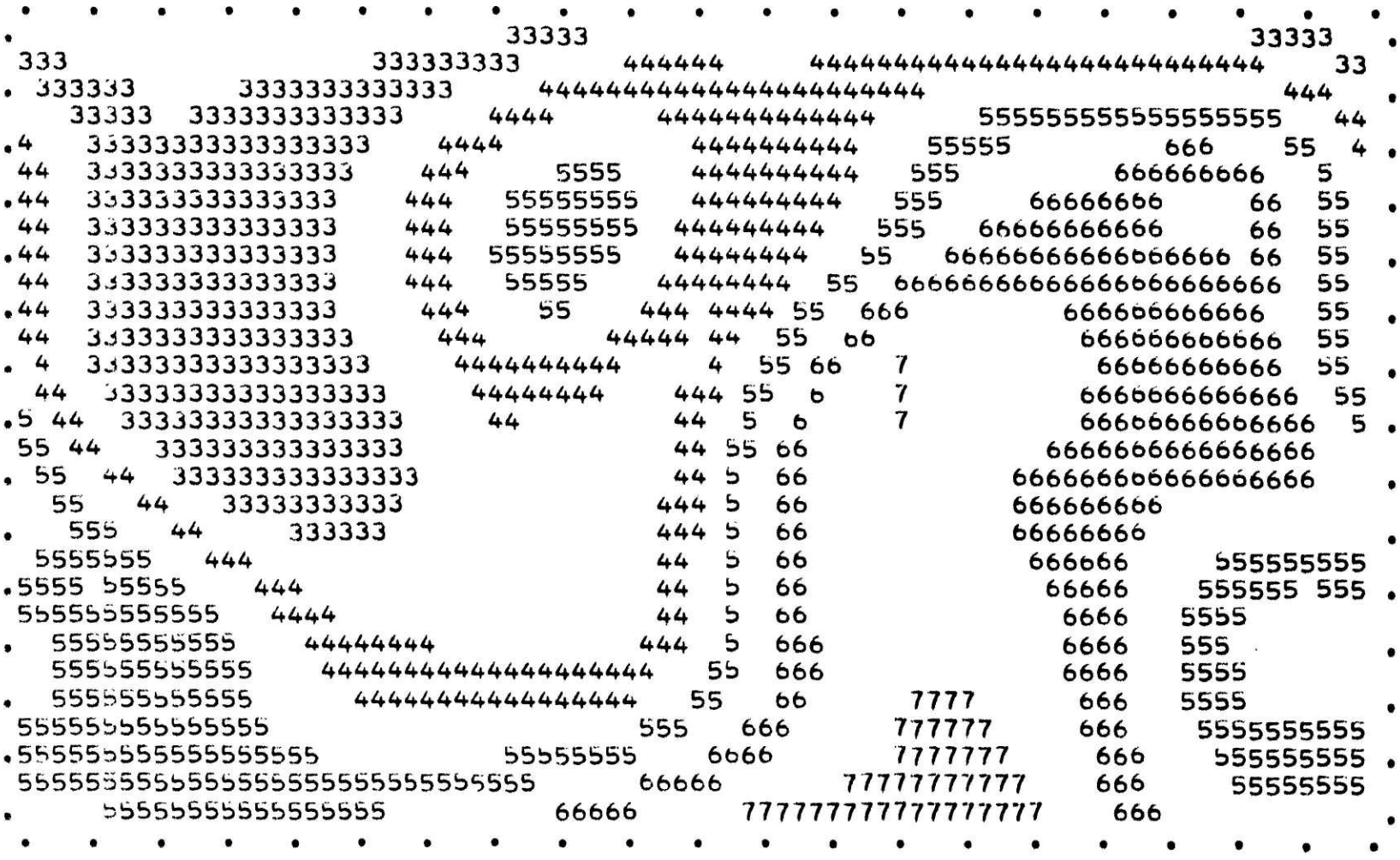

Figure 6.5.11 run 5 θ_5 after 7 days.

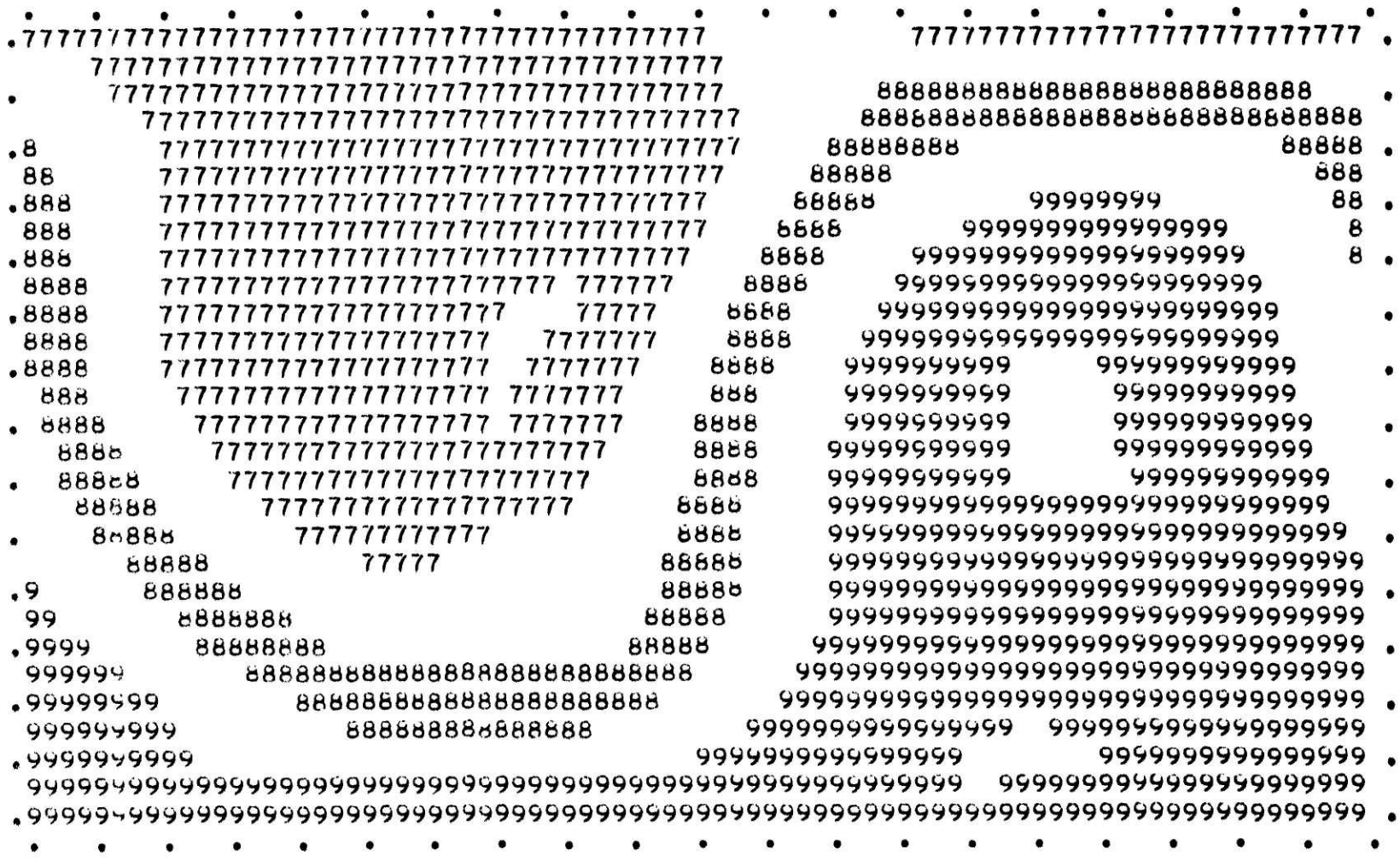

Figure 6.5.12 run 5 $\bar{M}_2^{\theta}$ after 7 days.

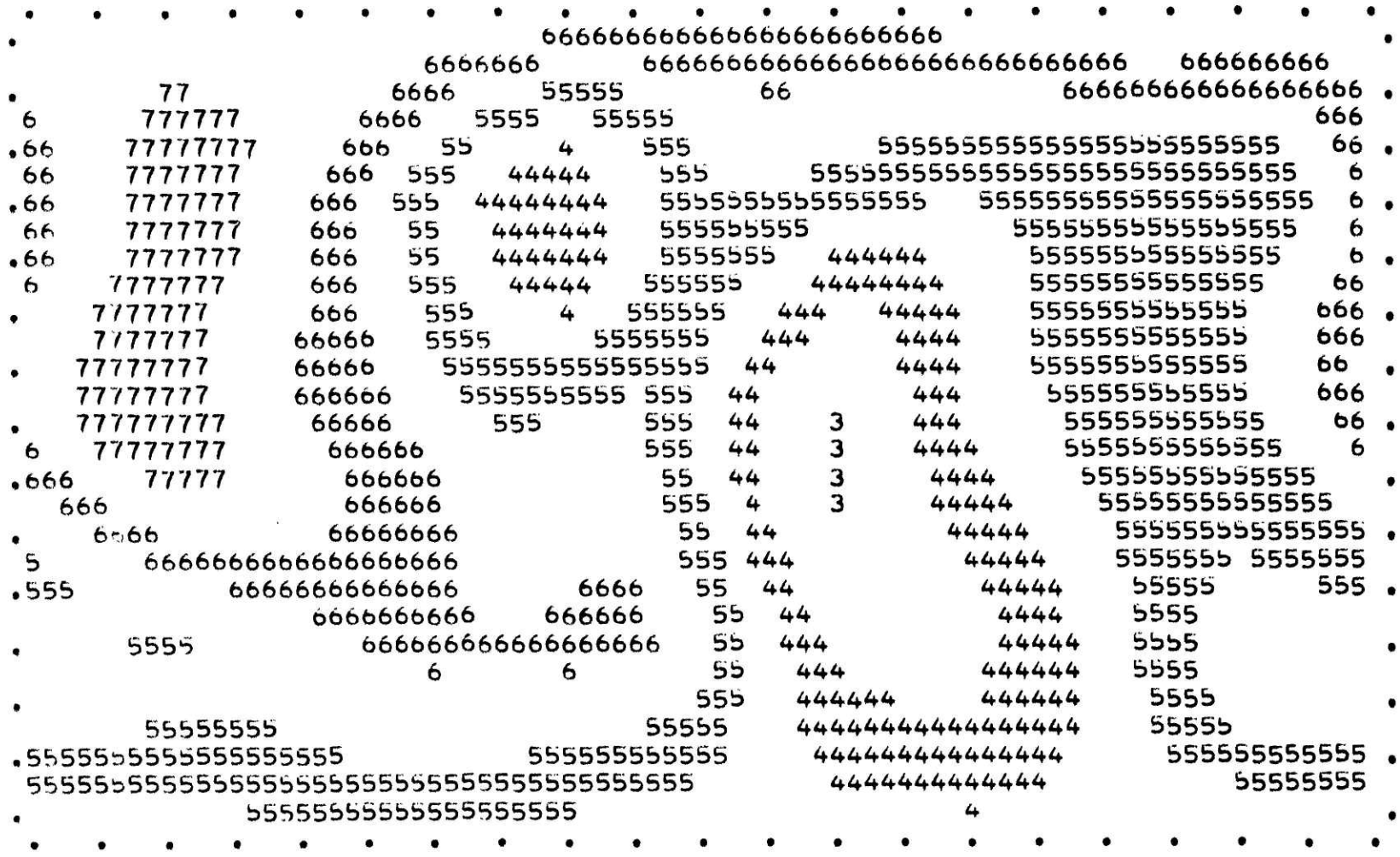

Figure 6.5 13 run 5 p_s after 8 days.

Figure 6.5.14 run 5 θ_5 after 8 days.

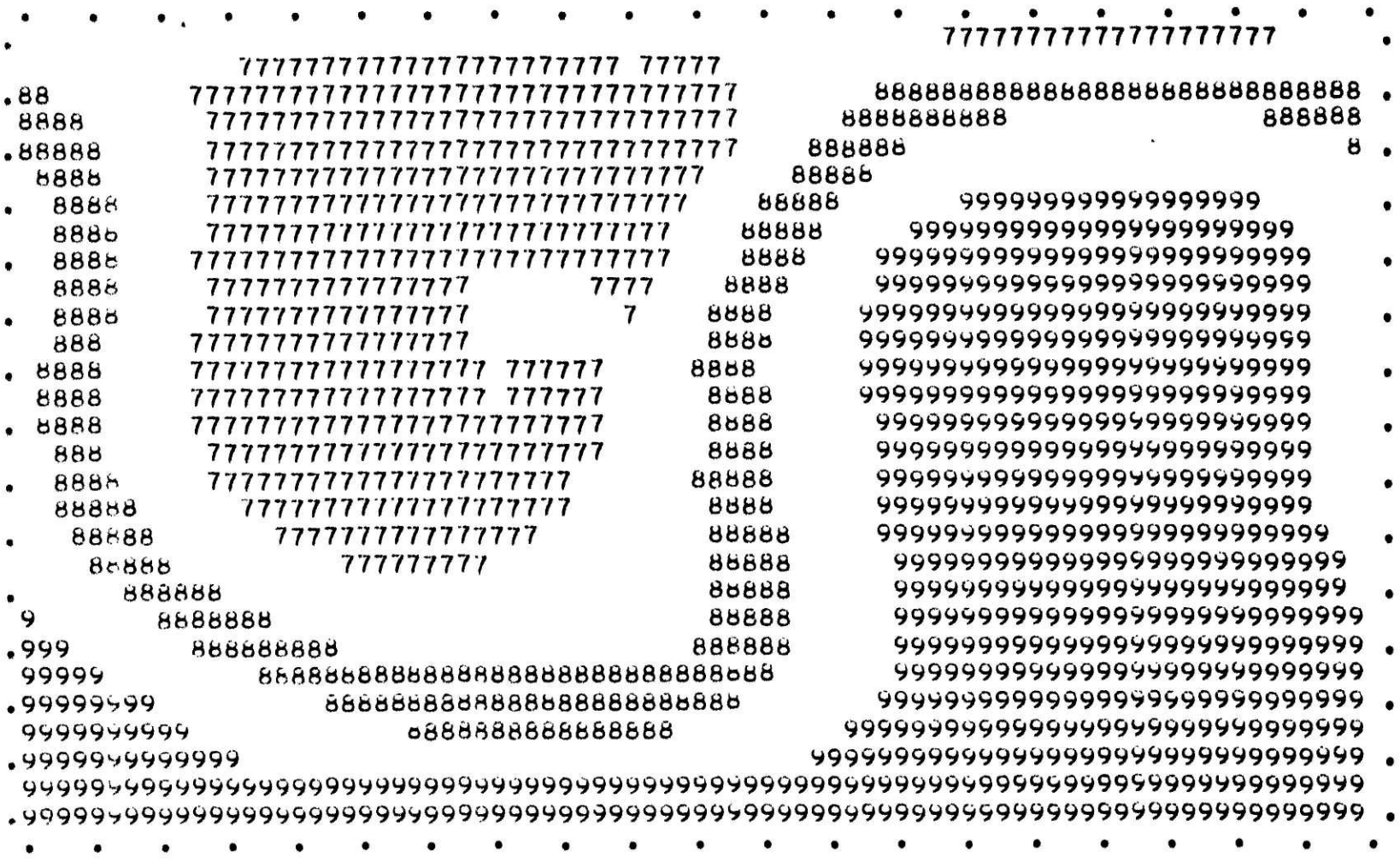

Figure 6.5.15 run 5 $\overline{M}_2$ after 8 days.

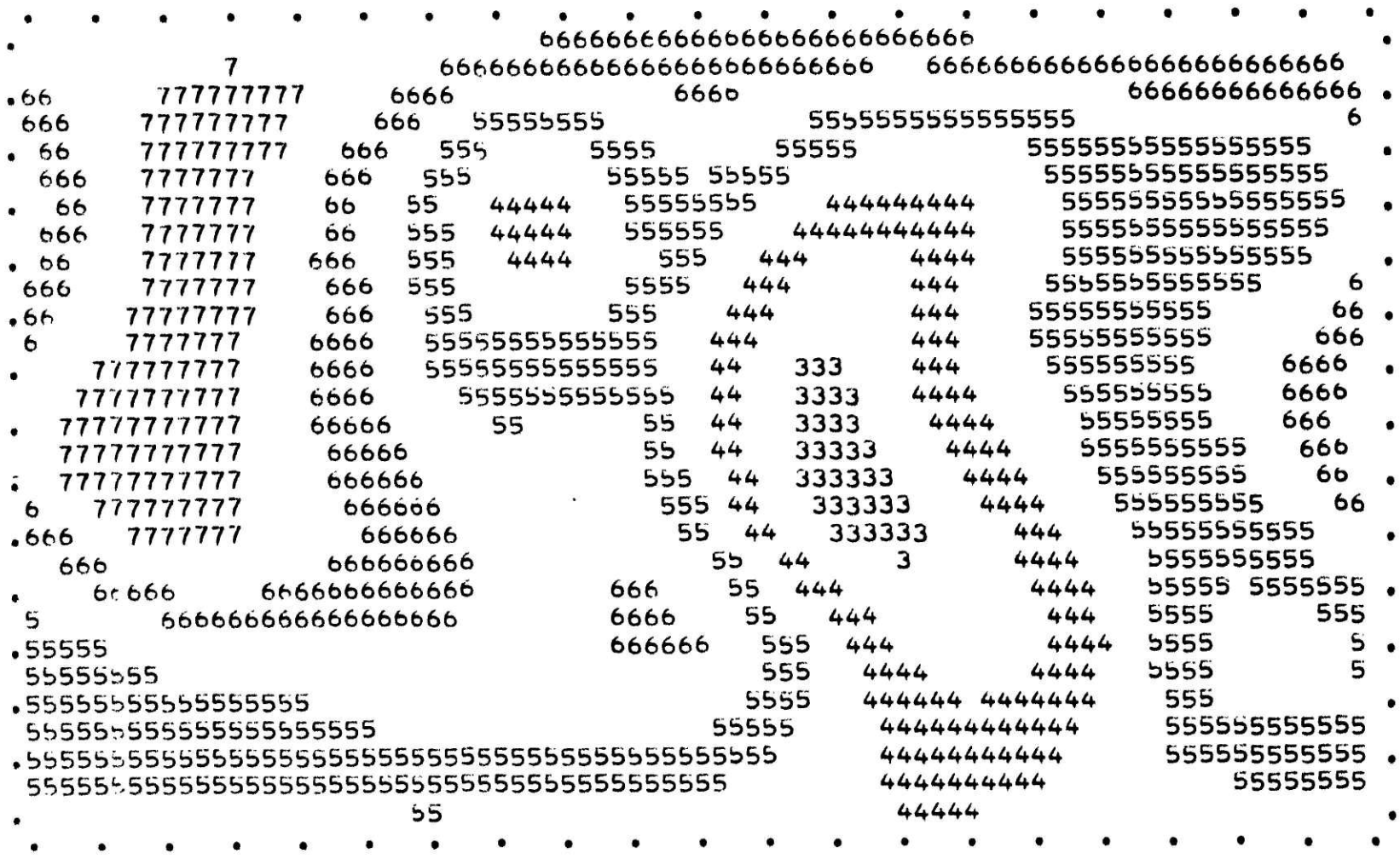

Figure 6.5.16 run 5 p_s after 9 days.

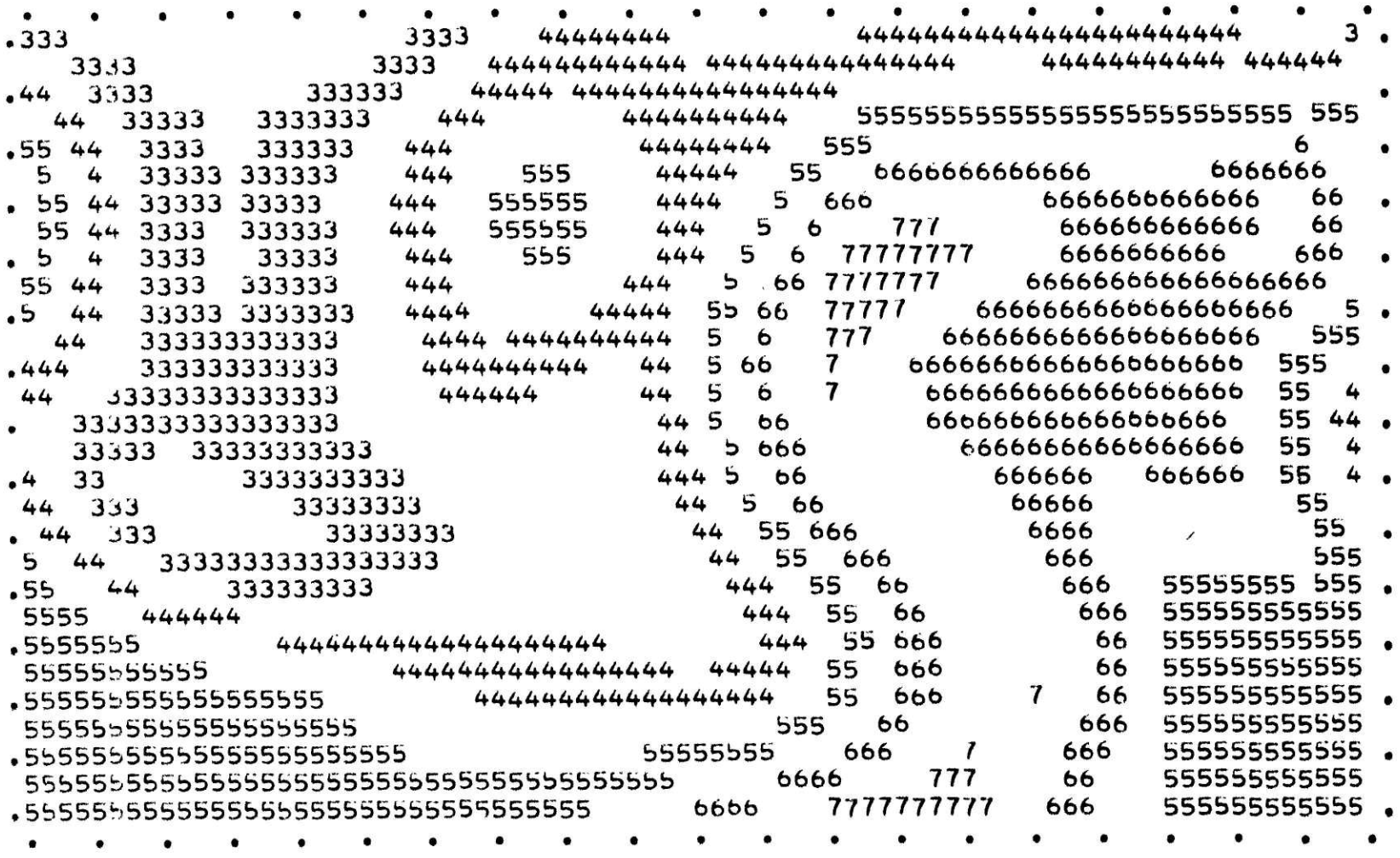

Figure 6.5.17 run 5 θ_s after 9 days.

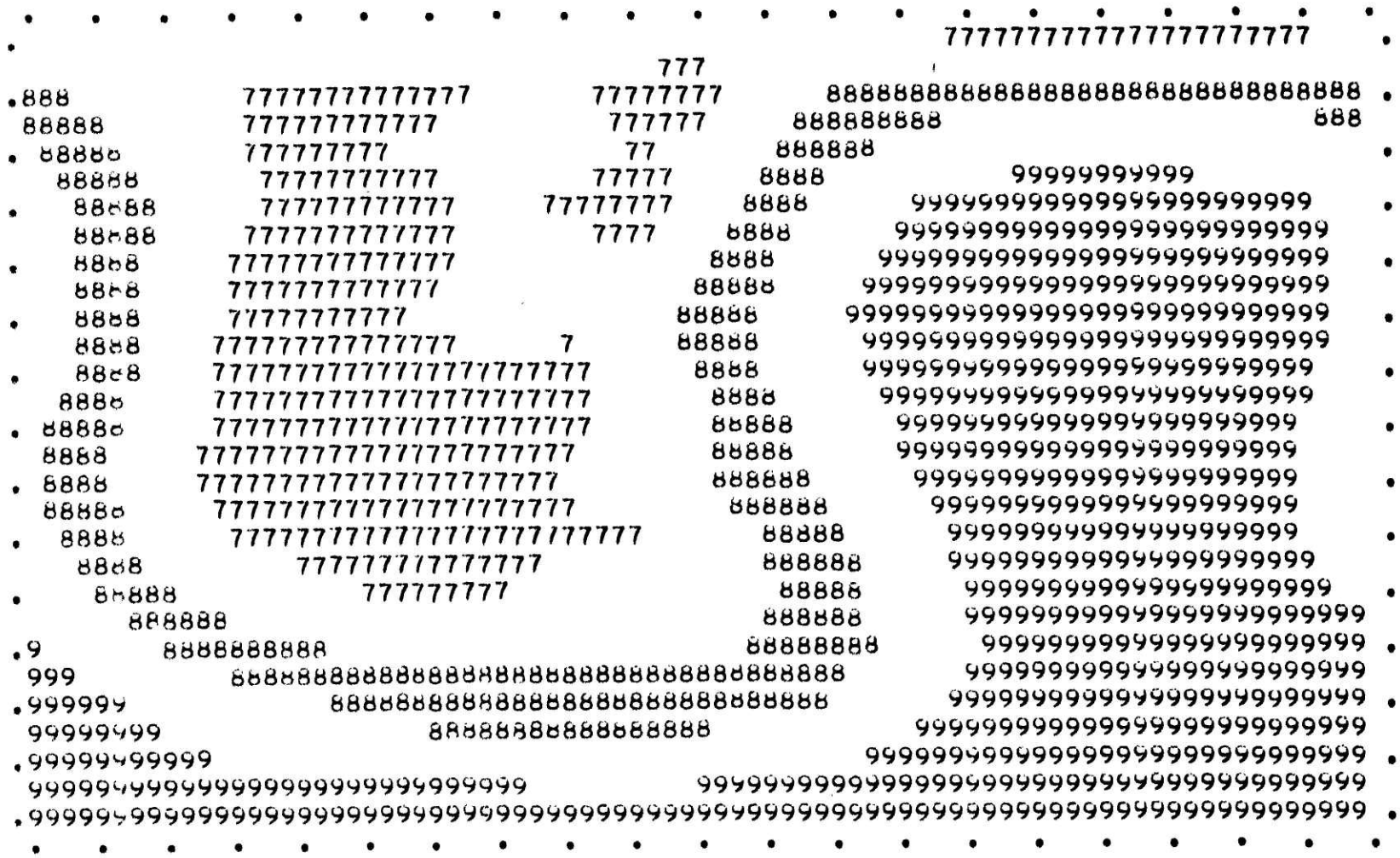

Figure 6.5.18 run 5 $\overline{M}_2^{\theta}$ after 9 days.

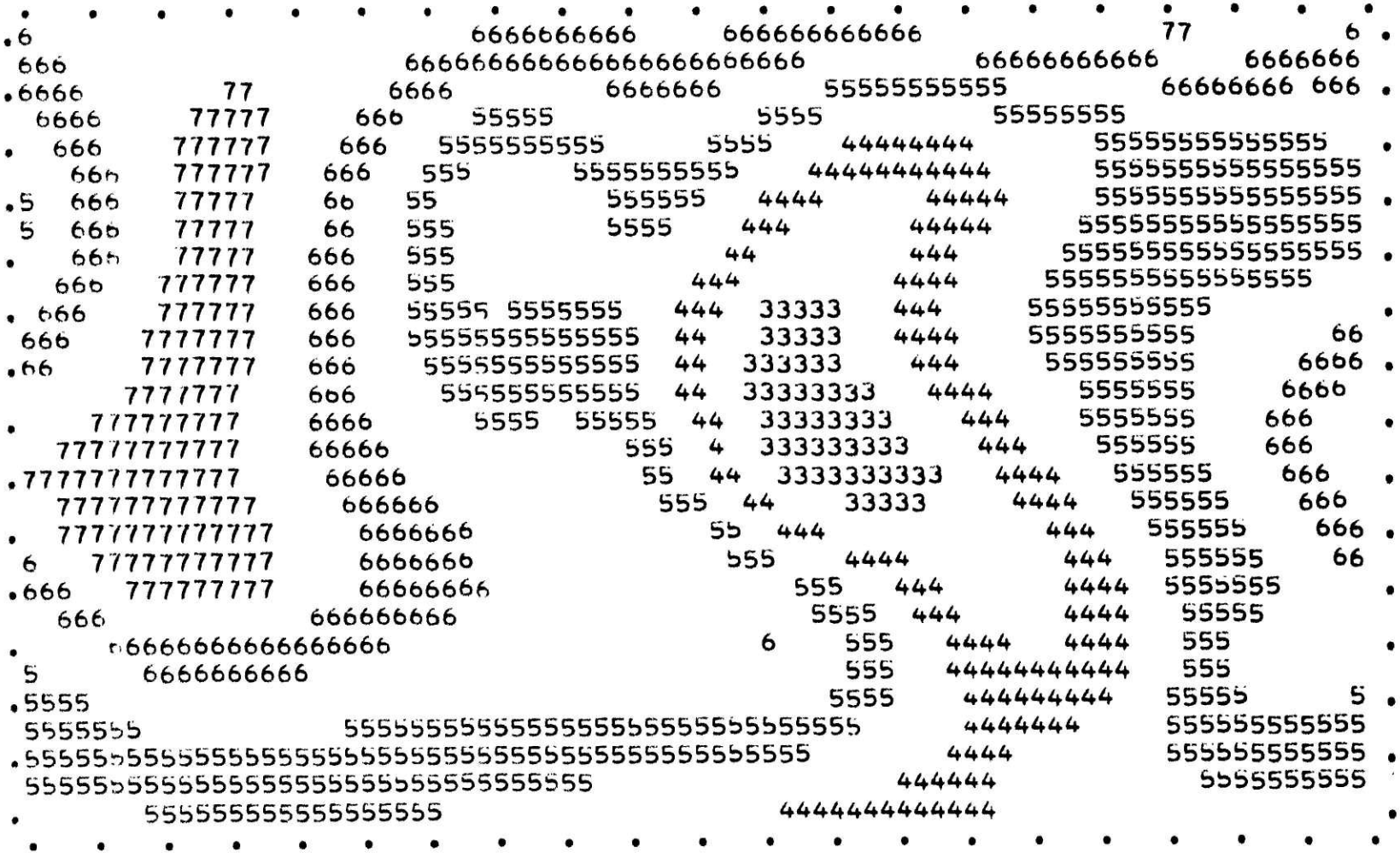

Figure 6.5.19 Run 5 p_s after 10 days.

Figure 6.5.20 run 5 θ_5 after 10 days.

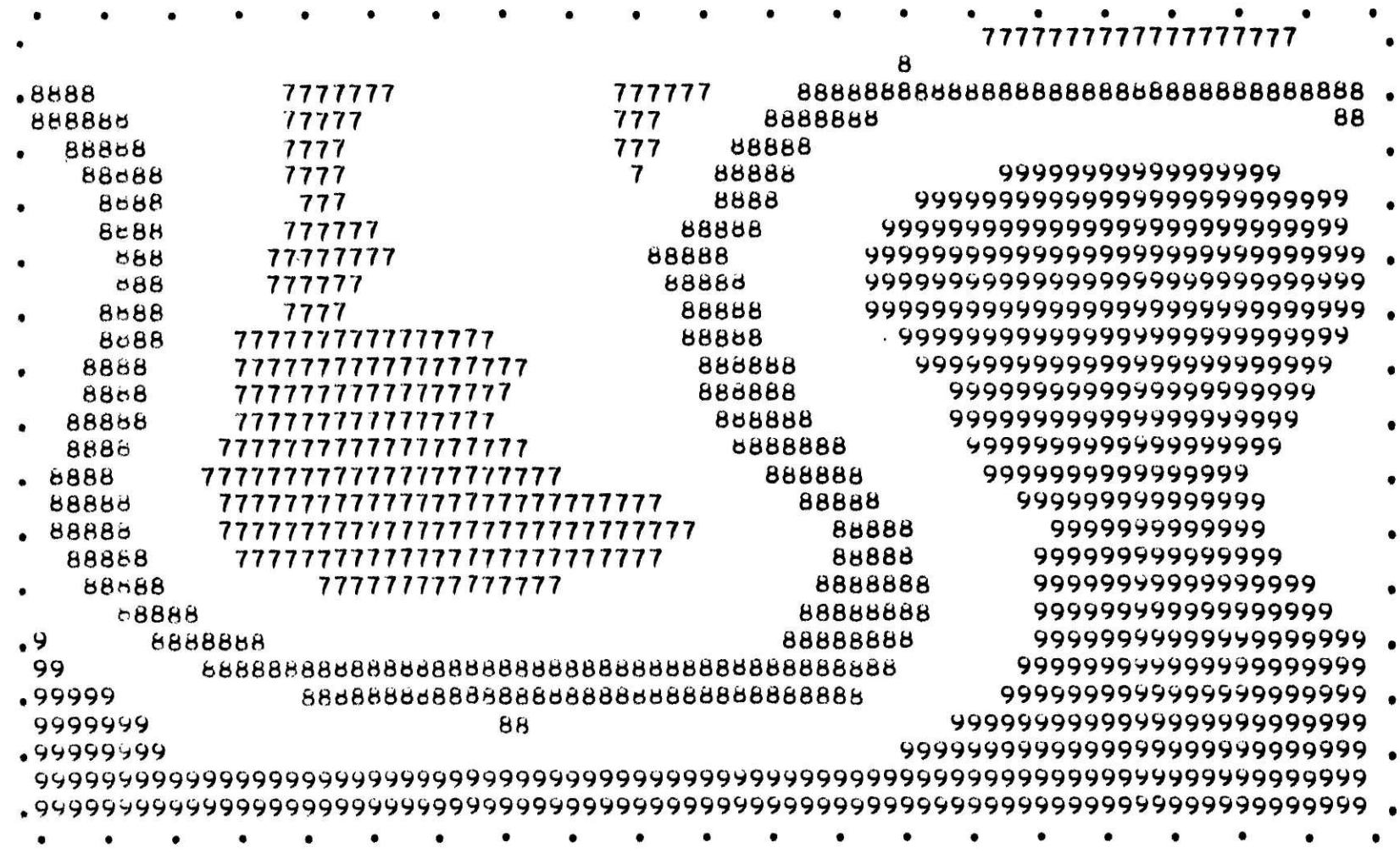

Figure 6.5.21 run 5 $\bar{\bar{M}}_2^{\theta}$ after 10 days.

Key to Chapter 6 figures Pattern	P_s $\times 10^2$ Pa	θ_s °K	M_2 $\times 10^2 m^2 s^{-2}$
----------	950	240	310
1111111111111111111111	955	245	311
1111111111111111111111	960	250	312
2222222222222222222222	965	255	313
2222222222222222222222	970	260	314
3333333333333333333333	975	265	315
3333333333333333333333	980	270	316
4444444444444444444444	985	275	317
4444444444444444444444	990	280	318
5555555555555555555555	995	285	319
5555555555555555555555	1000	290	320
6666666666666666666666	1005	295	321
6666666666666666666666	1010	300	322
7777777777777777777777	1015	305	323
7777777777777777777777	1020	310	324
8888888888888888888888	1025	315	325
8888888888888888888888	1030	320	326
9999999999999999999999	1035	325	327
9999999999999999999999	1040	330	328
**********	1045	335	329
**********			

Figure 6.6.1 Figure Key

Note that for runs 1, 2, and 3 the intersecting isentrope (=290°K) is indicated by a heavy dark line.

CHAPTER 7

CONCLUSIONS

A quadratically conservative isentropic model including diabatic terms has been developed. Under adiabatic conditions it conserves energy and can be run for two to three days before short waves start to develope. The periodic use of a high order filter removes the short waves but does not eliminate a spurious kink that developed after two days.

Numerical experiments with a two layer version of the model without the intersection of an isentrope with the ground prove sucessful and show no tendency to produce the kink observed in the intersecting case. Thus, good results can be obtained without requiring the extra work involved with an intersecting isentrope. This would not apply to a multilayer model as vertical resolution would be lost in the lowest layer near the poleward boundary. The fact that the kink does not appear in the runs without an intersecting isentrope indicates that the treatment of the intersection needs further developement.

The diabatic run using the two layer non-intersecting version of the model can be run sucessfully for ten days. This suggests that the model would be natural for investigating coastal cyclo- and frontogenesis or other ares where large heating contrasts exist. Since the increased resolution of the cyclones and fronts can be obtained, an isentropic model would be advantageous in such studies. The resolving of cyclones and fronts also suggests a solution to the tendency of general circulation models to give too shallow developement for cyclones and

to inadequately estimate their associated transports of momentum and heat. By using an isentropic model, one may avoid the necessity of using higher horizontal (or vertical) resolution that Stone et al. (1975) indicated is necessary to better represent the lows and their associated transports. The difficulty of the meridional boundary conditions, however, means that more work must be done before such a study could be undertaken. It is expected that by changing the meridional boundary conditions or eliminating the north and south walls, integrations could be performed for an indefinite length of time.

APPENDIX

Modifications for the Time Discontinuites

For case 1 θ_S , u_v, and v_v are extrapolated. This requires an adjustment in the associated time increments. If the present space fields are represented by subscript T, and the subscript v is for the present value of v, the equations for the time increments are:

$$\Delta t \cdot \frac{\partial \Delta \rho \bar{\theta}^{\theta}}{\partial t} = \Delta \rho_{v_T} \cdot \left(\frac{\theta_{S_T} + \theta_{v}}{2} \right) - \Delta \rho_{v} \cdot \left(\frac{\theta_S + \theta_v}{2} \right) \qquad (A.1)$$

$$\left(\Delta t \cdot \frac{\partial \Delta \rho u}{\partial t} \right)_v = \Delta \rho_{v_T} \cdot u_{v_T} - \Delta \rho_v \cdot u_v \qquad (A.2)$$

$$\left(\Delta t \cdot \frac{\partial \Delta \rho v}{\partial t} \right)_v = \Delta \rho_{v_T} \cdot V_{v_T} - \Delta \rho_v \cdot V_v \qquad (A.3)$$

These new values are then used in the next N-cycle step.

For case 2 θ_S and p_v have been redefined. The finite difference time increments are:

$$\left(\Delta t \cdot \frac{\partial \Delta \rho}{\partial t} \right)_v = \Delta \rho_{v_T} - \Delta \rho_v - \Delta \rho_{v-1} \qquad (A.4)$$

$$\left(\Delta t \cdot \frac{\partial \Delta \rho \bar{\theta}^{\theta}}{\partial t} \right) = \Delta \rho_{v_T} \cdot \left(\frac{\theta_{S_T} + \theta_v}{2} \right) - \left(\Delta \rho_v + \Delta \rho_{v-1} \right) \cdot \left(\frac{\theta_S + \theta_v}{2} \right) \qquad (A.5)$$

$$\left(\Delta t \cdot \frac{\partial \Delta \rho u}{\partial t} \right)_v = \Delta \rho_{v_T} \cdot u_{v_T} - \left(\Delta \rho_v + \Delta \rho_{v-1} \right) u_v \qquad (A.6)$$

$$\left(\Delta t \cdot \frac{\partial \Delta \rho v}{\partial t} \right)_v = \Delta \rho_{v_T} \cdot V_{v_T} - \left(\Delta \rho_v + \Delta \rho_{v-1} \right) V_v \qquad (A.7)$$

For case 3 p_r, Δp_r, Δp_{r+1}, u_r and v_r have all been redefined. The time increments are:

$$\left(\Delta t \cdot \frac{\partial \Delta p}{\partial t}\right)_r = \Delta p_{r_T} - \Delta p_r \qquad (A.8)$$

$$\left(\Delta t \cdot \frac{\partial \Delta p}{\partial t}\right)_{r+1} = \Delta p_{r+1_T} - \Delta p_{r+1} + \Delta p_r \qquad (A.9)$$

$$\left(\Delta t \cdot \frac{\partial \Delta p \bar{\theta}^{\theta}}{\partial t}\right) = \Delta p_{r_T}\left(\frac{\theta_{s_T} + \theta_r}{2}\right) - \Delta p_r \cdot \left(\frac{\theta_s + \theta_r}{2}\right) \qquad (A.10)$$

$\left(\Delta t \cdot \frac{\partial \Delta pu}{\partial t}\right)_r$ and $\left(\Delta t \cdot \frac{\partial \Delta pv}{\partial t}\right)$ as for case 1

$$\left(\Delta t \cdot \frac{\partial \Delta pu}{\partial t}\right)_{r+1} = \Delta p_{r+1_T} \cdot u_{r+1_T} - (\Delta p_{r+1} - \Delta p_r) \cdot u_{r+1} \qquad (A,11)$$

$$\left(\Delta t \cdot \frac{\partial \Delta pv}{\partial t}\right)_{r+1} = \Delta p_{r+1_T} \cdot v_{r+1_T} - (\Delta p_{r+1} - \Delta p_r) \cdot v_{r+1} \qquad (A,12)$$

For all the cases it can be seen that redefining one variable may require several time increments to be redfined.

REFERENCES

Bleck, R., 1973: Numerical forecasting experiments based on the conservation of potential vorticity on isentropic surfaces. J. Appl. Meteor., 12, 737-752.

____, 1974: Short-range predicition in isentropic coordinates with filtered and unfiltered numerical models. Mon. Wea. Rev., 102, 813-829.

____, 1977: Numerical simulation of lee cyclogenesis in the Gulf of Genoa, Mon. Wea. Rev., 105, 428-445.

Eliassen, A. and O. Hellevik, 1975: The design of a numerical model atmosphere with isentropic coordinate surfaces. NAVF Research Project No.D.10.09.2, Report No. 1, (Institute Report series, No. 13, September 1975. Institutt for Geofysikk, Universitetet i Oslo.)

____, and E. Raustein, 1968: A numerical integration experiment with a model atmosphere based on isentropic coordinates. Meteor. Annaler, 5, 45-63.

____ and ____, 1970: A numerical integration experiment with a six-level atmosheric model with isentropic information surface. Meteor. Annaler, 5, 429-449.

Friend, A.L., D. Djurić, and K. C. Brundidge, 1976: Numerical weather prediction using a combination of isentropic and sigma coordinates. Simulation of Large-Scale Atmospheric Processes, International Conference, Annaler der Meteorologie (Neue Folge) No. 11, 9-12.

Hellevik, O., 1976: Numerical integration experiments: cyclone developement. NAVF Research Project No.D.10.09.2, Report No. 2, (Institute Report series, No. 14, January 1976. Institutt for Geofysikk, Universitetet i Oslo).

Kálnay-Rivas, F., A. Bayliss, and J. Storch, 1977a: Experiments with the 4th order GISS model of the global atmosphere. To appear in Journ. of Comp. Phys.

____, 1977b: Numerical experiments with 4th order conservative finite difference equations. To appear in Journ of Comp. Phys.

Lorenz, F., 1971: An N-cycle time-differencing scheme for stepwise numerical integration. Mon. Wea. Rev., 99, 644-648.

Palmén, F., 1955: On the mean meridional drift of air in the friction layer of the west-wind belts. Quart. J. Roy. Meteor. Soc., 81, 459-461.

Reimer, E. 1976: An experiment in forecasting moist adiabatic processes with a model based on isentropic surfaces. Simulation of Large-Scale Atmospheric Processes, International Conference, Annaler der Meteorologie (Neue Folge) No. 11, 40-43.

Roads, J., 1977: Numerical experiments on the sensitivity of an atmospheric hydrologic cycle to the equilibrium temperature. PhD Thesis, Dept. of Meteorology, Massachusetts Institute of Technology.

Shapiro, M., 1975: Simulation of upper-level frontogenesis with a 20-level isentropic coordinate primitive equation model. Mon. Wea. Rev., 103, 591-604.

Shapiro, R., 1970: Smoothing, filtering, and boundary effects. Rev. Geophys. and Space Phys., 8, 359-387.

Starr, V. P., 1945: A quasi-Lagrangian system of hydrodynamical equations, J. Meteor., 2, 227-237.

Stone, P. H., S. Chow, H. M. Helfand, W. J. Quirk, and R. J. C. Somerville, 1975: Seasonal changes in the atmospheric heat balance simulated by the GISS general circulation model. Proceedings of the WMO/IAMAP Symposium on Long-Term Climatic Fluctuations, WMO Publication No. 421, 383-389.

Thompson, P., 1961: Numerical Weather Analysis and Prediction. New York, The Macmillan Company, 37-40.

Trevisan, A., 1976: Numerical experiments on the influence of orography on cyclone formation with an isentropic primitive equation model, J. Atmos. Sci., 33, 768-780.

ACKNOWLEDGEMENTS

The writer gratefully acknowledges the comments and suggestions of Prof. Arnt Eliassen. The comments and suggestions of the students of the Department of Meteorology at M.I.T., particularly those of Messrs. Neil Gordon and Gary Moore, were quite helpful. The writer wishes to thank Prof. Peter H. Stone for his comments on the resolution problem in general circulation models. The lucid comments, criticisms, and suggestions of Prof. Fredrick Sanders were extremely helpful and have given the writer further insight into the difficultes involved in using isentropic models. The financial, cerebral, and moral support of Prof. Edward N. Lorenz have proved invaluable and inspirational. Lastly, the writer is indebted to the help of Prof. Eugenia Kalnay-Rivas for her expertise in numerical methods, her insightfulness into the difficultes of this model, and her continued support during some of the more trying times. This thesis could not have been undertaken without her irreplaceable help.